

Insights Into And Manipulation Of Sulfated CNC Aggregation

Exploring TO as a probe for crystallite interaction and enzymatic hydrolysis as a method of selective surface modification

Master's thesis in Biotechnology (MPBIO)

WILLIAM LUNDSTRÖM

DEPARTMENT OF Chemistry and Chemical Engineering

CHALMERS UNIVERSITY OF TECHNOLOGY

Gothenburg, Sweden 2026

www.chalmers.se

Master's thesis 2026

Insights into and manipulation of CNC aggregation

Exploring TO as a probe for crystallite interaction and enzymatic hydrolysis as a method for selective surface modification

WILLIAM LUNDSTRÖM



CHALMERS
UNIVERSITY OF TECHNOLOGY

Department of Chemistry and Chemical Engineering
Division of Organic Chemistry
Gunnar Westman Group
Chalmers University of Technology
Gothenburg, Sweden 2026

Insights into and manipulation of CNC aggregation
Exploring TO as a probe for crystallite interaction and enzymatic hydrolysis as a method for selective surface modification
WILLIAM LUNDSTRÖM

© WILLIAM LUNDSTRÖM, 2026.

Supervisors:
Jelka Feldhusen, Department of Chemistry and Chemical Engineering; and
Elin Horn, Department of Physics and Astronomy
Examiner:
Gunnar Westman, Department of Chemistry and Chemical Engineering

Master's Thesis 2026
Department of Chemistry and Chemical Engineering
Division of Organic Chemistry
Gunnar Westman Group
Chalmers University of Technology
SE-412 96 Gothenburg
Telephone +46 31 772 1000

Cover: Assymetric unit of arylsulfatase from *Pseudomonas aeruginosa*. Adapted from reference [1], ©Structure 2001.

Typeset in LaTeX
Printed by Chalmers Reproservice
Gothenburg, Sweden 2026

Insights into and manipulation of CNC aggregation
Exploring TO as a probe for crystallite interaction and enzymatic hydrolysis as a method for selective surface modification
WILLIAM LUNDSTRÖM
Department of Chemistry and Chemical Engineering
Chalmers University of Technology

Abstract

This study investigates the aggregation behavior of crystalline nanocellulose (CNC) in aqeous suspension, and explores the viability of using sulfatases for controlled, selective surface desulfation. Thiazole orange (TO) and para-nitrophenyl sulfate (p-NPS) were synthesized and their purity was verified via NMR spectroscopy. The aggregation responses of TO in the presence of sulfated and non-sulfated, i.e. azitidinium-blocked, CNC were analyzed using UV-Vis absorbance and fluorescence spectrophotometry. Additionally, enzymatic assays of sulfatases from Helix pomatia and Pseudomonas aeruginosa on p-NPS in Tris and sodium acetate buffers were performed through UV-Vis absorbance spectrophotometry to evaluate catalytic activity. UV-Vis absorbance data corroborated that TO forms H-aggregates in the presence of CNC, while fluorescence results proved largely inconclusive due to Rayleigh scattering artifacts. Absorbance measurements indicated potential variations in aggregation behavior between the sulfated and blocked CNC batches. Ultimately, enzymatic desulfation of p-NPS was not successfully validated under the experimental conditions, likely resulting from enzyme degradation or suboptimal buffer parameters.

Keywords: crystalline nanocellulose, selective hydrolysis, sulfatase, enzymatic desulfation, thiazole orange, helix pomatia, pseudomaonas aeruginosa

Acknowledgements

I would like to extend my gratitude to the people at the Department of Life sciences, who took the time to answer my questions, and to Alma, who instructed me on the use of the fluorimeter. I want to thank my supervisors, Jelka and Elin, for all their help and advice throughout my thesis work, both in the and out of the lab. I particularly want to thank my examiner, Gunnar, for his continuous support, understanding, and engagement in my work.

William Lundström, Gothenburg, July 2026

List of Acronyms

Below is the list of acronyms that have been used throughout this thesis listed in alphabetical order:

AZ	azitidinium
CNC	crystalline nanocellulose
DI	de-ionized water
dsDNA	double-stranded DNA
DSP	disodium phosphate
EC	enzyme commission
IUBMB	international union of biochemistry and molecular biology
MCC	microcrystalline cellulose
MQ	Milli-Q
NaOAc	sodium acetate
NMR	nuclear magnetic resonance
p-NP	para-nitrophenyl
p-NPS	para-nitrophenyl sulfate
PAS	Pseudomonas aeruginosa sulfatase
RT	room temperature
SOP	standard operating procedure
TO	thiazole orange
Tris	Tris(hydroxymethyl)aminomethane
UV	ultraviolet
Vis	visible
WT%	weight percentage

Nomenclature

Below is the nomenclature of parameters and variables that have been used throughout this thesis.

Parameters

λ_{ex}	Excitation wavelength
λ_{em}	Emission wavelength
ϵ	Molar attenuation coefficient
l	Optical path length
$\overline{m}_{watchglass}$	Technical replicate average watchglass weight

Variables

A	Absorbance
c	Concentration
DW_{CNC}	Dry weight of CNC
$m_{CNC(aq)}$	Weight of added CNC suspension
$\overline{m}_{watchglass+CNC}$	Technical replicate average weight of the combined watchglass and suspension
C	Concentration of NaOH at the point of equivalence
V_e	Volume of NaOH at the point of equivalence
M_s	Total weight of the suspension
D_s	Concentration of the suspension

Contents

List of Acronyms **ix**

Nomenclature **xi**

List of Figures **xv**

List of Tables **xxi**

1 Introduction **1**
1.0.1 Aim . . . 1
1.0.2 Objectives . . . 1
1.0.3 Scope and Limitations . . . 2
1.0.4 Societal Impact . . . 3
1.1 Literature Review . . . 3

2 Theory **7**
2.1 Crystalline Nanocellulose . . . 7
2.2 Cyanine Dyes . . . 10
2.2.1 Thiazole Orange . . . 10
2.3 Enzymatic assay substrate . . . 11
2.4 Sulfatases . . . 12
2.4.1 Sulfatase from Helix pomatia . . . 13
2.4.2 Sulfatase from Pseudomonas aeruginosa . . . 13
2.5 Hypothesis of selective desulfation . . . 14
2.6 Spectrophotometry . . . 14

3 Methodology **17**
3.1 Chemicals . . . 17
3.2 Preparation of CNC suspension . . . 18
3.2.1 Preparation of tris buffer . . . 19
3.2.2 Preparation of sodium acetate buffer . . . 19
3.2.3 Preparation of disodium phosphate buffer . . . 19
3.2.4 Synthesis of Thiazole Orange . . . 19
3.2.5 Synthesis of para-Nitrophenyl sulfate . . . 19
3.2.5.1 Standard Method . . . 20
3.2.5.2 Alternate Method . . . 20
3.3 Spectroscopy . . . 20

3.3.1 UV-Vis Absorption Spectroscopy 20
3.3.2 Fluorescence Spectroscopy 20
3.3.3 Nuclear Magnetic Resonance Spectroscopy 21

4 Results **23**
4.1 Validation of Thiazole Orange synthesis by NMR spectroscopy 23
4.2 Validation of p-NPS synthesis by NMR spectroscopy 25
4.3 Absorbance spectra of buffer solutions 29
4.4 Absorbance spectra for TO 31
4.5 Absorbance spectra for CNC 32
4.6 Absorbance spectra for TO and CNC 33
4.7 Fluorescence spectra for TO 35
4.8 Fluorescence spectra for CNC 36
4.9 Fluorescence spectra for CNC and TO 39
4.10 Absorbance Spectra for p-NPS 41
4.11 Absorbance spectra of sulfatases 48
4.12 Enzymatic assays via absorbance spectroscopy 51
4.12.1 Helix pomatia 1 and pNPS (std) in 0.015 M Tris 51
4.12.2 Helix pomatia 1 and pNPS (std) in 0.5 M Tris 52
4.12.3 Helix pomatia 2 and (recrystalized) pNPS (std) in 0.5 M Tris 54
4.12.4 Helix pomatia 1 and (recrystalized) p-NPS (std) in 0.5 M NaOAc 55
4.12.5 Helix pomatia 2 and recrystallized p-NPS (std) in 0.5 M NaOAc 56
4.12.6 Pseudomonas aeruginosa sulfatase and recrsytallized p-NPS (alt) in 0.05 M Tris 57
4.12.7 Pseudomonas aeruginosa sulfatase and recrystallized p-NPS (alt) in DI 58

5 Discussion **61**

6 Conclusion **65**

A Supporting figures **I**
A.1 NMR spectra I
A.1.1 NMR spectra of p-NPS by standard method I
A.1.2 NMR spectra of p-NPS by alternate method III
A.1.3 NMR spectra of TO VII

B Standard Operating Procedures **XIX**
B.1 Synthesis of CNC XIX
B.1.1 Measurement of dry weight and sulfate content XIX
B.2 Potentiometric and Conductometric Titration XIX

List of Figures

1.1 UV-Vis measurement of para-nitrophenyl sulfate (p-NPS) and sulfatase from *Helix pomatia* in 0.5 M Tris(hydroxymethyl)aminomethane (Tris) buffer (pH 7.4), with a new spectra recorded every 5 minutes for 2 h (t0-t120). The spectra at t0 is a reference without sulfatase. Adapted from reference [8], ©Elin Horn 2024. 4

1.2 UV-Vis measurement of p-NPS and sulfatase from *Helix pomatia* in 0.5 M sodium acetate (NaOAc) buffer (pH 6.2), with a new spectra recorded every 5 minutes for 2 h (t0-t120). The spectra at t0 is a reference without sulfatase. Adapted from reference [8], ©Elin Horn 2024. 4

1.3 Dimer, and H and J aggregates of thiazole orange (TO). Adapted from reference [12], ©Journal of Materials Chemistry C 2013 5

1.4 Absorption spectra of different concentrations of TO and 0.1 wt% crystalline nanocellulose (CNC) in 25 mM disodium phosphate (DSP) buffer. Adapted from reference [7], ©Simon Jademyr 2016. 5

1.5 Emission spectra of different concentrations TO and 0.1 wt% CNC in 25 mM DSP buffer, excited at 290 nm. Adapted from reference [7], ©Simon Jademyr 2016. 6

2.1 a) Chemical structure of cellulose and the repeating unit cellobiose are illustrated. b) Representation of unit cell of cellulose Iα structure. Carbon, oxygen, and hydrogen atoms are represented by cyan, red, and white colors, respectively. Adapted from reference [16], ©Science Advances 2022. 7

2.2 a) A 36-chain microfibril model of cellulose Iα crystalline structure with a hexagonal shape generated with Cellulose Builder software, displaying different crystallographic planes. b) A longitudinal view of parallel sheets of cellulose chains. Each molecular sheet is shifted along the c axis by + c/4. Adapted from reference [16], ©Science Advances 2022. 8

2.3 Orientation of sulfate groups on the CNC surface. To the right the crystal structure of cellulose is displayed, highlighting two of the lattice planes. Adapted from reference [8], ©Elin Horn 2024. 8

2.4 A schematic of the isotropic and anisotropic phases of CNC suspensions, and the ordering of crystallites into a chiral nematic structure. a) Helical twists of individual crystallites. b) Helical twists of layers of semi-parallell crystallites, i.e. cholesteric Adapted from reference [20], ©Food and Bioprocess Technology 2020. 9
2.5 Schematic illustration of the smectic, nematic, and cholesteric phases of liquid crystals. Adapted from reference [21], ©Smart Glass World 2026. 9
2.6 Schematic illustration of phase changes for *thermotropic* liquid crystals. Adapted from reference [24], ©Anna Fox 2009. 10
2.7 The chemical structure of Thiazole Orange. Adapted from reference[29], ©MedChemExpress 2026. 11
2.8 The chemical structure of p-NPS. Adapted from reference [31], ©Thermo Scientific Chemicals 2026. 12
2.9 The potential stereochemical outcomes at the chiral secondary carbon atom of a substrate in the hydrolysis of sulfate esters catalyzed by sulfatases. Adapted from reference [35], ©Methods in Enzymology 2010. 13
2.10 (a) shows the hexagonal cross section of CNC, where the yellow dots represents sulfate groups on the surface. (b) represents the CNC surface after chemical hydrolysis, resulting in a randomized desulfation pattern. (c) shows a selective desulfation pattern and how the CNC surface potentially could look after enzymatic methods have been applied. Adapted from reference [8], ©Elin Horn 2024. 14
2.11 Example of second order artefacts in a broad fluorescence emission spectrum of a solution of 2-aminopyridine mixed with Ludox excited at 300 nm. Adapted from reference [41], ©Edinburgh Instruments 2021. 15

4.1 Nuclear magnetic resonance (NMR) spectra of TO. 24
4.2 NMR spectra of p-NPS synthesized by the "standard method". 26
4.3 NMR spectra of p-NPS synthesized by the "alternate method". 28
4.4 UV-Vis absorbance spectrum of 0.5 M Tris buffer at 37 °C. 29
4.5 Average absorbance of technical triplicates of tris buffer, ±1 standard deviation, prepared from three separate sources of tris base, here arbitrarily denoted "l", "18", and "K6". 0.1 g tris base were solved in DI, giving the corresponding concentration of 412.75 mM. 30
4.6 Average absorbance of technical triplicates of NaOAc buffer, ±1 standard deviation. 30
4.7 Average absorbance of technical triplicates of 5 mM DSP buffer, ±1 standard deviation. 31
4.8 Absorbance spectra of TO solved in 5 mM DSP to concentrations of 17.5, 35, and 70 µM, in the ultraviolet (UV)-visible (Vis) range between 200 and 700 nm. the experiment was performed on December 1st 2025. 31

4.9 Absorbance spectra of TO solved in 5 mM DSP to concentrations of 17.5, 35, and 70 µM, in the UV-Vis range between 200 and 700 nm. The experiment was performed on December 12th 2025. 32
4.10 Average absorbance of technical triplicates, ±1 standard deviation, of aqueous suspensions of sulfated and "non-sulfated" CNC at 0.05, 0.1, and 0.75 wt%. 32
4.11 Average absorbance of technical triplicates, ±1 standard deviation, of 0.05 weight percentage (WT%) aqueous suspension of sulfated CNC (265 µmol sulfate/g CNC) and 17.5, 35, and 70 µM TO solved in 5 mM DSP buffer, respectively. The molar ratio of TO to surface sulfate on the CNC is 1:1. Signals adjusted for the background signal of 5 mM DSP buffer. 33
4.12 Average absorbance of technical triplicates, ±1 standard deviation, of 0.05 WT% aqueous suspension of sulfated CNC (265 µmol sulfate/g CNC) and 17.5, 35, and 70 µM TO solved in 5 mM DSP buffer, respectively. The molar ratio of TO to surface sulfate on the CNC is 2:1. Signals adjusted for the background signal of 5 mM DSP buffer. . 34
4.13 Average absorbance of technical triplicates, ±1 standard deviation, of 0.1 WT% aqueous suspension of sulfated CNC (265 µmol sulfate/g CNC) and 17.5, 35, and 70 µM TO solved in 5 mM DSP buffer, respectively. The molar ratio of TO to surface sulfate on the CNC is 2:1. Signals adjusted for the background signal of 5 mM DSP buffer. . 34
4.14 Emission of 17.5, 35, and 70 µM TO in 5 mM DSP buffer in the 300-700 nm range, excited at 290 nm. Signals showns are averages of technical triplicates, ±1 standard deviation, and normalized to the emission of solvent, DSP. Experiment performed on December 1st 2025. 35
4.15 Emission of 17.5, 35, and 70 µM TO in 5 mM DSP buffer in the 300-700 nm range, excited at 290 nm. Signals showns are averages of technical triplicates, ±1 standard deviation, and normalized to the emission of solvent, DSP. The experiment was performed on December 15th 2025. 36
4.16 Emission of 0.05, 0.1, and 0.75 WT% sulfated (265 µmol sulfate per g CNC) and non-sulfated (252 µmol sulfate per g CNC blocked by azitidinium (AZ) salts) CNC, in aqueous suspension. Scanned in the 300-700 nm range, and excited at 290 nm. Signals showns are averages of technical triplicates, ±1 standard deviation, and normalized to the emission of solvent, de-ionized water (DI) water. The experiment was performed on December 5th 2025. 37
4.17 Emission of 0.05, 0.1, and 0.75 WT% sulfated (265 µmol sulfate per g CNC) and non-sulfated (252 µmol sulfate per g CNC blocked by AZ salts) CNC, in aqueous suspension. Scanned in the 300-800 nm range, and excited at 380 nm. Signals showns are averages of technical triplicates, ±1 standard deviation, and normalized to the emission of solvent, DI water. The experiment was performed on December 18th 2025. 38

4.18 Emission of 0.05, 0.1, and 0.75 WT% sulfated (265 µmol sulfate per g CNC) and non-sulfated (252 µmol sulfate per g CNC blocked by AZ salts) CNC, in aqueous suspension. Scanned in the 300-800 nm range, and excited at 500 nm. Signals showns are averages of technical triplicates, ±1 standard deviation, and normalized to the emission of solvent, DI water. The experiment was performed on December 18th 2025 39
4.19 Emission of 0.05 WT% sulfated (265 µmol sulfate per g CNC) CNC in aqueous suspension and, respectively, 17.5, 35, and 70 µM TO in 5 mM DSP buffer. The molar ratio of TO to surface sulfate on the CNC is 2:1. Signals are normalized to the emission of the buffer, 5 mM DSP. The excitation wavelength, λ_{ex}, was 290 nm, and the scanned range was between 300 and 700 nm, and the excitation and emission slit widths was set to 2.5 nm. The experiment was performed on December 2nd. 40
4.20 Emission of 0.1 WT% sulfated (265 µmol sulfate per g CNC) CNC in aqueous suspension and, respectively, 17.5, 35, and 70 µM TO in 5 mM DSP buffer. The molar ratio of TO to surface sulfate on the CNC is 2:1. Signals are normalized to the emission of the buffer, 5 mM DSP. The excitation wavelength, λ_{ex}, was 290 nm, and the scanned range was between 300 and 700 nm, and the excitation and emission slit widths was set to 2.5 nm. The experiment was performed on December 15th. 41
4.21 Absorbance of p-NPS synthesized by the standard method, solved in 37 °C DI water. Scans were taken at an interval of 5 min for a total duration of 60 min, in the 200-500 nm range. The experiment was performed on September 15th 2025. 42
4.22 Absorbance of p-NPS synthesized by the standard method, solved in 15 mM Tris buffer at 37 °C. Scans were taken at an interval of 5 min for a total duration of 120 min, in the 200-500 nm range. The experiment was performed on October 9th 2025. 43
4.23 Absorbance of recrystallized p-NPS synthesized by the standard method, solved in 0.5 M NaOAc buffer at 37 °C. Scans were taken at an interval of 2.5 min for a total duration of 60 min, in the 200-500 nm range. The experiment was performed on November 4th 2025. 44
4.24 Absorbance of recrystallized p-NPS synthesized by the standard method, solved in 0.5 M NaOAc buffer at 37 °C. Scans were taken at an interval of 2.5 min for a total duration of 30 min, in the 200-500 nm range. The experiment was performed on November 6th 2025. 45
4.25 Absorbance at 37 °C of filtered and recrystalized pNPS, synthesized by the alternate method, solved in DI. Scans were taken at an interval of 5 min for a total duration of 60 min, in the 200-500 nm range. The experiment was performed on October 30th 2025. 46
4.26 Absorbance in the 200-500 nm range at 37 °C of filtered and recrystalized pNPS, synthesized by the alternate method, solved in DI. The experiment was performed on November 4th 2025. 46

4.27 Absorbance of p-NPS synthesized by the alternative method, solved in 0.2 M Tris buffer at 37 °C, in the 200-500 nm range. The experiment was performed on October 15th 2025. 47
4.28 Absorbance at 37 °C of filtered and recrystalized p-NPS, synthesized by the alternate method, solved in 50 mM Tris buffer. Scans were taken at an interval of 5 min for a total duration of 35 min, in the 200-500 nm range. The experiment was performed on October 27th 2025. 48
4.29 Absorbance of *Helix pomatia* sulfatase (source 1), in 15 mM Tris buffer at 37 °C. Scans were taken every 5 minutes for 120 minutes, between 200-500 nm. The experiment was performed on October 9th. 49
4.30 Absorbance of *Helix pomatia* sulfatase (source 2), in 0.5 M Tris buffer at 37 °C, in the 200-500 nm range. The experiment was performed on November 6th. 50
4.31 Absorbance of *Helix pomatia* sulfatase (source 2), in 0.5 M NaOAc buffer at 37 °C, in the 200-500 nm range. The experiment was performed on November 6th. 50
4.32 Enzymatic assay of *Helix pomatia* sulfatase (source 1) on p-NPS synthesized by the standard method, in 0.015 M Tris buffer at 37 °C. Scans where made every 5 minutes for 120 minutes, in the 200-500 nm range, on October 9th 2025. 51
4.33 Enzymatic assay of *Helix pomatia* sulfatase (source 1) on p-NPS synthesized by the standard method, in 0.015 M Tris buffer at room temperature (RT). Scans where made every 5 minutes for 120 minutes, in the 200-500 nm range, on October 9th 2025. 52
4.34 Enzymatic assay of *Helix pomatia* sulfatase (source 1) on p-NPS synthesized by the standard method, in 0.5 M Tris buffer at 37 °C. Scans where made every 5 minutes for 120 minutes, in the 200-500 nm range, on October 8th 2025. 53
4.35 Enzymatic assay of *Helix pomatia* sulfatase (source 1) on p-NPS synthesized by the standard method, in 0.5 M Tris buffer at RT. Scans where made every 5 minutes for 120 minutes, in the 200-500 nm range, on October 8th 2025. 54
4.36 Enzymatic assay of *Helix pomatia* sulfatase (source 2) on recrystallized p-NPS, synthesized by the standard method, in 0.5 M Tris buffer at 37 °C. Scans where made every 2.5 minutes for 15 minutes, in the 200-500 nm range, on November 6th 2025. 55
4.37 enzymatic assay of *Helix pomatia* sulfatase (source 1) sulfatase on recrystallized p-NPS, synthesized by the standard method, in 0.5 M NaOAc buffer at 37 °C. Scans where made every 2.5 minutes for 60 minutes, in the 200-500 nm range, on November 4th 2025. 56
4.38 Enzymatic assay of *Helix pomatia* sulfatase (source 2) sulfatase on recrystallized p-NPS, synthesized by the standard method, in 0.5 M NaOAc buffer at 37 °C. Scans where made every 2.5 minutes for 30 minutes, in the 200-500 nm range, on November 6th 2025. 57

4.39 Enzymatic assay of Pseudomonas aeruginosa sulfatase (PAS) on recrystallized p-NPS, synthesized by the alternative method, in 50 mM Tris buffer at 37 °C. Scans where made every 5 minutes for 35 minutes, in the 200-500 nm range, on October 27th 2025. 58
4.40 Enzymatic assay of PAS on recrystallized p-NPS, synthesized by the alternative method, in DI water at 37 °C. Scans where made every 5 minutes for 60 minutes, in the 200-500 nm range, on October 30th . . 59

B.1 Typical potentiometric titration curve for sulfated CNC against NaOH.XXI

List of Tables

3.1 **Chemicals list** 17

1
Introduction

Nanocrystalline cellulose (CNC), also known as Cellulose Nanocrystals, are nanoscale crystalline pieces of cellulose polymers that - like most other nanomaterials - have shown a breadth of interesting properties because of its diminutive dimensions. Cellulosic materials such as CNC are intrinsically renewable, and depending on treatment, also sustainable and bio-compatible [2]. Applications in food packaging has shown performance gains relative to conventional materials in preliminary studies [3], as it similarly have shown when used as a doping material in cement and paints [4]. A wide range of use-cases in the healthcare sector are also being explored, including in drug delivery, tissue scaffolds, and wound-dressing gausses [4]; and recently, CNC has also gained attention in the field of electronics, ranging from super-capacitors, sensors, and flexible batteries, to printable electronics [4, 5]. Being a high strength yet lightweight material, it is even considered for vehicle construction and body armor [4].

As is the case for most nanomaterials, the material properties of nanocrystalline cellulose (CNC) films (and other such materials) are heavily dependent on not only the chemical composition and structure of its constituents, but crucially also the aggregate structure formed by them that in and of itself gives rise to properties not found in said constituents [6]. Thus, any insight into determining and modifying the chemical composition (e.g. sulfate content), and subsequently the formation of this aggregate structure, is of great interest for the eventual manipulation and practical application of CNC materials.

1.0.1 Aim

The aim of this project is to further the understanding of how crystallites of CNC interact and aggregate during film formation, and how this process might be controlled by modifying the surface structure of said crystallites. Specifically of interest is how the abundance and orientation of the superficial sulfate groups affect the aggregation process, and whether sulfatases could be a novel method of controlling this process thanks to its hypothesized *selectivity*, i.e. non-symmetry regarding which faces of the crystallites it could efficiently desulfate.

1.0.2 Objectives

To achieve the overall aim of the project, and with a foundation in the work previously done on the topic, the following seven specific objectives were identified:

1. Using absorbance spectrophotometry, verify and replicate the cyanine dye aggregation response to changes of dye concentration and dry weight of CNC, previously identified by Jademyr [7].
2. Using fluorescence (emission) spectrophotometry, verify and replicate the fluorescence of DNA-cyanine dye complexes, in absence and presence of CNC, previously identified by Jademyr [7].
3. Examine the potential correlation between sulfate content of CNC suspension and aggregation behavior through absorbance and fluorescence spectrophotometry of two batches of cnc: one sulfated (with sulfate content determined by potentiometric titration), and one (effectively) non-sulfated.
4. Study the dehydration phase of CNC film formation by time-lapse image capture using fluorescence microscopy, utilizing the fluorescent properties of intercalation between CNC-bound TO and double-stranded DNA (dsDNA).
5. Verify and replicate the enzymatically catalyzed desulfation of p-NPS previously achieved by Horn [8], i.e. that of *H. pomatia* sulfatase in tris- and sodium acetate buffers.
6. Expand the scope compared to the previous desulfation study by testing an alternate enzyme, *P. aeruginosa* sulfatase, under the same conditions as H. pomatia in tris- and sodium acetate buffers.
7. Granted successful replication of enzymatic desulfation, evaluate the use of chelators as an appropriate method of sulfatase inhibition, and thus as an additional mode of controlling the surface sulfate levels on CNC.

1.0.3 Scope and Limitations

The scope of CNC material studied in this project is limited to aqeuous suspensions of sulfated CNC, diluted to 0.05, 0.1, and 0.75 WT%. Two batches were used, at $265\,\mu mol\,g^{-1}$ and $252\,\mu mol\,g^{-1}$ sulfate on CNC. The latter was blocked by AZ salts and considered non-sulfated, to enable comparisons of sulfated and non-sulfated batches.
Sulfatases are classification of enzymes capable of hydrolyzing sulfate-ester bonds [9], such as those linking the surface sulfate groups on crystallites of CNC. Potentially, many are applicable for use in this context, necessitating a limitation of which specific enzymes to study. The choice fell on sulfatase from *H. pomatia* and *P. aeruginosa*, due to their availability in the lab, and time- and resource limitations making purchase and delivery of new enzymes unfeasible.

Enzymatic activity is studied through enzymatic assays, specifically absorbance measurements limited to the UV-visual spectrum between 200 and 500 nm. Only two buffers are used due to the previous use in the study by Horn: Tris buffer and sodium acetate buffer [8]. Only two temperatures where used for absorbance measurements: physiological and RT, i.e. 37 °C and approximately 20 °C. The substrate used for the assays is limited to p-NPS, though two synthesis pathways are employed.

As for aggregation behavior, it is studied through absorbance measurements at the same wavelengths, and through fluorescence spectroscopy between either 300-700 or 300-800 nm, and excited at either 290, 380, or 500 nm. All in 5 mM DSP buffer for comparability to the Jademyr study [7], and at RT due to instrument specifications. Target buffer parameters, a concentration of 5 mM (aq) and a pH of 7.0, at 25 °C, are based on previous research by Karlsson et al. [10]. Only one fluorescent cyanine dye is studied, thiazole orange (TO), chosen due to it being the most promising of the examined pair in the Jademyr study [7].

Due to many batches of buffer solutions being used throughout the duration of the project, and the different levels of dilutions employed, pH was not prioritized as a strictly fixed parameter, and rather accepted to vary within narrow target ranges around the optima: pH 7.1-7.4 for Tris buffers, pH 5-6 for sodium acetate buffers, and pH 6.9-7.1 for DSP, respectively.

1.0.4 Societal Impact

By targeting the knowledge gap that currently exists regarding the viability of using enzymatic desulfation as a novel tool in modifying CNC, as well as the role of the surface sulfate groups, that this tool would affect, in aggregation behavior, this project is one step on the path to practical implementation of CNC. As a renewable, sustainable, and bio-compatible material with applications in electronics, healthcare, and construction, CNC could help reduce the use of fossil-based and carbon intensive materials, be the basis of innovative and sustainable industries and products, and bring advances in the healthcare sector. Additionally, since CNC is fabricated from cellulose, one can imagine utilizing current waste streams in the forestry and agricultural industries to source material for CNC production, valorizing unused materials and increasing the circularity of the economy. Thus, this project relates to several of the United Nations' sustainable development goals (SGDs), but particularly goals 3, good health and well-being; 9, fostering innovation and sustainable industry; and 12, responsible consumption and production [11].

1.1 Literature Review

Elin Horn have previously assayed the activity of *Helix pomatia* sulfatase on p-NPS and CNC in Tris and sodium acetate buffers [8]. *Figure* 1.1 shows an assay of sulfatase from *Helix pomatia* on p-NPS in 0.5 M, pH 7.4 Tris buffer, exemplifying a successful enzymatic desulfation of p-NPS. The peak at 280 nm, representing sulfated p-NPS, decreases over time as the peak at 410 nm, representing the desulfated species, para-nitrophenyl (p-NP), increases correspondingly.

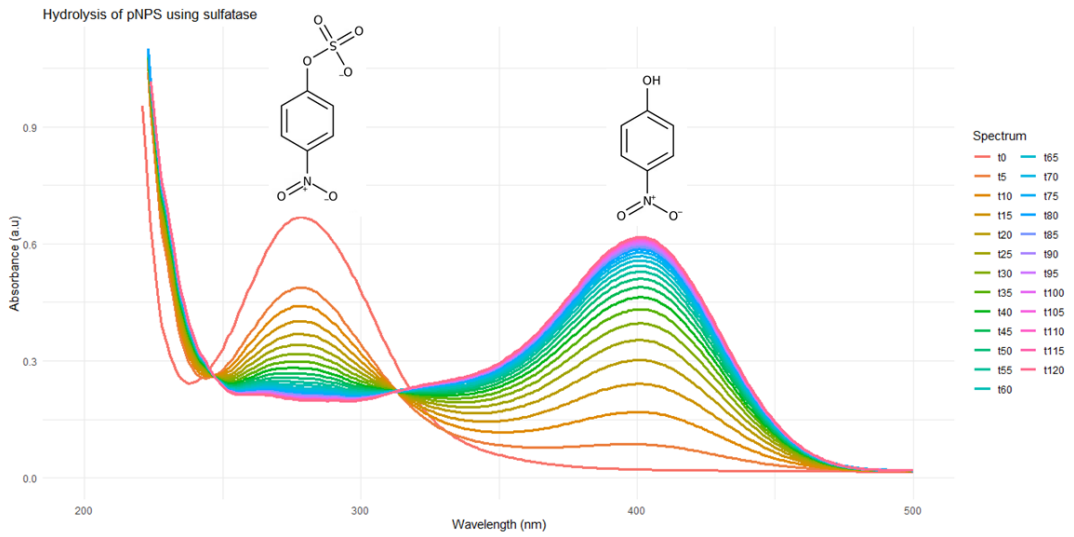

Figure 1.1: UV-Vis measurement of p-NPS and sulfatase from *Helix pomatia* in 0.5 M Tris buffer (pH 7.4), with a new spectra recorded every 5 minutes for 2 h (t0-t120). The spectra at t0 is a reference without sulfatase. Adapted from reference [8], ©Elin Horn 2024.

Figure 1.2 shows an assay of sulfatase from *Helix pomatia* on p-NPS in 0.5 M, pH 6.2 sodium acetate buffer, exemplifying successful enzymatic desulfation also in acetate buffer.

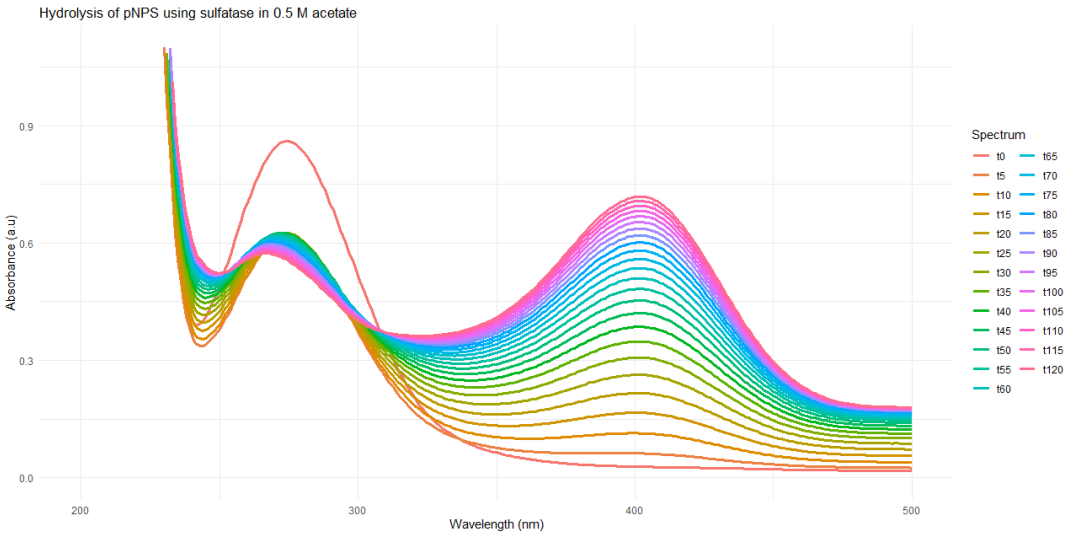

Figure 1.2: UV-Vis measurement of p-NPS and sulfatase from *Helix pomatia* in 0.5 M NaOAc buffer (pH 6.2), with a new spectra recorded every 5 minutes for 2 h (t0-t120). The spectra at t0 is a reference without sulfatase. Adapted from reference [8], ©Elin Horn 2024.

Main conclusions by Horn applicable to the this project where that: NaOAc buffer was noticeably more efficacious for enzymatic desulfation of CNC than Tris, though not apparent of p-NPS; and that pH lower than 7 was preferable to avoid alkaline

autohydrolysis (chemical desulfation) [8].

Simon Jademyr have previously synthesized the cyanine dye TO, and studied CNC aggregation and interaction with cyanine dyes using UV-Vis and fluorescence spectrophotometry [7]. Three TO aggregation responses where considered in the context, parallell H-aggregates, antiparallell J-aggregates, and dimers, as illustrates by the schematic in *Figure* 1.3.

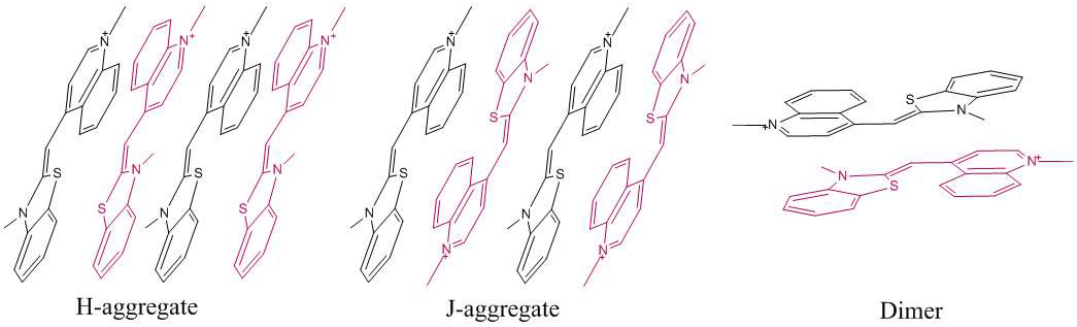

Figure 1.3: Dimer, and H and J aggregates of TO. Adapted from reference [12], ©Journal of Materials Chemistry C 2013

Absorption spectra of different concentrations of TO and 0.1 wt% CNC in 25 mMDSP buffer, displayed in *Figure* 1.4, exemplifies the main conclusion by Jademyr that is relevant to this project: that TO forms dimers with itself, and H-aggregates in the presence of CNC [7].

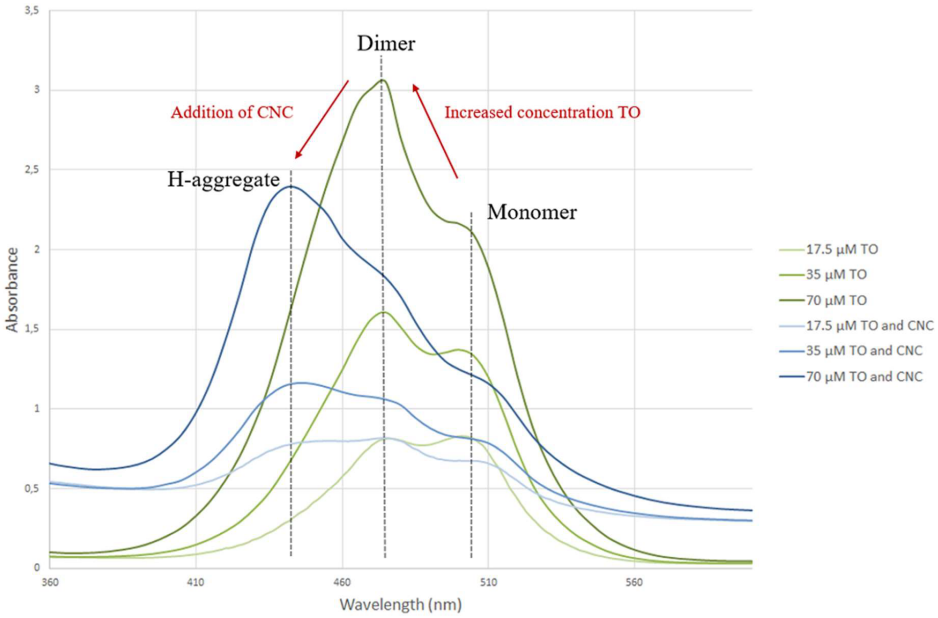

Figure 1.4: Absorption spectra of different concentrations of TO and 0.1 wt% CNC in 25 mM DSP buffer. Adapted from reference [7], ©Simon Jademyr 2016.

Figure 1.5 show the emission spectra of different concentrations TO and 0.1 wt% CNC in 25 mM DSP buffer, excited at 290 nm.

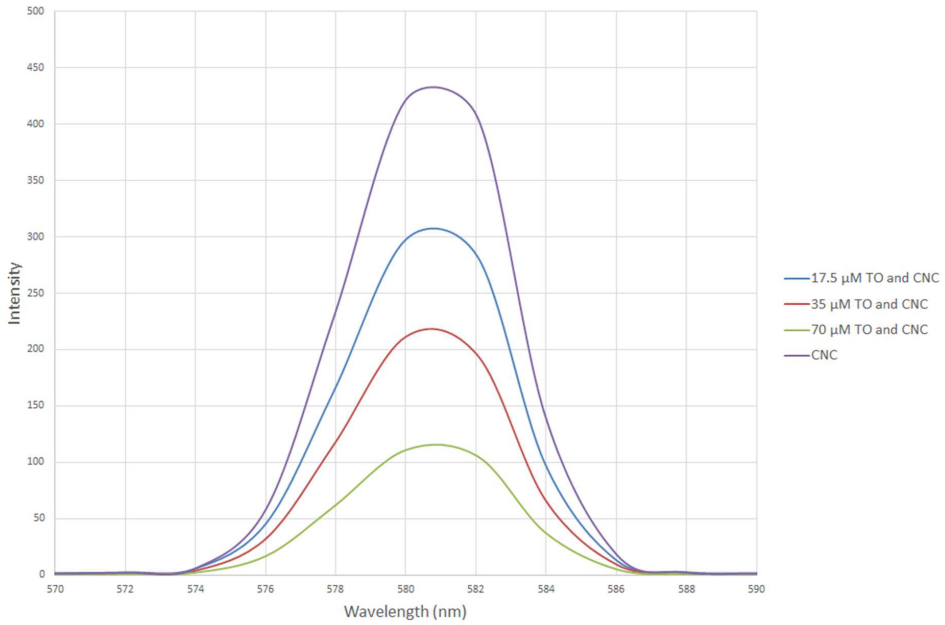

Figure 1.5: Emission spectra of different concentrations TO and 0.1 wt% CNC in 25 mM DSP buffer, excited at 290 nm. Adapted from reference [7], ©Simon Jademyr 2016.

2

Theory

2.1 Crystalline Nanocellulose

CNC is a derivative of cellulose and is obtained through sulfuric acid hydrolysis of lignocellulose, specifically microcrystalline cellulose (MCC), the crystalline regions of the cellulose fiber. *Figure* 2.1 shows the chemical structure of the repeating cellobiose unit of cellulose and its unit cell. During sulfuric acid hydrolysis, anionic sulfate half-ester groups replaces some hydroxyl groups at the surface, resulting in sulfated CNC [13]. The dimensions are generally found to be a length of 200 nm, a width of 10-20 nm, and a thickness of a few nm [14], which qualifies it as a nanomaterial as at least one dimension is in the range of 1-100 nm [15].

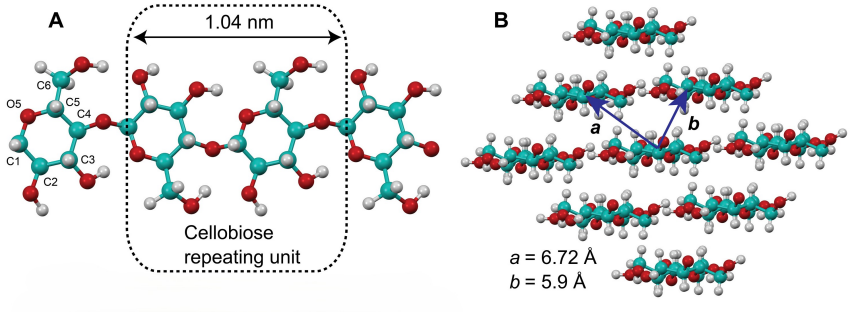

Figure 2.1: a) Chemical structure of cellulose and the repeating unit cellobiose are illustrated. b) Representation of unit cell of cellulose Iα structure. Carbon, oxygen, and hydrogen atoms are represented by cyan, red, and white colors, respectively. Adapted from reference [16], ©Science Advances 2022.

The cross section of crystallites of CNC have approximate hexagonal geometry, as exemplified in *Figure 2.2*. Due to the nature of the packing of the repeating units of cellulose, the accessible side chains and their angles are different on each of the six faces.

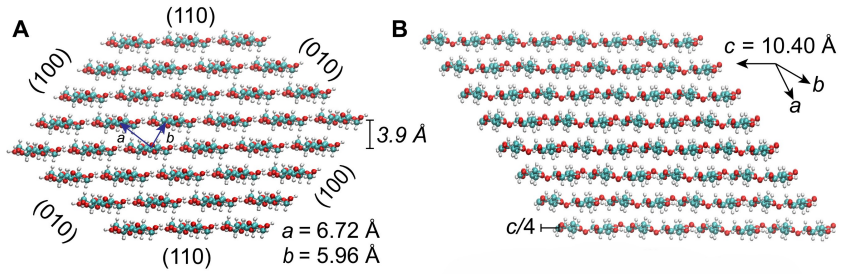

Figure 2.2: a) A 36-chain microfibril model of cellulose Iα crystalline structure with a hexagonal shape generated with Cellulose Builder software, displaying different crystallographic planes. b) A longitudinal view of parallel sheets of cellulose chains. Each molecular sheet is shifted along the c axis by + c/4. Adapted from reference [16], ©Science Advances 2022.

The schematic in *Figure* 2.3 illustrates a CNC crystallite and its exposed surface sulfates, as well as their non-symmetrical orientation. Heise et al. have found the spatial distribution of functional groups of CNC to affect the crystallites' affinity for self-assembly and adhesive interactions with non-cellulosic interfaces [17]. Studies focusing on surface sulfate groups corroborate the fact, linking them to thermal stability, dispersion, and aggregation of the crystallites among other things [18].

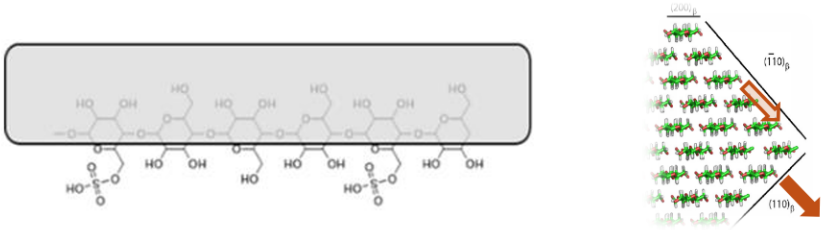

Figure 2.3: Orientation of sulfate groups on the CNC surface. To the right the crystal structure of cellulose is displayed, highlighting two of the lattice planes. Adapted from reference [8], ©Elin Horn 2024.

In aqueous suspension, CNC crystallites self-assemble into liquid crystal phases [19]. As such a suspension is dehydrated during the manufacture of film, the crystallites aggregate into layers that are directionally offset from each other, forming helical structures of varying pitch and height, i.e. a cholesteric - also known as chiral nematic - structure. The bulk material thus changes from an homogeneous, isotropic liquid, to an anisotropic solid. A schematic overview of this phenomenon and potential resulting structure is presented in *Figure 2.4*, with *Figure* 2.5 detailing the differences between various aggregate structures or phases that are common among liquid crystals.

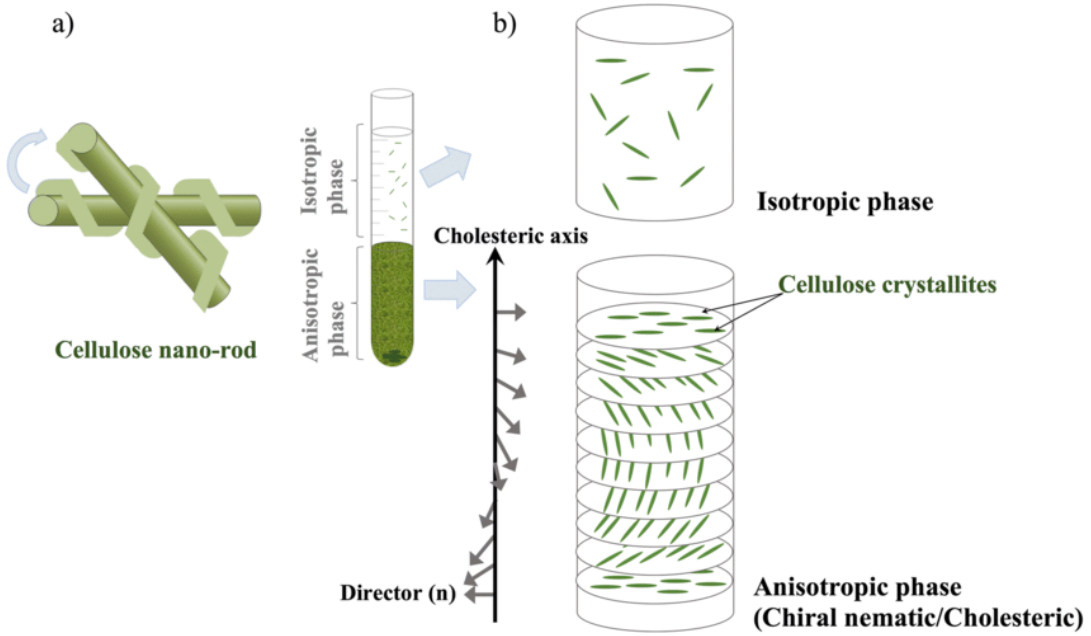

Figure 2.4: A schematic of the isotropic and anisotropic phases of CNC suspensions, and the ordering of crystallites into a chiral nematic structure. a) Helical twists of individual crystallites. b) Helical twists of layers of semi-parallell crystallites, i.e. cholesteric Adapted from reference [20], ©Food and Bioprocess Technology 2020.

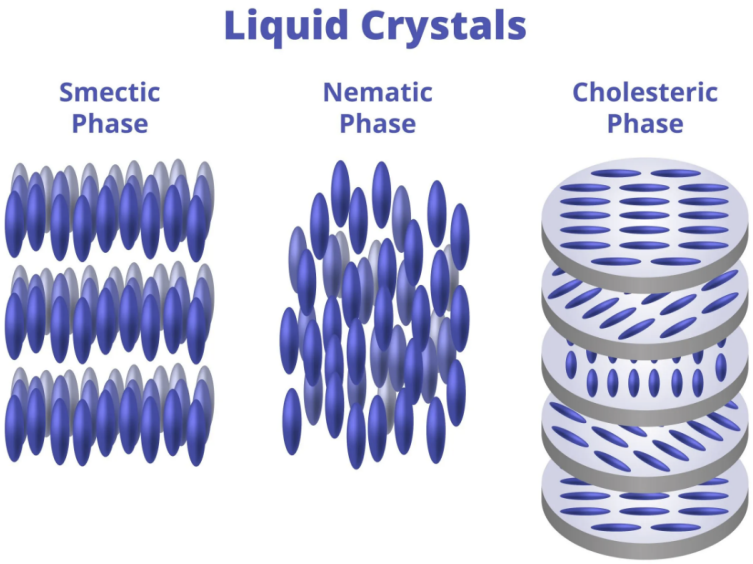

Figure 2.5: Schematic illustration of the smectic, nematic, and cholesteric phases of liquid crystals. Adapted from reference [21], ©Smart Glass World 2026.

Liquid crystals can be categorized by which parameter mainly trigger phase changes: thermotropic liquid crystals, which experience phase changes due to temperature; lyotropic, which do the same due to the density; and metallotropic, which respond

to low-temperature inorganic, metal-based compositions [21]. CNC form cholesteric lyotropic liquid crystals in aqueous suspensions, but may exhibit thermotropic behaviour in other media [22]. *Figure* 2.6 illustrate phase changes for thermotropic liquid crystals when increasing the temperature. For lyotropic crystals the phase changes effectively occur in the inverse order when solute concentration is increased, getting more crystalline with higher concentration, but their phases are often also temperature dependent (thermotropic) [23].

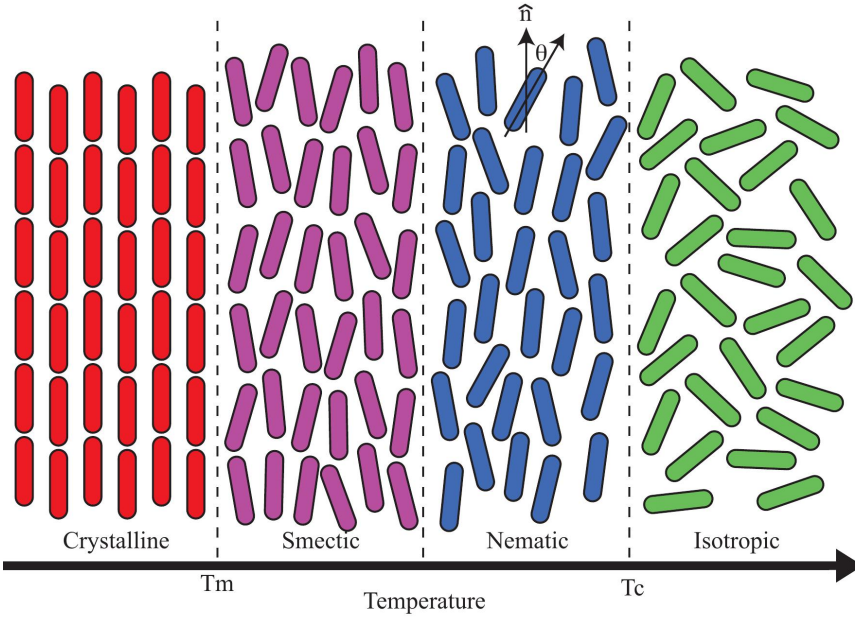

Figure 2.6: Schematic illustration of phase changes for *thermotropic* liquid crystals. Adapted from reference [24], ©Anna Fox 2009.

2.2 Cyanine Dyes

Cyanine dyes are commonly used to label a variety of biomolecules, such as peptides and proteins, antibodies, and nucleic acid probes, for use in fluorescence detection techniques [25]. They are characterized by their polymethine (i.e. carbon) chain, linking two nitrogen atoms independently part of aromatic rings, so called heteroaromatic moiteys, such as pyrrole, thiazole, or indole [25]. Cyanines are either: 1), open or closed-chained, i.e. symmetric; or 2), so called hemicyanines, i.e. asymmetric with one nitrogen atom being non-cyclic instead of the standard aromatic [25, 26].

2.2.1 Thiazole Orange

Thiazole orange (TO) (CAS number 107091-89-4) is an asymmetric anthocyanine dye, with a molecular weight of 476.61 $g \cdot mol^{-1}$ and a chemical structure that importantly consists of two aromatic systems connected by a methine bridge, as seen in *Figure* 2.7. The dye fluoresces when the two rings are coplanar, and is thus overall only slightly fluorescent when in solution due to the free rotation its methine bridge allows [27, 28]. When its aromatic system is rotationally restricted, however,

a significant relative increase in fluoerscence can be observed [27, 28]. This effectively conditional fluorescence, which gives TO its common use in staining nucleic acids (as it fluoresces when rotionally restricted by intercalating between their bases), also makes the dye a fitting indicator of aggregation and crystallite interaction in CNC suspensions when conjugated to its surface sulfate groups. A commercial TO product has been found to have excitation peaks at 510, 488, and 470 nm, and a peak emission at 527 nm [29].

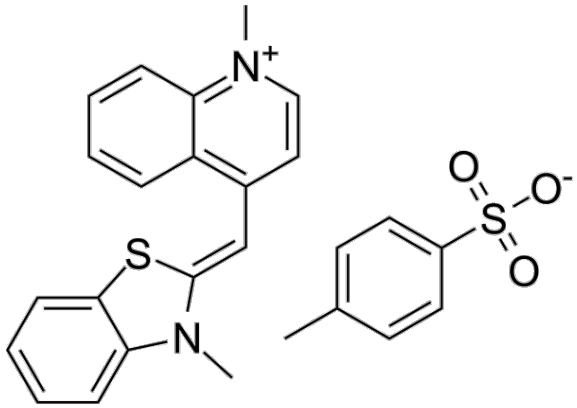

Figure 2.7: The chemical structure of Thiazole Orange. Adapted from reference[29], ©MedChemExpress 2026.

2.3 Enzymatic assay substrate

Due to the complexity of working with suspensions of CNC, a model substrate to use in place of it is preferential during enzymatic assays. The potassium salt of p-NPS was chosen due to its successful use in previous experiments by Horn [8]. It is a small, simple molecule with an accessible sulfate group, bound to the para-position of a nitrophenyl group with a sulfate ester bond. A common counterion is K^+. It's properties makes it a favorable substrate for assaying sulfatase activity [30]. The chemical structure is displayed in *Figure* 2.8.

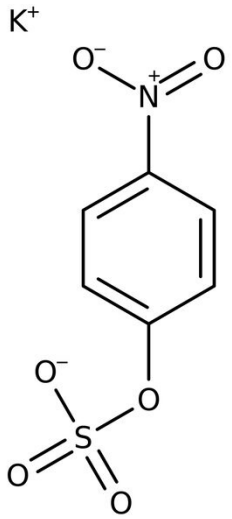

Figure 2.8: The chemical structure of p-NPS. Adapted from reference [31], ©Thermo Scientific Chemicals 2026.

2.4 Sulfatases

Sulfatases, or sulfuric ester hydrolases, are a class of enzymes (i.e. protein) that catalyze the hydrolysis of sulfate ester bonds, so called desulfation, giving them the enzyme commission (EC) number 3.1.6. as classified by the international union of biochemistry and molecular biology (IUBMB) [32]. EC numbers are are classification scheme for enzymes based on the reaction they catalyze [33]. Other common methods to hydrolyze sulfate ester bonds are to change pH, such as with strong acids, or to increase the temperature to enable autohydrolysis, i.e. heat-induced hydrolysis. Unlike these methods, enzymatic catalysis is possible at both physiological pH and temperature (or even at room temperature) simultaneously, and thus potentially more appropriate for biological and other sensitive substrates. There is an added benefit of it being safer, for the lack of corrosive acids, and more energy efficient, for the lack of heating.

The IUBMB divides sulfatases into three classifications based on catalytic mechanism and co-factors: type I, with 3-oxo-L-alanine as the key catalytic residue; type II, which are non-heme iron-dependent dioxygenases; and type III, whose catalytic domain forms a $metallo-\beta-lactamase$ fold and binds two zinc ions as cofactors [32]. The SulfAtlas database, on the other hand, divides the class of enzymes into four families based on (genetic) sequence homology: the S1 family, or formylglycine-dependent sulfatases; the S2 family, being alkylsulfodioxygenases; the S3 family, which encompass the alkylsulfohydrolases; and the S4 family, constituted by the arylsulfohydrolases [34]. *Figure* 2.9 illustrates the two mechanisms of sulfate ester hydrolysis performed by sulfatases.

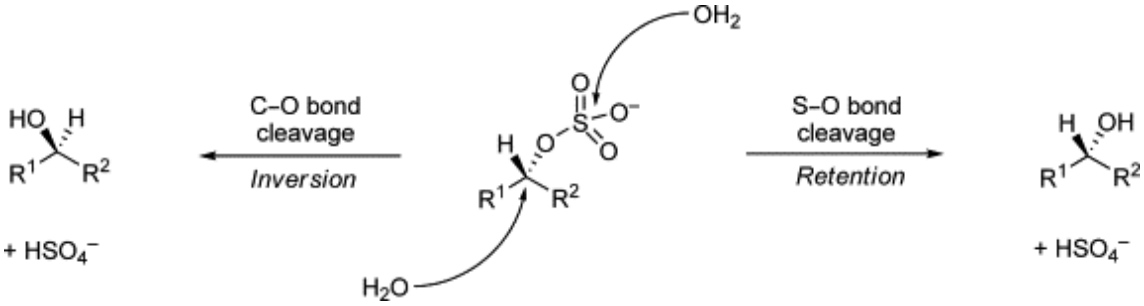

Figure 2.9: The potential stereochemical outcomes at the chiral secondary carbon atom of a substrate in the hydrolysis of sulfate esters catalyzed by sulfatases. Adapted from reference [35], ©Methods in Enzymology 2010.

Enzymatic activity may be stopped through several methods, commonly by denaturation through heat or drastic pH changes - both generally applicable - but also through a variety of inhibitors more specific to each enzyme. Thermal denaturation risks unintended autohydrolysis of sulfate ester bonds, as previously described, making it unsuitable for inhibition of sulfatase if the goal is selective desulfatation of CNC. Similar concerns arise with the use of sudden and drastic pH changes, so called "pH shock". An alternative approach that does not affect the substrate noticeably is to use inhibitors or chemicals that target the enzymes' catalytic domains directly, such as chelators irreversibly binding to metal co-factors in type I sulfatases.

2.4.1 Sulfatase from Helix pomatia

In this report, sulfatase from *Helix pomatia* (colloquially called roman snail) specifically refers to the product S2696-5KU from Sigma-Aldrich, with CAS number 9016-17-5 [36]. It has the EC number 3.1.6.1 [36], making it a type I sulfatase according to IUBMB specifications [32]. It has recommended storage temperature of -20C, and an approximate molecular weight of 85 kDa [36]. and a is specified by the manufacturer to have a catalytic activity (for desulfation) of 10 000 units per g solid [36]. One unit will hydrolyze 1.0 µmol of P-Nitrocatechol Sulfate per hour at pH 5.0 at 37 °C [36]. Some studies suggest the presence of at least three different sulfatases in *Helix pomatia* [37].

2.4.2 Sulfatase from Pseudomonas aeruginosa

Pseudomonas aeruginosa is a Gram-negative bacterium capable of both aerobic and anaerobic growth, that is readily found in most human-impacted environments, and capable of utilizing over a 100 organic molecules as carbon and energy sources. It grows well at 37 °C but survives in the temperature range of 4 to 42 ℃, and is known for its ability to break down polycyclic aromatic hydrocarbons [38].
Sulfatase from *P. aeruginosa*, or PAS, is a globular molecule with external dimensions of 55 x 55 x 50 Å, determined by Boltes et al. (2001) with a resolution of 1.3 Å [1]. Its primary role is to supply sulfur for bacterial growth by the release of inorganic sulfate from sulfate esters [1]. In this project, a product from Sigma-Aldrich derived from the PAO1 strain of *P. aeruginosa* was used: SAE0213 [39]. It has a

recommended storage temperature of -25 to −10 °C, a retest period (minimun shelf life) of 2 years, and with a specified catalytic activity of 2000 units per mL [39]. One unit will hydrolyze 1.0 µmol of p-nitrocatechol sulfate per hour at pH 8.0, at 37 °C [39]. Being a arylsulfatase, it is a type I sulfatase [32].

2.5 Hypothesis of selective desulfation

The hypothesis, first proposed by professor Westman and later investigated by Horn [8], is in this report referred to as the *hypothesis of selective desulfation*. It is based on the non-symmetrical distribution of surface sulfates between the six different faces of CNC crystals, in and of itself a result of them being crystals (i.e. with uniform internal orientation), with the angle and distance of protrusion of sulfate groups from each radial plane being different, as previously illustrated by figures 2.2 and 2.3. Thus, the hypothesis states, also the accessibility to big molecules such as desulfatases ought to be different on each of the planes, which by careful choice of enzyme enables a selective rather than randomized desulfation pattern, as illustrated by *Figure 2.10*.

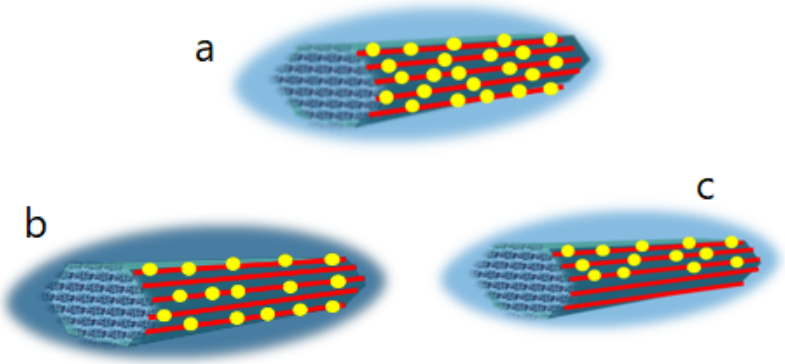

Figure 2.10: (a) shows the hexagonal cross section of CNC, where the yellow dots represents sulfate groups on the surface. (b) represents the CNC surface after chemical hydrolysis, resulting in a randomized desulfation pattern. (c) shows a selective desulfation pattern and how the CNC surface potentially could look after enzymatic methods have been applied. Adapted from reference [8], ©Elin Horn 2024.

2.6 Spectrophotometry

Spectrophotometry is an experimental method to measure the absorption of light by a chemical substance as a beam of light passes through the sample solution [40]. The basic principle is that each compound absorbs or transmits over a certain range of wavelengths, and that it is characteristic (though not necessarily unique) for each compound [40]. This measurement is commonly used to quantify the amount of a known chemical substance in a given solution [40]. UV-Vis spectrophotometers uses light over the ultraviolet range and visible range, i.e. between 185 - 400 nm and 400

- 700 nm respectively [40].

The absorbance is calculated automatically by the instrument according to lambert-beers law in equation 2.1.

$$A = \varepsilon lc \tag{2.1}$$

Rayleigh scattering is a known potential source of false positive fluorescent signals in fluorescence spectrophotometry, particularly of scattering samples such as powders, crystals, and colloidal suspensions [41]. This type of scattering artifact is characterized by narrow, high intensity peaks at the excitation wavelength, i.e. first order diffraction, and integer multiples of the excitation wavelength, second and third order diffraction etc., and is illustrated in *Figure* 2.11 [41].

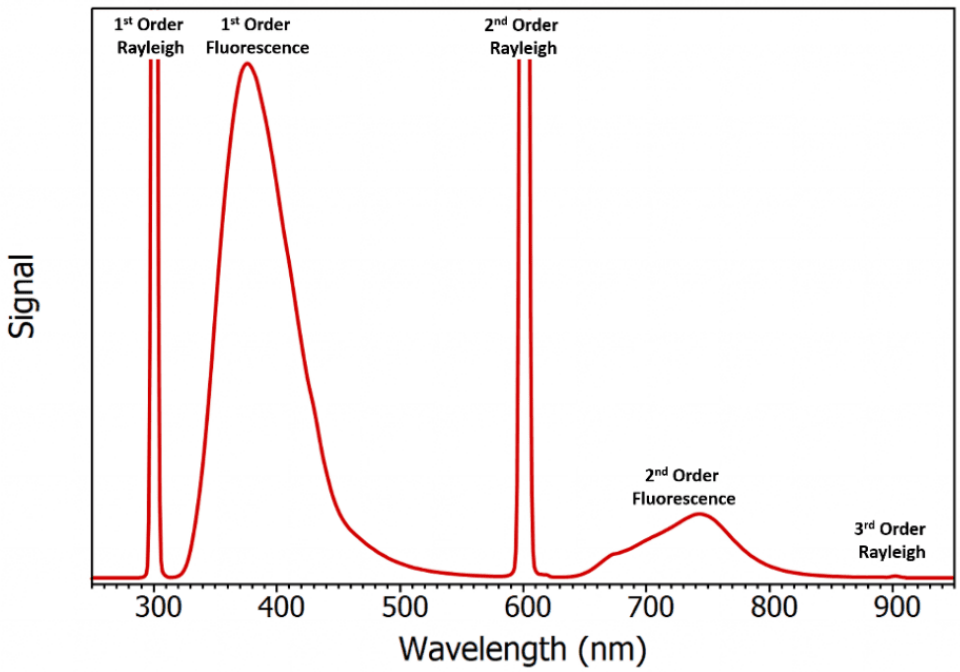

Figure 2.11: Example of second order artefacts in a broad fluorescence emission spectrum of a solution of 2-aminopyridine mixed with Ludox excited at 300 nm. Adapted from reference [41], ©Edinburgh Instruments 2021.

Another complicating factor is the inner filter effect. It occurs when the optical density (concentration) of the sample is high, and results in decreased fluorescent intensity non-linear to concentration, either through attenuation (absorbtion) of excitation light before it reaches the center of the cuvette where measurments are taken, called the primary effect, or through reabsorbtion of the emitted fluorescence before exiting the cuvette, called the secondary effect [42].

3
Methodology

3.1 Chemicals

Table 3.1 lists the name, and formula where applicable, of each chemical used in the project.

Table 3.1: Chemicals list

Chemical Name	**Formula**
Sulfatase from Helix pomatia (S2696-5KU)*	N/A
Arylsulfatase, Enhanced, Recombinant (SAE0213-10KU)**	N/A
Quinaldinium Tosylate	$C_{17}H_{17}NO_3S$
N-methyl thiomethylbenzothiazole	$C_9H_9NS_2$
Dichloromethane	CH_2Cl_2
Triethylamine	$C_6H_{15}N$
Methanol	CH_3OH
Sulfuric acid	H_2SO_4
Microcrystalline cellulose (MCC)	N/A
Tris(hydroxymethyl)aminomethane (Tris base)	$C_4H_{11}NO_3$
Hydrochloric acid	HCl
Sodium acetate	NaOAc
Acetic acid	HOAc
Disodium phosphate (DSP)	Na_2HPO_4
Sodium hydroxide	NaOH
Carbon disulfide	CS_2
N,N-dimethylaniline	$C_8H_{11}N$
Chlorosulfonic acid	HSO_3Cl
p-Nitrophenol	$C_6H_5NO_3$
Potassium hydroxide	KOH
Tetrahydrofuran (THF)	C_4H_8O
Sulfur trioxide pyridine complex	$C_5H_5NSO_3$
Potassium tert-butoxide (t-BuOK)	C_4H_9KO
Sodium chloride	NaCl
Azitidinium (AZ) salts	N/A

*Product from Sigma-Aldrich [36]
**Product from Sigma-Aldrich [39]

3.2 Preparation of CNC suspension

The "sulfated CNC" suspension were synthesized by sulfuric acid hydrolysis of cellulosic material according to previous studies [7, 43]. A round-bottom flask containing 64 w/w% H_2SO_4 was lowered into a heating bath set to 45 °C and was left to stabilize in temperature for one hour. Hydrolysis was initiated with addition of 40 g MCC to the round-bottom flask, and stopped after two hours by pouring the acid-cellulose mixture into 7 L DI water. The solution was centrifuged for 15 min at 4300 rpm and the excess water decanted, while dialysis membranes with a molecular weight cut-off of 12-14000 g/mol were hydrated. Membranes were filled, closed, and left in large plastic containers filled with DI water. The water was exchanged periodically over several days until conductivity measured below 5 µS (microsiemens).

The dry weight of the CNC suspension was determined through total solids determination. Three watch-glasses were autoclaved, dryed overnight in an oven at 100 °C, and measured thrice on a scale to 4 decimal accuracy, after which approximately 5 g of CNC suspension - enough to cover the bottom of the glasses evenly - were added to each using glass pipettes while still on the scales after taring. The glasses were then placed back in the oven overnight at the same temperature to ensure full evaporation of the liquid content, and each weighed thrice again. Analytical and technical triplicates were used to improve the accuracy of the weight measurements. The technical replicate average watchglass weights, $\bar{m}_{watchglass}$ (g), were used to calculate the dry weight, DW (w/w%), separately for each of the analytical replicates according to equation 3.1, where $m_{CNC(aq)}$ is the weight of added CNC suspension, and $\bar{m}_{watchglass+CNC}$ is the technical replicate average weight of the combined watchglass and suspension after dehydration. In turn, the average of the three calculated dry weights, i.e. the analytical replicates, was calculated and considered the true value. All weights were tabulated at the moment of measurement.

$$DW_{CNC} = \bar{m}_{watchglass} + m_{CNC(aq)} - \bar{m}_{watchglass+CNC} \tag{3.1}$$

The sulfate content of the suspension, in micromole sulfate per g of CNC, was determined by triplicate potentiometric titrations according to established standard operating procedure (SOP) at the department of chemistry and chemical engineering at Chalmers. See *Appendix B*, section B.2 for details.

As for the "non-sulfated" batch of CNC, an August 2025 batch, designated *Antibacterial Screening Suspension 6-N-6*, was used. Originally made for a previous and unrelated study, the batch was considered functionally devoid of surface sulfate groups due to blocking by added azitidinium salt(s), regardless of the suspension originally having had a sulfate content of 252 µmol g^{-1}. Excluding this addition of azitidinium salt(s) at the end, the batch was synthesized according to the same SOP used for the "sulfated batch".

Both batches were diluted in DI water to 0.75, 0.1, and 0.05 wt%.

3.2.1 Preparation of tris buffer

For 100 ml 0.5 M Tris(hydroxymethyl)aminomethane (Tris) buffer, 6.057 ± 0.01 g Tris base was weighed, then solved in approximately 80 ml DI water using magnetic stirrers. pH was adjusted to within the 7.1-7.4 range by addition of concentrated hydrochloric acid, HCl (aq., 37%), using a pipette. DI water was added until total volume was 100 ml, and final pH determined by pH-meter. Three sources of Tris was used, but not distinguished, except when explicitly stated during independent testing for contamination.

3.2.2 Preparation of sodium acetate buffer

For 100 ml 0.5 M sodium acetate (NaOAc) buffer,4.102 ± 0.01 g NaOAc was weighed, then solved in approximately 80 ml DI water using magnetic stirrers. pH was adjusted to within the 5-6 range by addition of concentrated acetic acid, HOAc (aq., 98%), using a pipette. DI water was added until total volume was 100 ml, and final pH determined by pH-meter.

3.2.3 Preparation of disodium phosphate buffer

An aqueous solution of disodium phosphate (DSP) was chosen as the buffer for spectrophotometric experiments due to its successful use in a previous and related study by Jademyr, with Karlsson et al. having found the following parameters appropriate: a pH of 7 (adjusted with HCl or NaOH depending on initial pH), a molarity of 5 mM, and a temperature of 25 °C [7, 10].

For 200 ml 5 mM disodium phosphate (DSP) buffer, 0.142 ± 0.01 g DSP was weighed, then solved in approximately 160 ml DI water using magnetic stirrers. pH was adjusted to 7 ± 0.1 by addition via pipette of concentrated hydrochloric acid, HCl (aq., 37%), or sodium hydroxide, NaOH, depending on preliminary pH measurement. DI water was added until total volume was 200 ml, and final pH determined by pH-meter.

3.2.4 Synthesis of Thiazole Orange

Quinaldinium Tosylate (329 mg, 1 mmol) and N-methyl thiomethylbenzothiazole (367 mg, 1 mmol) was dispered in Dichloromethane (5 ml) and Triethylamine (150 mg, 1.5 mmol) was added. The reaction immediately turned red upon addition of Triethylamine. The reaction was stirred over night, the solvent was evaporated and the residue was recrystallized from a water:MeOH (7:3) mixture to obtain the product.

3.2.5 Synthesis of para-Nitrophenyl sulfate

Two synthesis pathways were utilized in the synthezis of the potassium salt form of para-nitrophenyl sulfate (p-NPS) (CAS number 6217-68-1): the method used by Horn [8], for the purposes of this report called the "standard method", and a method

established in the 2017 patent by inventor Kenichi Mori [44], for the purposes of this report called the "alternate method". The chemicals, their name, formula, and source where applicable, are listed in 3.1.

3.2.5.1 Standard Method

To 5 ml carbon disulfide N,N-dimethylaniline (4.7 ml, 37 mmol) and chlorosulfonic acid (0.9 ml, 14 mmol) was added. The suspension was stirred for 5 min (RT) and p-Nitrophenol (1.4 g, 10 mmol) was slowly added. The resulting slurry was heated (50 °C) and stirred for 90 min. Thereafter, the temperature was lowered (25 °C) and the reaction was stirred overnight. The suspension was cooled on ice. 20 ml of 4 M KOH was carefully added and the stirring was continued for another 30 min. Afterwards, the slurry was filtered and warm water was added for recrystallization. The resulting crystals was characterised using NMR. 1H NMR (600 MHz, DMSOd6): δ 7.40 (d, J=9.24 Hz, 2H), 8.20 (d, J=9.24 Hz, 2H). 13C NMR (600 MHz, DMSO-d6): δ 125.6 (2xC) 120.1 (2xC).

3.2.5.2 Alternate Method

Substitute the 100 mL four-necked flask with Ar, add 50 mL of THF, 2.21 g (15.9 mmol; 318 mM) of p-nitrophenol, 3.13 g (19.7 mmol; 394 mM) of sulfur trioxide pyridine complex and add 2 And stirred for a while (sulfation step). Further, 1.78 g (15.9 mmol; 318 mM) of t-BuOK was added and the mixture was stirred at 25 ° C for 2 hours, whereupon precipitation of crystals was observed (neutralization step). The formed slurry was filtered, and the crystals were washed with 10 mL of THF. The obtained wet crystals were dried under reduced pressure at 40 ° C for 12 hours to obtain 4.32 g of dry crystals.

3.3 Spectroscopy

3.3.1 UV-Vis Absorption Spectroscopy

Spectrophotometry in the UV to Vis range, specifically between 200 nm and 500 nm, was performed on an Agilent Technologies Cary 3500 Multicell UV-Vis Spectrophotometer to assay enzymatic activity, and to study aggregation response of CNC and TO [45].

3.3.2 Fluorescence Spectroscopy

Emission spectroscopy in the 300-700 nm and 300-800 nm range was performed to study the aggregation response of CNC and TO. Excitation wavelength λ_{ex} was set to either 380 nm or 500 nm, and excitation and emission slit widths of 2.5 nm.

3.3.3 Nuclear Magnetic Resonance Spectroscopy

NMR spectroscopy was used to validate the purity and successful synthesis of TO and p-NPS.

4

Results

4.1 Validation of Thiazole Orange synthesis by NMR spectroscopy

Excerpt of data from NMR spectroscopy of TO is presented in *Figure* 4.1. *Subfigure* 4.1a shows the spectra in the 2.0-9.0 ppm range, with peaks highlighted. There is a 1H singlet at 6.80 ppm, and 2H singlets at 4.10, 3.90, and 2.34 ppm. *Subfigure* 4.1b shows the spectra in the 6.7-8.8 ppm range, with peaks highlighted. There is a 1H singlet at 6.82 (also visible in 4.1a), 1H doublets at 7.83, 8.32, and 8.61 ppm, a 2H doublet at 7.23, 2H multiplets at 7.36, 7.54, and 7.94 ppm, and a 3H multiplet at 7.73 ppm. See *Appendix* A.1.3 for all spectra.

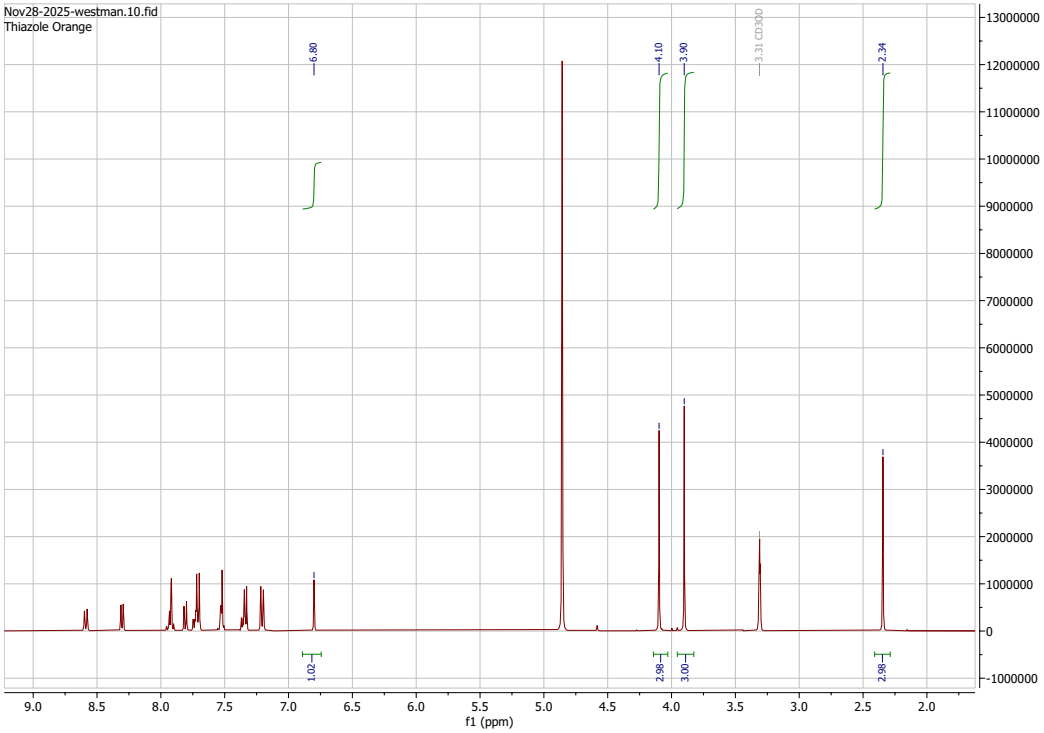

(a) NMR spectra of TO in the range of 2.0-9.0 ppm.

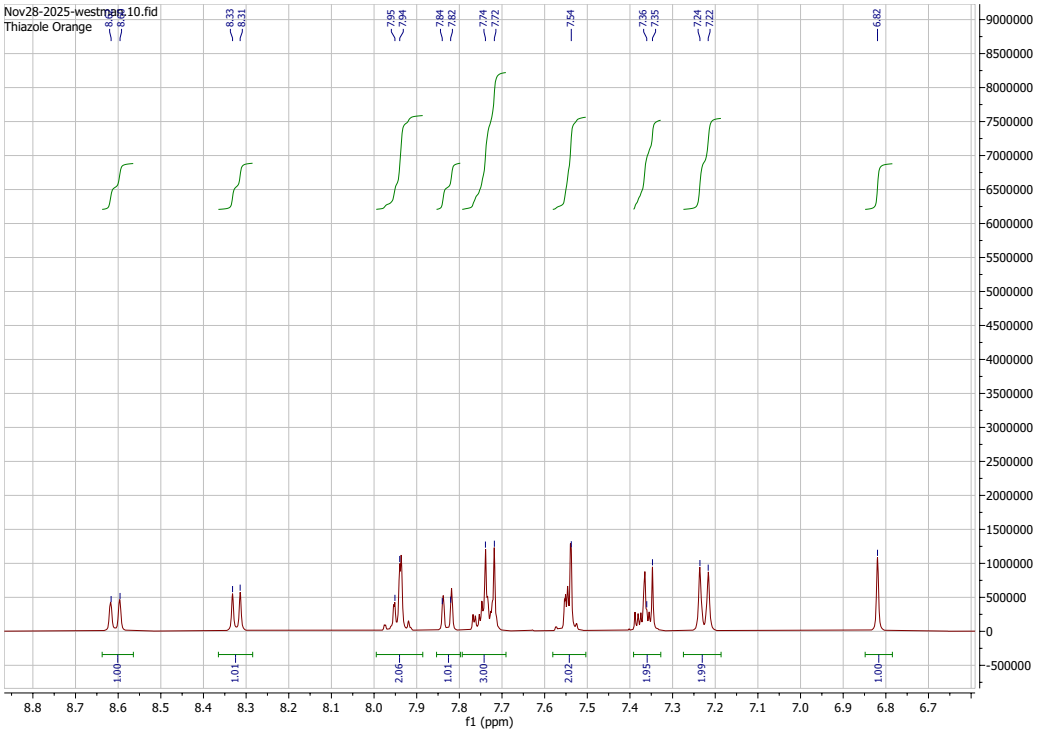

(b) NMR spectra of TO in the range of 6.7-8.8 ppm.

Figure 4.1: NMR spectra of TO.

4.2 Validation of p-NPS synthesis by NMR spectroscopy

Excerpt of data from NMR spectroscopy of p-NPS synthesized by the standard method is presented in *Figure* 4.2. For the full set of NMR-spectra, see *Appendix* A.1.1.

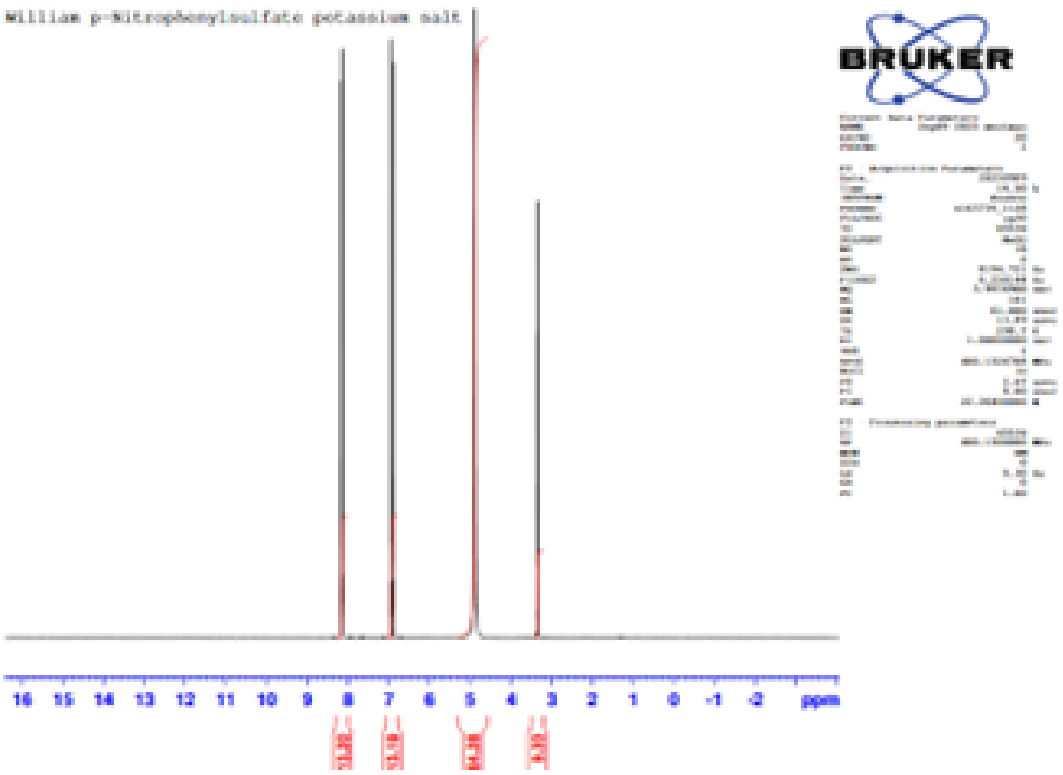

(a) NMR spectra of p-NPS (std.) in the (-2)-16 ppm range.

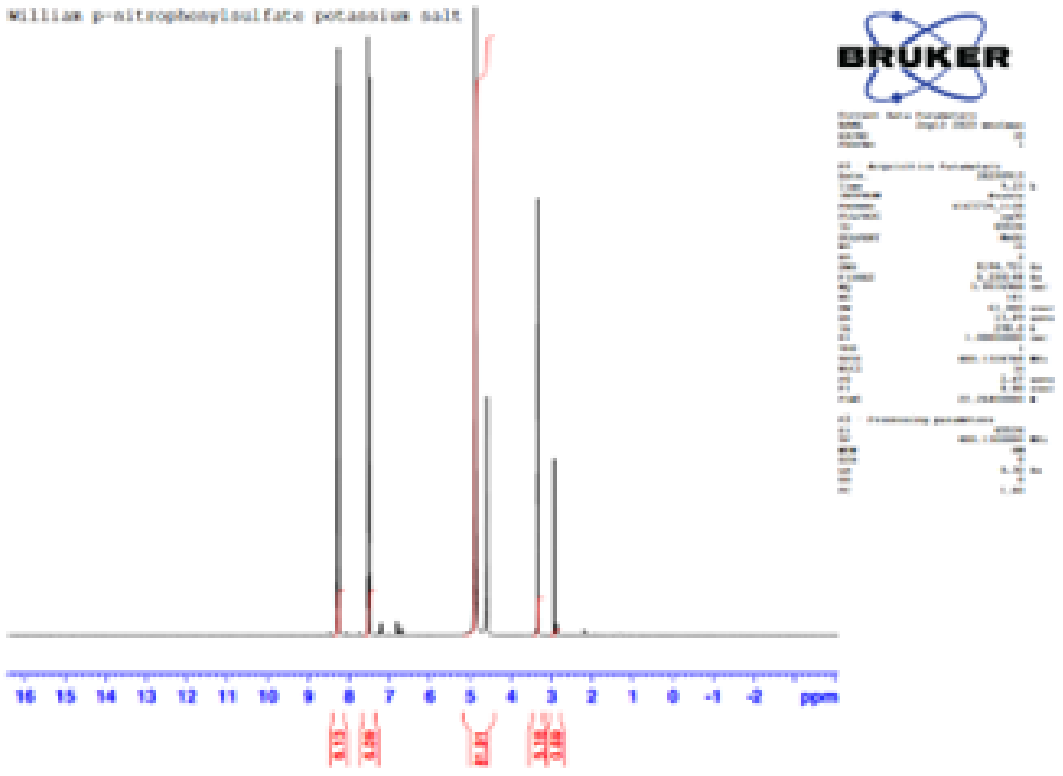

(b) NMR spectra of p-NPS (std.) in the (-2)-16 ppm range.

Figure 4.2: NMR spectra of p-NPS synthesized by the "standard method".

Excerpt of data from NMR spectroscopy of p-NPS synthesized by the alterative method is presented in *Figure* 4.3. *Subfigure* 4.3a shows the spectra in the (-4)-16 ppm range. *Subfigure* 4.3b shows the spectra in the 4.5-8.5 ppm range, with some peaks highlighted. There are 5H multiplets at 7.42 and 8.2 ppm. For all spectra, see *Appendix* A.1.2.

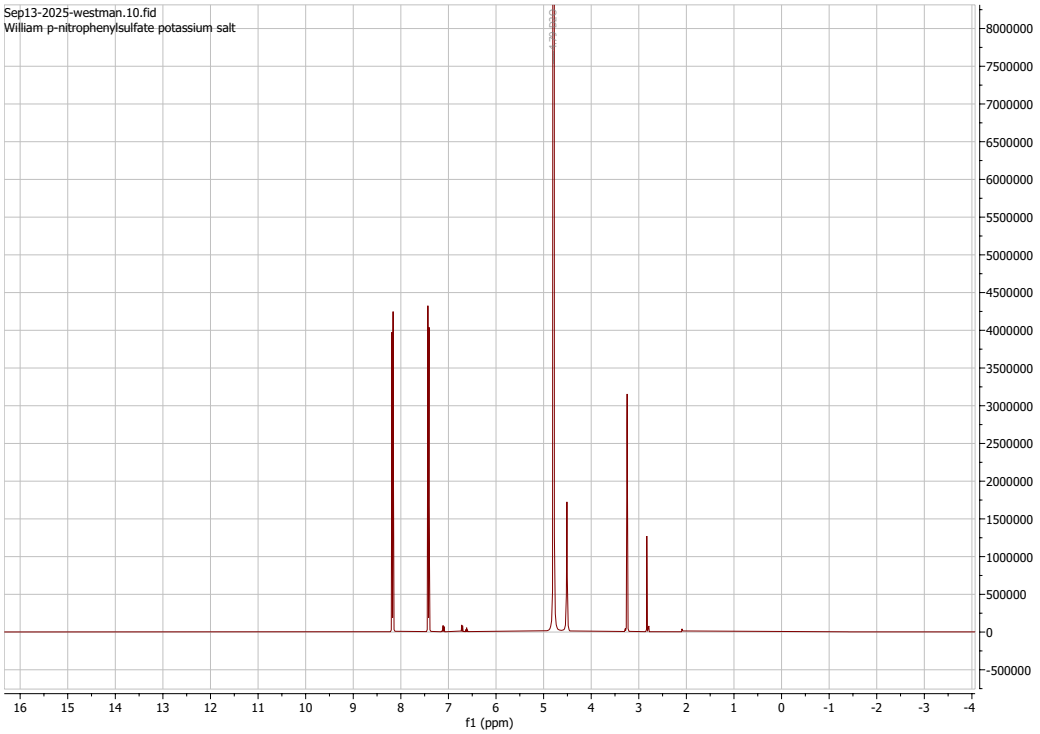

(a) NMR spectra of p-NPS in the (-4)-16 ppm range.

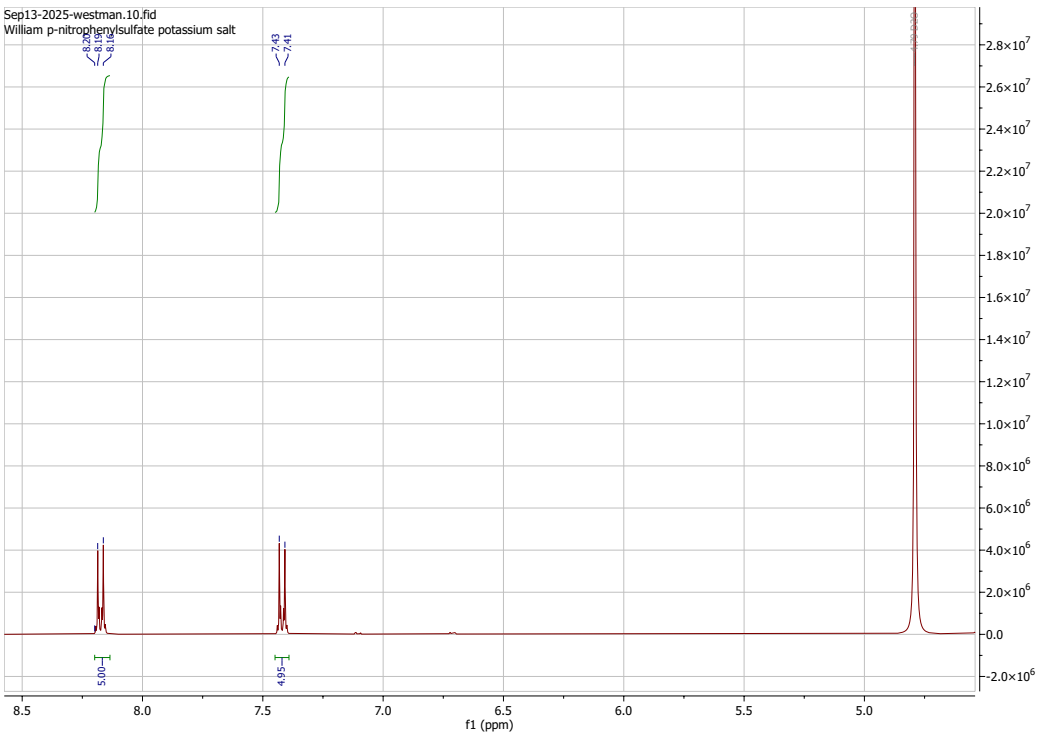

(b) NMR spectra of p-NPS in the (-4)-16 ppm range.

Figure 4.3: NMR spectra of p-NPS synthesized by the "alternate method".

4.3 Absorbance spectra of buffer solutions

Figure 4.4 shows the absorbance of 0.5 M Tris buffer in the UV-Vis range between 200 and 500 nm, at 37 °C. The absorbance was scanned on October 9th 2025.

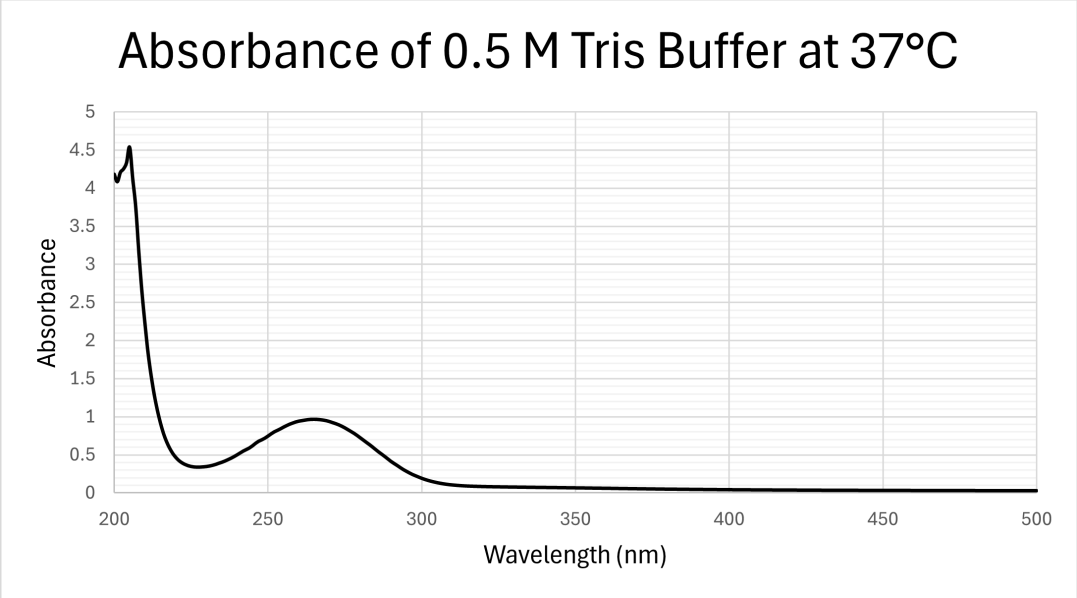

Figure 4.4: UV-Vis absorbance spectrum of 0.5 M Tris buffer at 37 °C.

Three sources of Tris base were spectrographically tested to rule out possible source contamination as a cause of the unexpectedly low sulfatase activity detailed in section 4.12. *Figure* 4.5 show the average absorbance of technical triplicates, ±1 standard deviation, of 412.75 mM aqeuous solutions of each source: arbitrarily denoted "l", "18", and "K6".

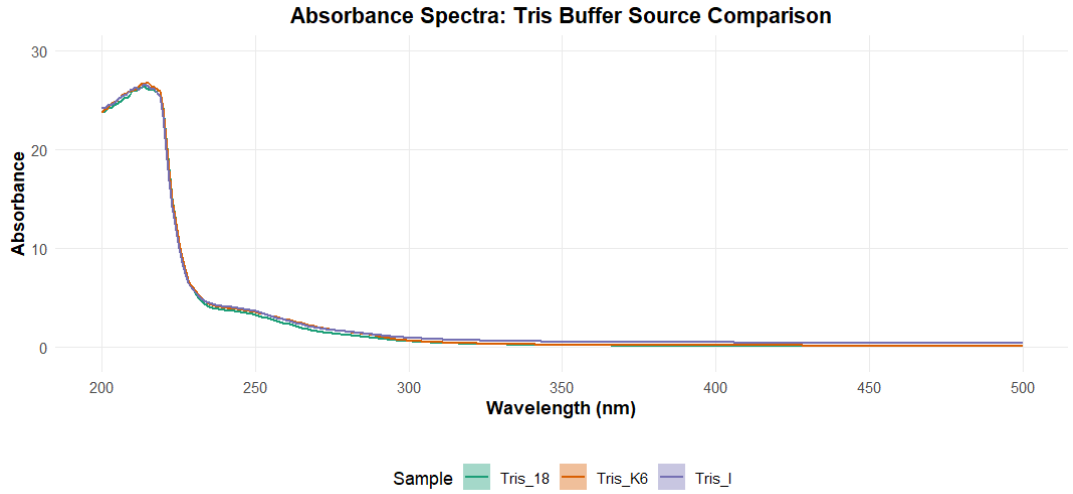

Figure 4.5: Average absorbance of technical triplicates of tris buffer, ±1 standard deviation, prepared from three separate sources of tris base, here arbitrarily denoted "l", "18", and "K6". 0.1 g tris base were solved in DI, giving the corresponding concentration of 412.75 mM.

Figure 4.6 shows the average absorbance of technical triplicates, ±1 standard deviation, of sodium acetate buffer at RT.

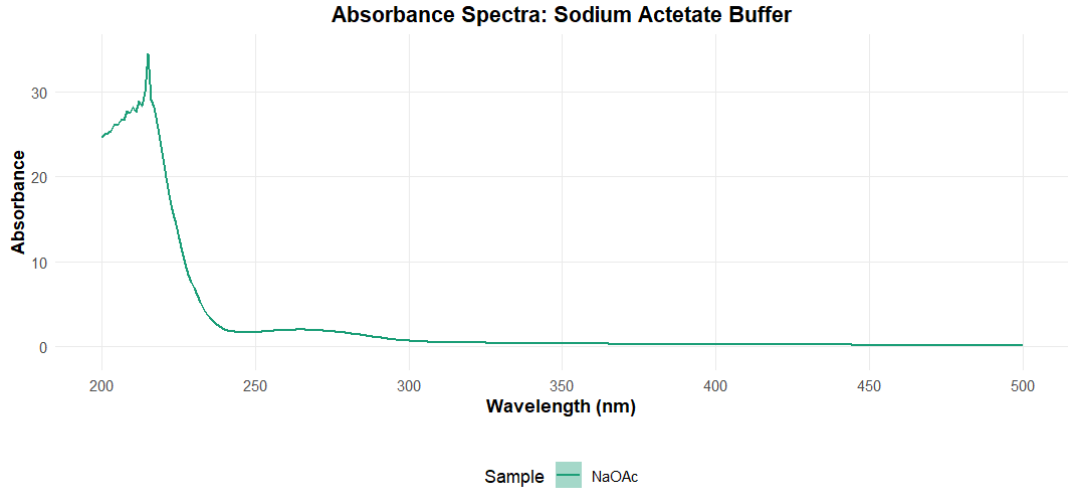

Figure 4.6: Average absorbance of technical triplicates of NaOAc buffer, ±1 standard deviation.

Figure 4.7 shows the average absorbance of technical triplicates, ±1 standard deviation, of 5 mM DSP buffer at RT.

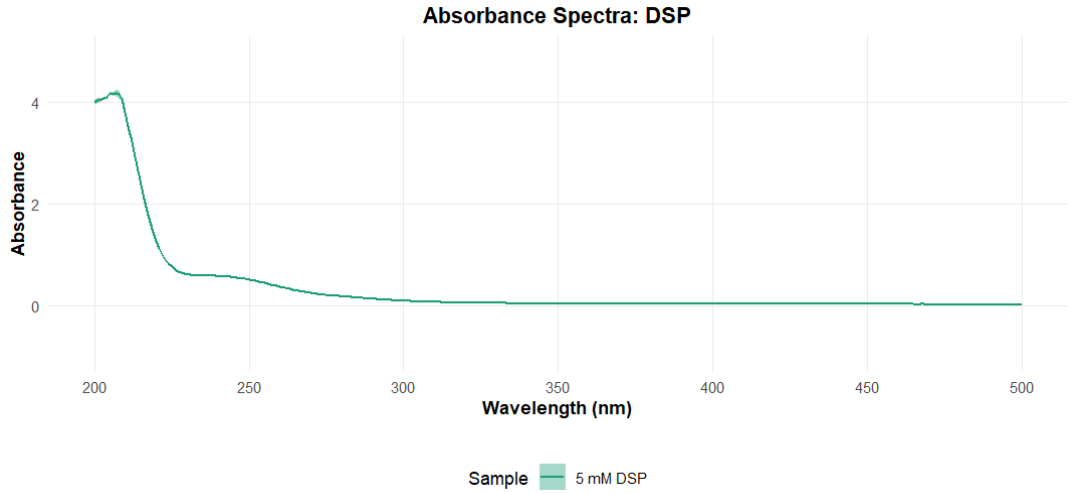

Figure 4.7: Average absorbance of technical triplicates of 5 mM DSP buffer, ±1 standard deviation.

4.4 Absorbance spectra for TO

Figures 4.8 and 4.9 show the average absorbance of technical triplicates, ±1 standard deviation, of 17.5, 35, and 70 µM TO solved in 5 mM DSP in the UV-Vis spectra between 200 and 700 nm, on December 1st and 12th, respectively.

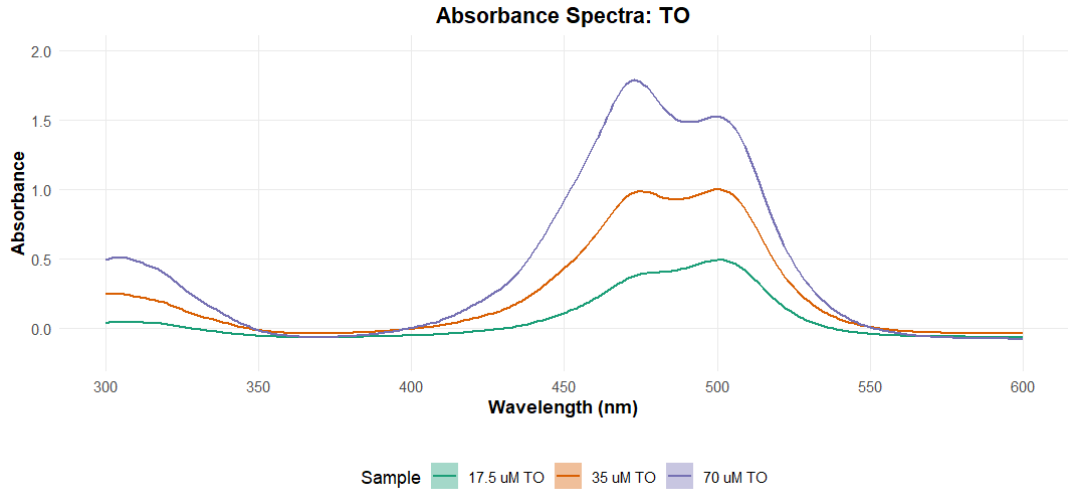

Figure 4.8: Absorbance spectra of TO solved in 5 mM DSP to concentrations of 17.5, 35, and 70 µM, in the UV-Vis range between 200 and 700 nm. the experiment was performed on December 1st 2025.

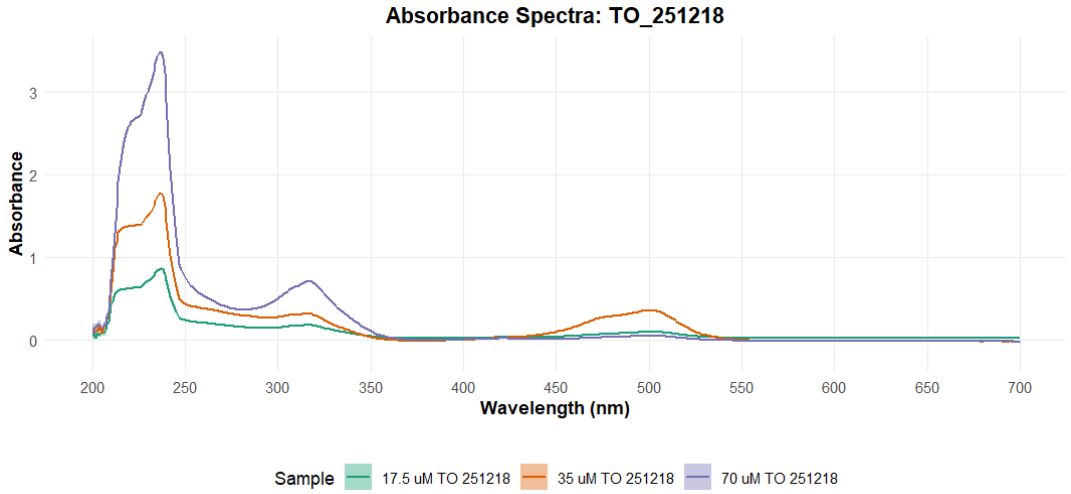

Figure 4.9: Absorbance spectra of TO solved in 5 mM DSP to concentrations of 17.5, 35, and 70 µM, in the UV-Vis range between 200 and 700 nm. The experiment was performed on December 12th 2025.

4.5 Absorbance spectra for CNC

The absorbance of the two batches of aqueous CNC suspensions, sulfated and non-sulfated at dry weights (i.e. concentrations) of 0.05 wt%, 0.1 wt%, and 0.75 wt%, between 300 and 600 nm in the UV and visible range, is displayed in *Figure* 4.10. The sulfated batch is denoted "sulf" and the non-sulfated batch, or more correctly a sulfated batch with blocked sulfate groups, is denoted "no sulf". The signals are normalized to the absorbance of DI.

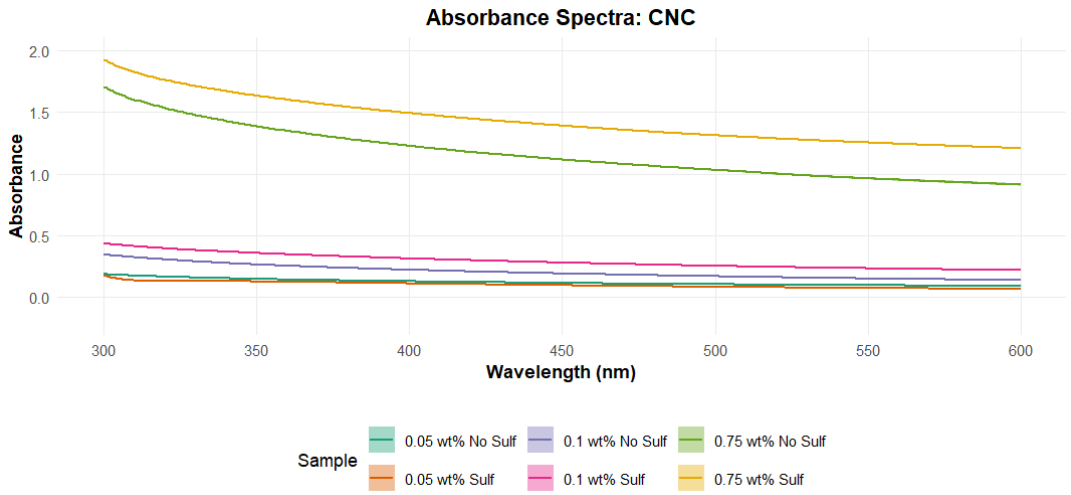

Figure 4.10: Average absorbance of technical triplicates, ±1 standard deviation, of aqueous suspensions of sulfated and "non-sulfated" CNC at 0.05, 0.1, and 0.75 wt%.

4.6 Absorbance spectra for TO and CNC

Figure 4.11 shows the absorbance spectra of 0.05 WT% aqueous suspension of sulfated CNC and 17.5, 35, and 70 µM TO solved in 5 mM DSP buffer, respectively. The absorbance signals are the average of technical triplicates, ±1 standard deviation, and and normalized to the absorbance of 5 mM DSP buffer. The molar ratio of TO to surface sulfate on the CNC is 1:1. The surface sulfate content of the batch was determined to 265 µmol sulfate per g CNC using potentiometric titration as outlined in section 3.2.

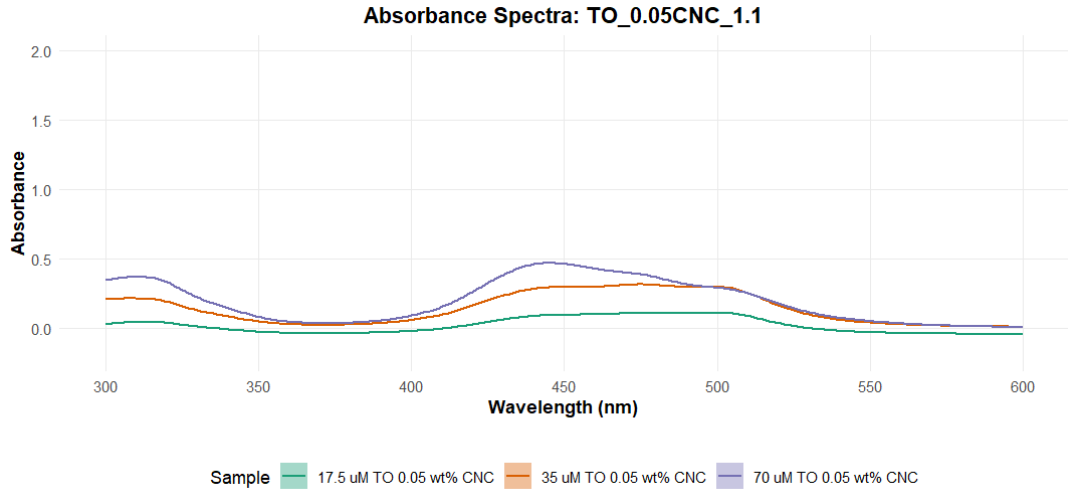

Figure 4.11: Average absorbance of technical triplicates, ±1 standard deviation, of 0.05 WT% aqueous suspension of sulfated CNC (265 µmol sulfate/g CNC) and 17.5, 35, and 70 µM TO solved in 5 mM DSP buffer, respectively. The molar ratio of TO to surface sulfate on the CNC is 1:1. Signals adjusted for the background signal of 5 mM DSP buffer.

Figure 4.12 shows the absorbance spectra of 0.05 WT% aqeuous suspension of the sulfated CNC (265 µmol sulfate/g CNC) and 17.5, 35, and 70 µM TO solved in 5 mM DSP buffer, respectively. The absorbance signals are the average of technical triplicates, ±1 standard deviation, and and normalized to the absorbance of 5 mM DSP buffer. The molar ratio of TO to surface sulfate on the CNC is 2:1.

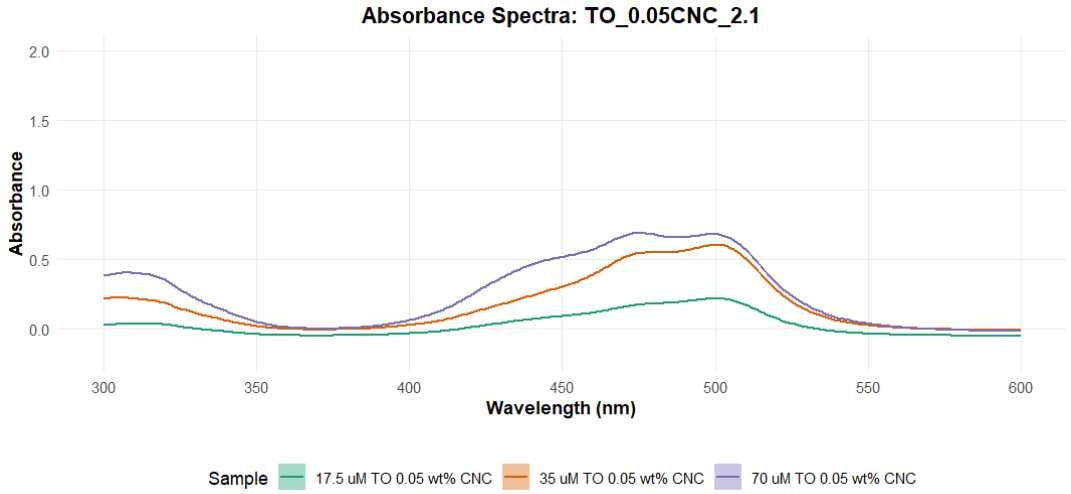

Figure 4.12: Average absorbance of technical triplicates, ±1 standard deviation, of 0.05 WT% aqueous suspension of sulfated CNC (265 µmol sulfate/g CNC) and 17.5, 35, and 70 µM TO solved in 5 mM DSP buffer, respectively. The molar ratio of TO to surface sulfate on the CNC is 2:1. Signals adjusted for the background signal of 5 mM DSP buffer.

Figure 4.13 shows the absorbance spectra of 0.1 WT% aqueous suspension of the sulfated CNC (265 µmol sulfate/g CNC) and 17.5, 35, and 70 µM TO solved in 5 mM DSP buffer, respectively. The absorbance signals are the average of technical triplicates, ±1 standard deviation, and and normalized to the absorbance of 5 mM DSP buffer. The molar ratio of TO to surface sulfate on the CNC is 2:1.

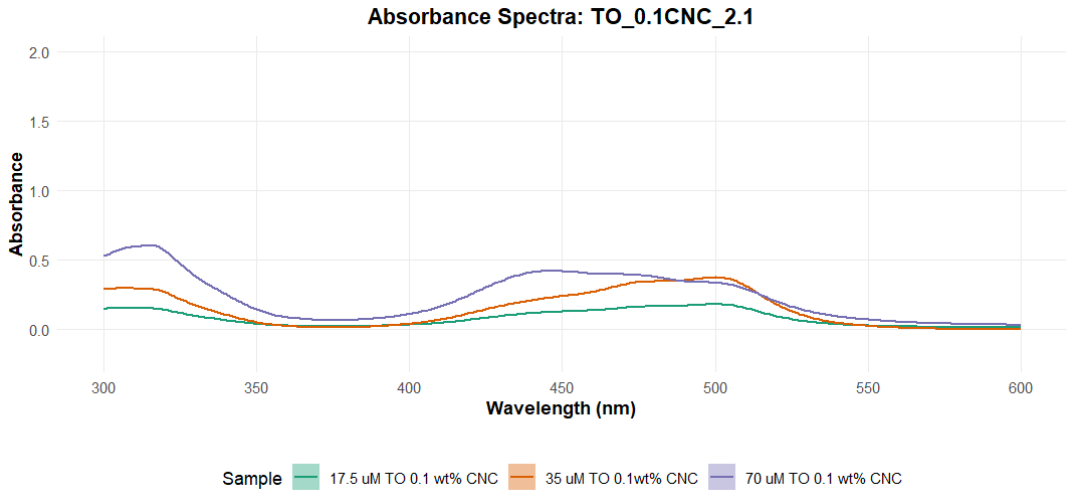

Figure 4.13: Average absorbance of technical triplicates, ±1 standard deviation, of 0.1 WT% aqueous suspension of sulfated CNC (265 µmol sulfate/g CNC) and 17.5, 35, and 70 µM TO solved in 5 mM DSP buffer, respectively. The molar ratio of TO to surface sulfate on the CNC is 2:1. Signals adjusted for the background signal of 5 mM DSP buffer.

4.7 Fluorescence spectra for TO

Figures 4.14 and 4.15 shows the average emission of technical triplicates, ±1 standard deviation, of 17.5, 35, and 70 µM TO in 5 mM DSP buffer, on December 1st and 15th, respectively. Signals are normalized to the emission of solvent, 5 mM DSP buffer. The excitation wavelength, λ_{ex}, was 290 nm, the scanned range was between 300 and 700 nm, and the excitation and emission slit width was set to 2.5 nm.

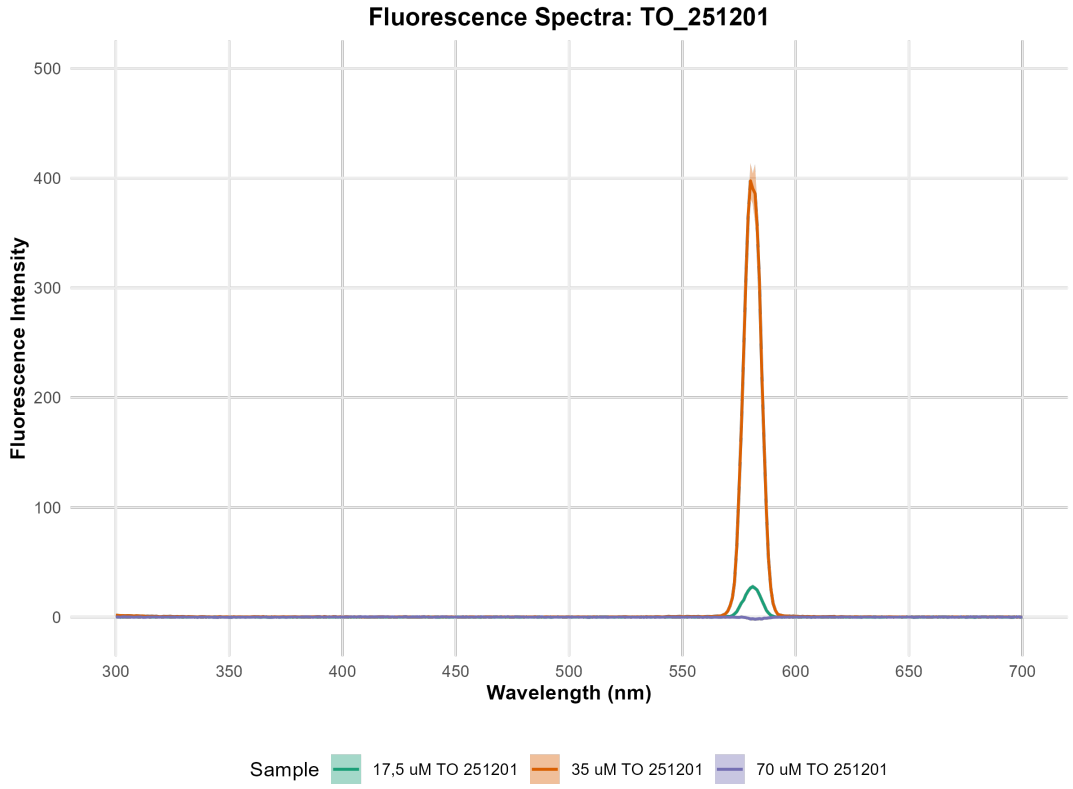

Figure 4.14: Emission of 17.5, 35, and 70 µM TO in 5 mM DSP buffer in the 300-700 nm range, excited at 290 nm. Signals showns are averages of technical triplicates, ±1 standard deviation, and normalized to the emission of solvent, DSP. Experiment performed on December 1st 2025.

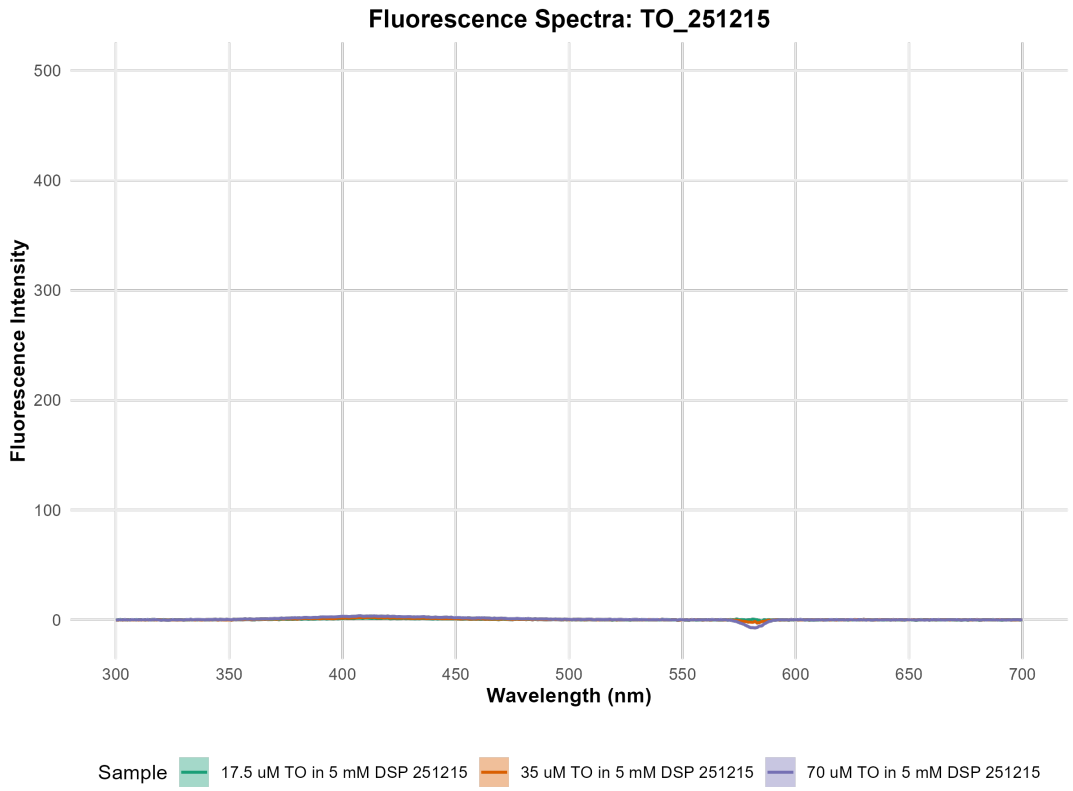

Figure 4.15: Emission of 17.5, 35, and 70 µM TO in 5 mM DSP buffer in the 300-700 nm range, excited at 290 nm. Signals showns are averages of technical triplicates, ±1 standard deviation, and normalized to the emission of solvent, DSP. The experiment was performed on December 15th 2025.

4.8 Fluorescence spectra for CNC

Figure 4.16 shows the average emission of technical triplicates, ±1 standard deviation, of 0.05, 0.1, and 0.75 WT% sulfated (265 µmol sulfate per g CNC) and non-sulfated (252 µmol sulfate per g CNC blocked by AZ salts) CNC, in aqueous suspension. Signals are normalized to the emission of solvent, DI water. The excitation wavelength, λ_{ex}, was 290 nm, the scanned range was between 300 and 700 nm, and the excitation and emission slit widths was set to 2.5 nm. The experiment was performed on December 5th.

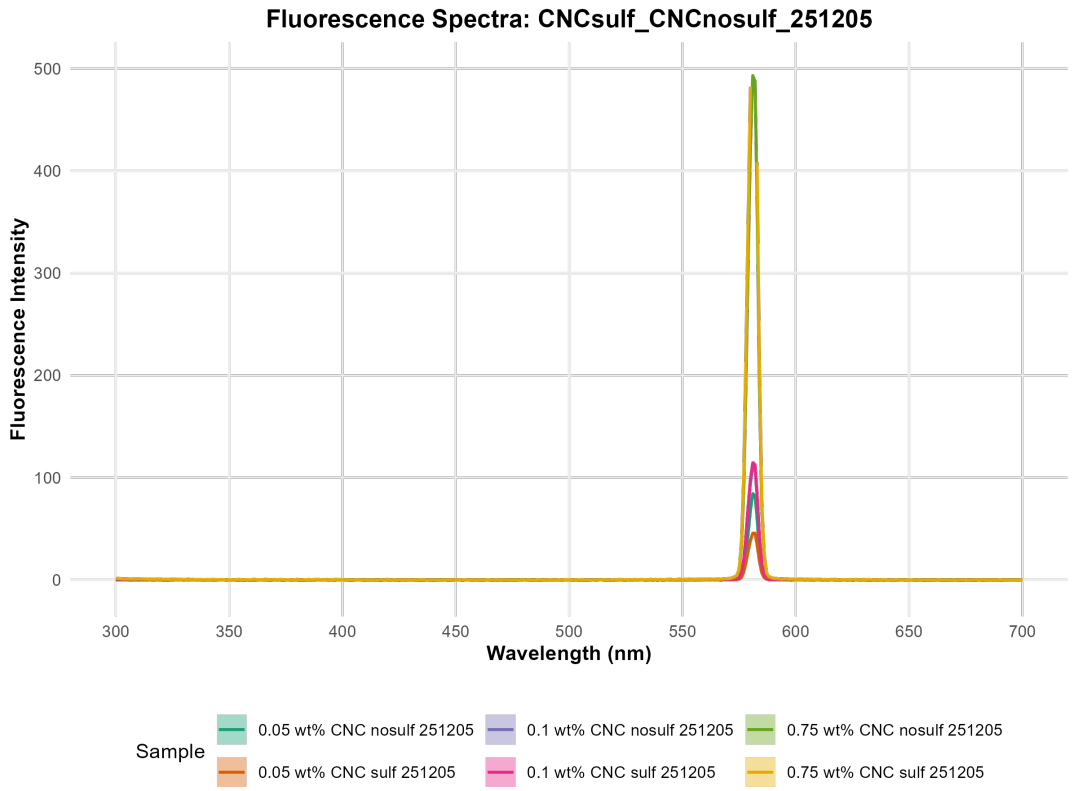

Figure 4.16: Emission of 0.05, 0.1, and 0.75 WT% sulfated (265 µmol sulfate per g CNC) and non-sulfated (252 µmol sulfate per g CNC blocked by AZ salts) CNC, in aqueous suspension. Scanned in the 300-700 nm range, and excited at 290 nm. Signals shown are averages of technical triplicates, ±1 standard deviation, and normalized to the emission of solvent, DI water. The experiment was performed on December 5th 2025.

Figure 4.17 shows the average emission of technical triplicates, ±1 standard deviation, of 0.05, 0.1, and 0.75 WT% sulfated (265 µmol sulfate per g CNC) and non-sulfated (252 µmol sulfate per g CNC blocked by AZ salts) CNC, in aqueous suspension. Signals are normalized to the emission of solvent, DI water. The excitation wavelength, λ_{ex}, was 380 nm, and the scanned range was between 300 and 800 nm, and the excitation and emission slit widths was set to 2.5 nm. The experiment was performed on December 18th.

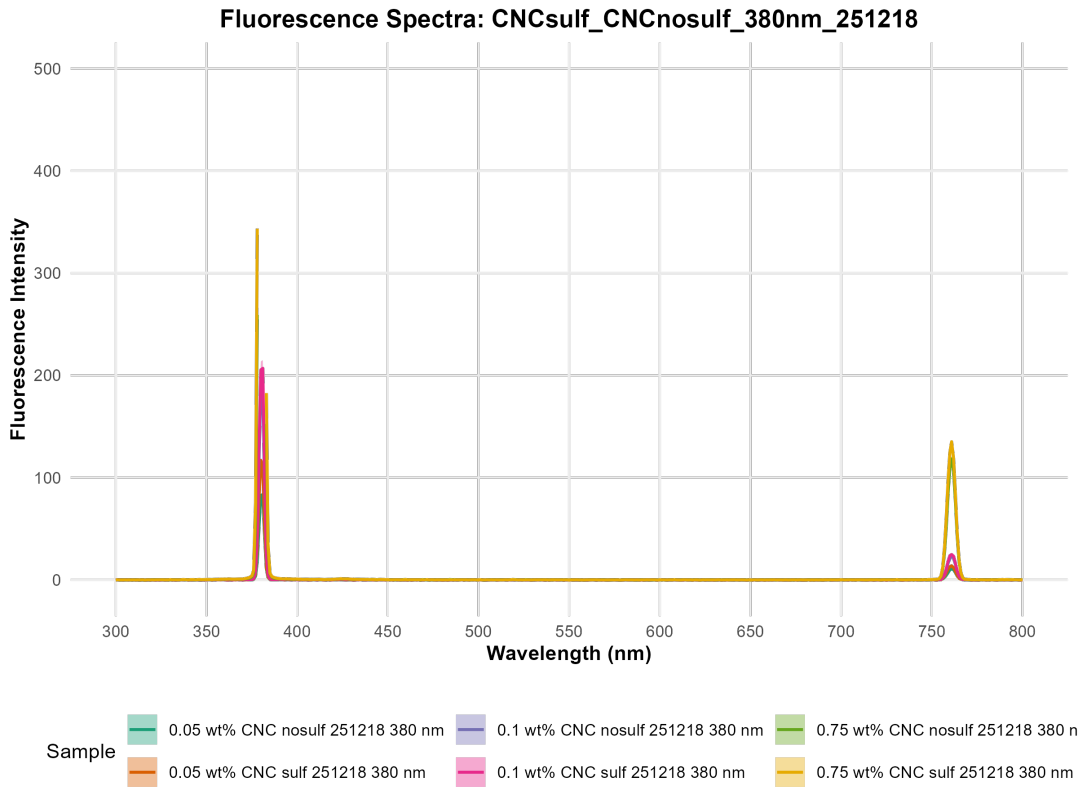

Figure 4.17: Emission of 0.05, 0.1, and 0.75 WT% sulfated (265 µmol sulfate per g CNC) and non-sulfated (252 µmol sulfate per g CNC blocked by AZ salts) CNC, in aqueous suspension. Scanned in the 300-800 nm range, and excited at 380 nm. Signals shown are averages of technical triplicates, ±1 standard deviation, and normalized to the emission of solvent, DI water. The experiment was performed on December 18th 2025.

Figure 4.18 shows the average emission of technical triplicates, ±1 standard deviation, of 0.05, 0.1, and 0.75 WT% sulfated (265 µmol sulfate per g CNC) and non-sulfated (252 µmol sulfate per g CNC blocked by AZ salts) CNC, in aqueous suspension. Signals are normalized to the emission of solvent, DI water. The excitation wavelength, λ_{ex}, was 500 nm, and the scanned range was between 300 and 800 nm, and the excitation and emission slit widths was set to 2.5 nm. The experiment was performed on December 18th.

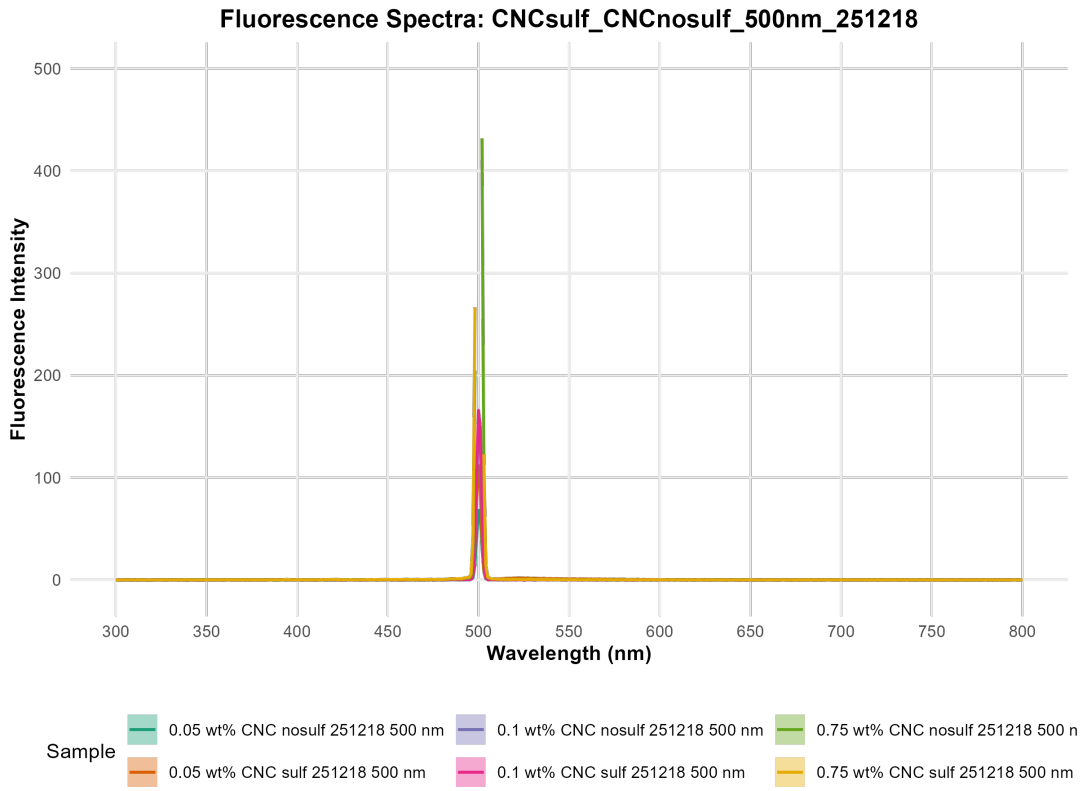

Figure 4.18: Emission of 0.05, 0.1, and 0.75 WT% sulfated (265 µmol sulfate per g CNC) and non-sulfated (252 µmol sulfate per g CNC blocked by AZ salts) CNC, in aqueous suspension. Scanned in the 300-800 nm range, and excited at 500 nm. Signals showns are averages of technical triplicates, ±1 standard deviation, and normalized to the emission of solvent, DI water. The experiment was performed on December 18th 2025

4.9 Fluorescence spectra for CNC and TO

Figure 4.19 shows the average emission of technical triplicates, ±1 standard deviation, of 0.05 WT% sulfated (265 µmol sulfate per g CNC) in aqueous suspension and, respectively, 17.5, 35, and 70 µM TO in 5 mM DSP buffer. The molar ratio of TO to surface sulfate on the CNC is 2:1. Signals are normalized to the emission of the buffer. The excitation wavelength, λ_{ex}, was 290 nm, and the scanned range was between 300 and 700 nm, and the excitation and emission slit widths was set to 2.5 nm. The experiment was performed on December 2nd.

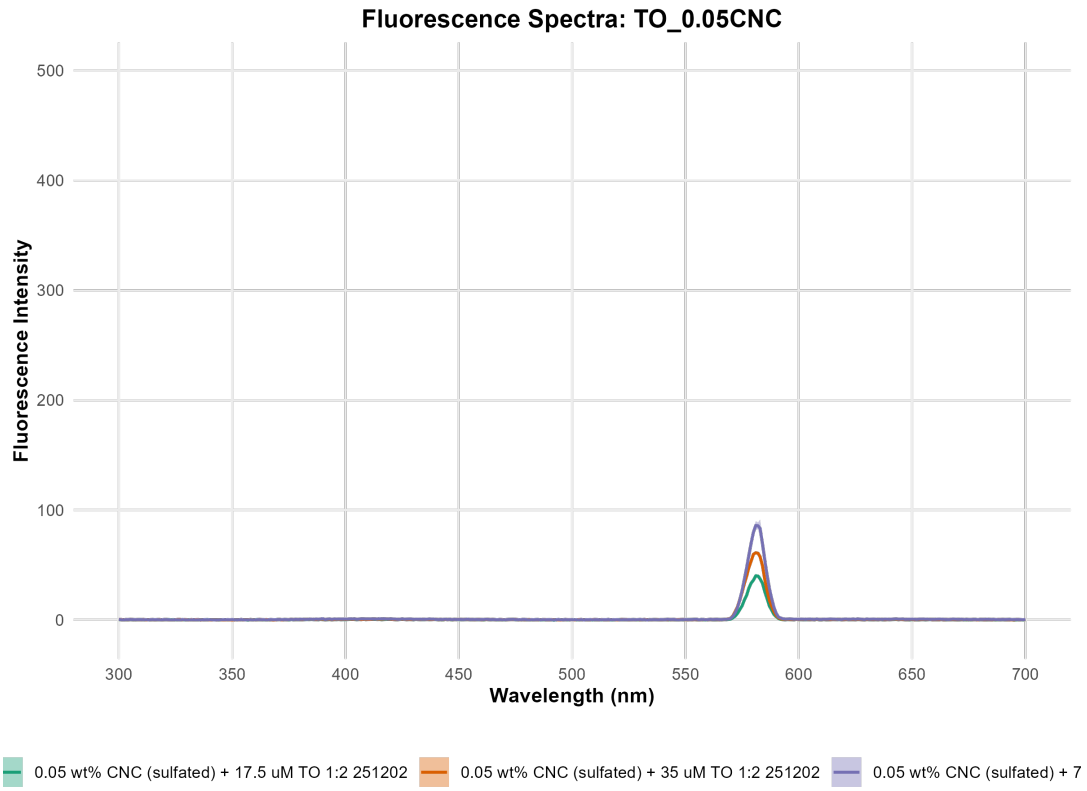

Figure 4.19: Emission of 0.05 WT% sulfated (265 µmol sulfate per g CNC) CNC in aqueous suspension and, respectively, 17.5, 35, and 70 µM TO in 5 mM DSP buffer. The molar ratio of TO to surface sulfate on the CNC is 2:1. Signals are normalized to the emission of the buffer, 5 mM DSP. The excitation wavelength, λ_{ex}, was 290 nm, and the scanned range was between 300 and 700 nm, and the excitation and emission slit widths was set to 2.5 nm. The experiment was performed on December 2nd.

Figure 4.20 shows the average emission of technical triplicates, ±1 standard deviation, of 0.1 WT% sulfated (265 µmol sulfate per g CNC) in aqueous suspension and, respectively, 17.5, 35, and 70 µM TO in 5 mM DSP buffer. The molar ratio of TO to surface sulfate on the CNC is 2:1. Signals are normalized to the emission of the buffer. The excitation wavelength, λ_{ex}, was 290 nm, and the scanned range was between 300 and 700 nm. The experiment was performed on December 15th.

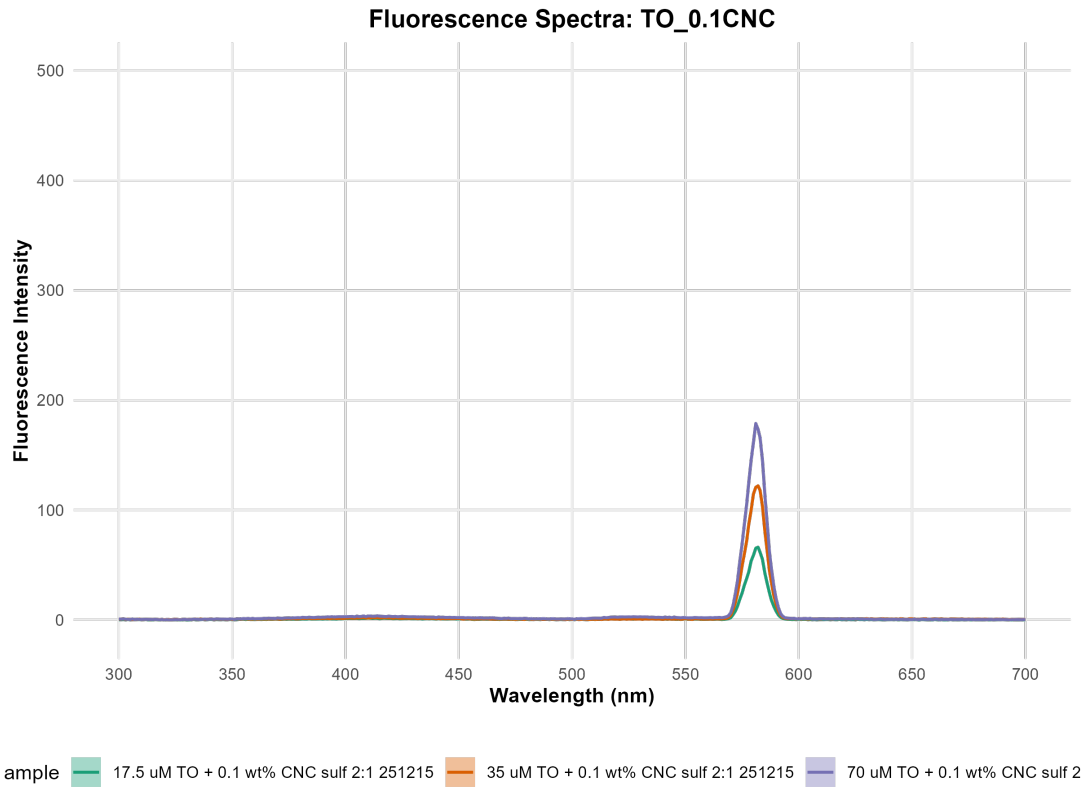

Figure 4.20: Emission of 0.1 WT% sulfated (265 µmol sulfate per g CNC) CNC in aqueous suspension and, respectively, 17.5, 35, and 70 µM TO in 5 mM DSP buffer. The molar ratio of TO to surface sulfate on the CNC is 2:1. Signals are normalized to the emission of the buffer, 5 mM DSP. The excitation wavelength, λ_{ex}, was 290 nm, and the scanned range was between 300 and 700 nm, and the excitation and emission slit widths was set to 2.5 nm. The experiment was performed on December 15th.

4.10 Absorbance Spectra for p-NPS

Figure 4.21 shows the absorbance of p-NPS synthesized by the standard method, solved in DI water at 37 °C in the UV-Vis range between 200 and 500 nm. Scans were done every 5 minutes for 60 minutes. The experiment was performed on September 15th.

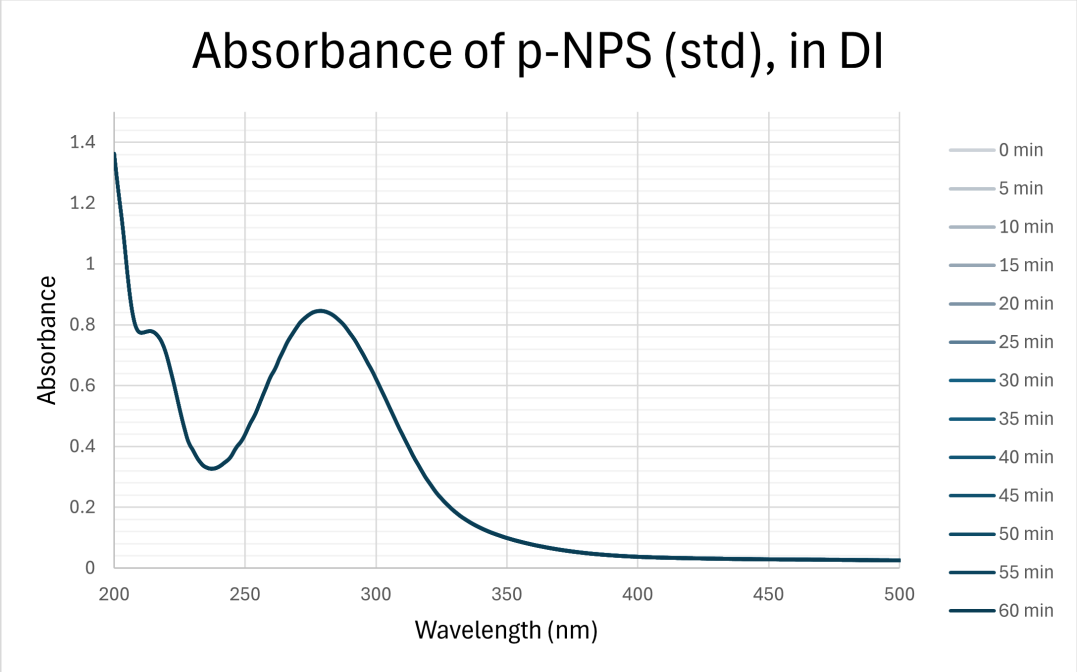

Figure 4.21: Absorbance of p-NPS synthesized by the standard method, solved in 37 °C DI water. Scans were taken at an interval of 5 min for a total duration of 60 min, in the 200-500 nm range. The experiment was performed on September 15th 2025.

Figure 4.22 shows the absorbance of p-NPS synthesized by the standard method, solved in 0.015 M Tris buffer at 37 °C. Scans were done every 5 minutes for 120 minutes in the UV-Vis range between 200 and 500 nm. The experiment was performed on October 9th.

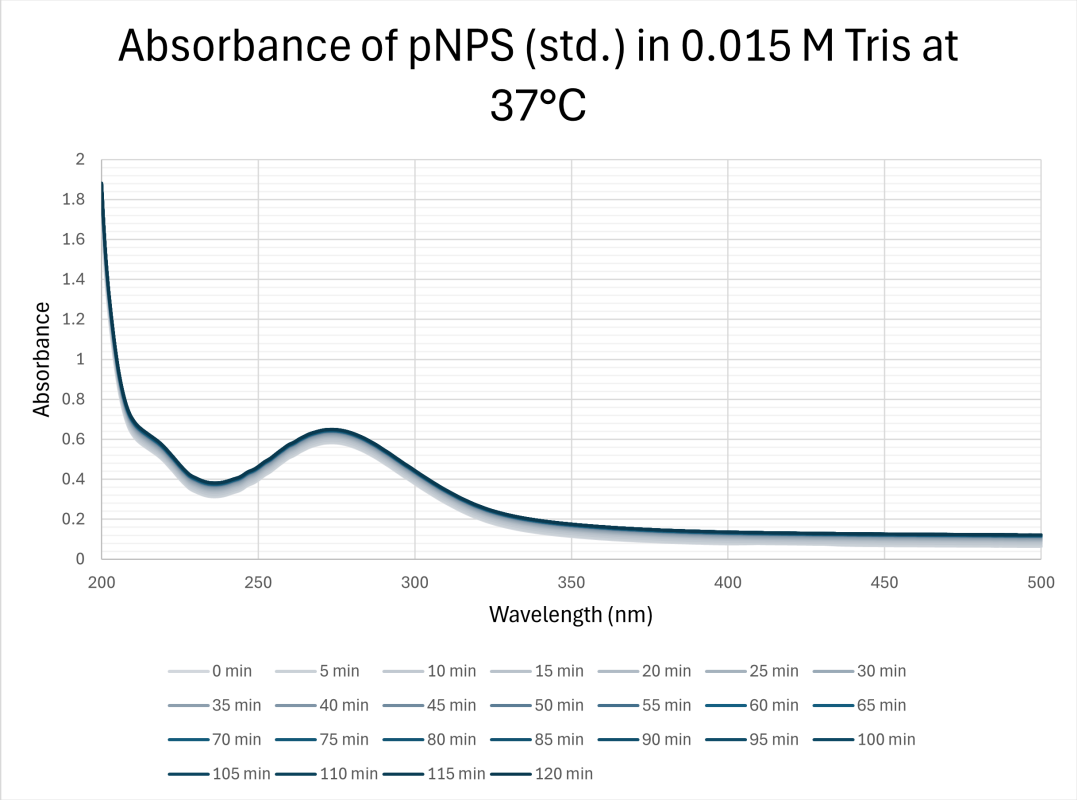

Figure 4.22: Absorbance of p-NPS synthesized by the standard method, solved in 15 mM Tris buffer at 37 °C. Scans were taken at an interval of 5 min for a total duration of 120 min, in the 200-500 nm range. The experiment was performed on October 9th 2025.

Figure 4.23 shows the absorbance of recrystalized p-NPS, synthesized by the standard method, solved in 0.5 M NaOAc buffer at 37 °C. Scans were done every 2.5 minutes for 60 minutes in the UV-Vis range between 200 and 500 nm. The experiment was performed on November 4th.

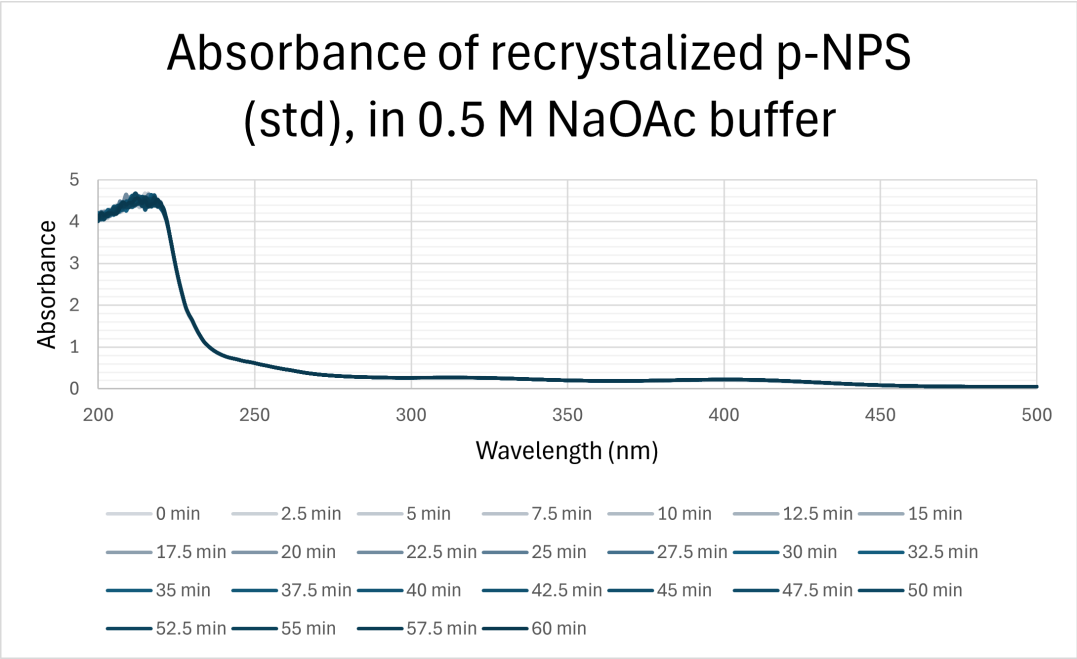

Figure 4.23: Absorbance of recrystallized p-NPS synthesized by the standard method, solved in 0.5 M NaOAc buffer at 37 °C. Scans were taken at an interval of 2.5 min for a total duration of 60 min, in the 200-500 nm range. The experiment was performed on November 4th 2025.

Figure 4.23 shows the absorbance of recrystalized p-NPS, synthesized by the standard method, solved in 0.5 M NaOAc buffer at 37 °C. Scans were done every 2.5 minutes for 30 minutes in the UV-Vis range between 200 and 500 nm. The experiment was performed on November 6th.

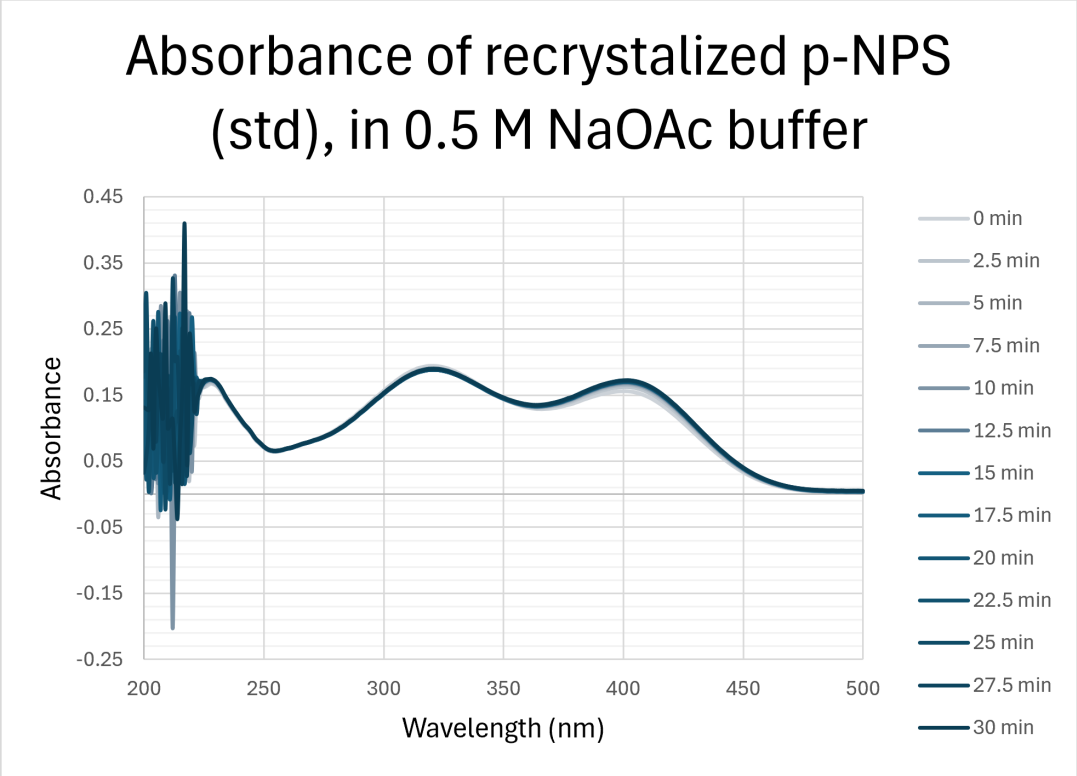

Figure 4.24: Absorbance of recrystallized p-NPS synthesized by the standard method, solved in 0.5 M NaOAc buffer at 37 °C. Scans were taken at an interval of 2.5 min for a total duration of 30 min, in the 200-500 nm range. The experiment was performed on November 6th 2025.

Figure 4.25 shows the absorbance of recrystalized p-NPS, synthesized by the alternative method, solved in DI water at 37 °C. Scans were done every 5 minutes for 60 minutes in the UV-Vis range between 200 and 500 nm. The experiment was performed on October 30th.

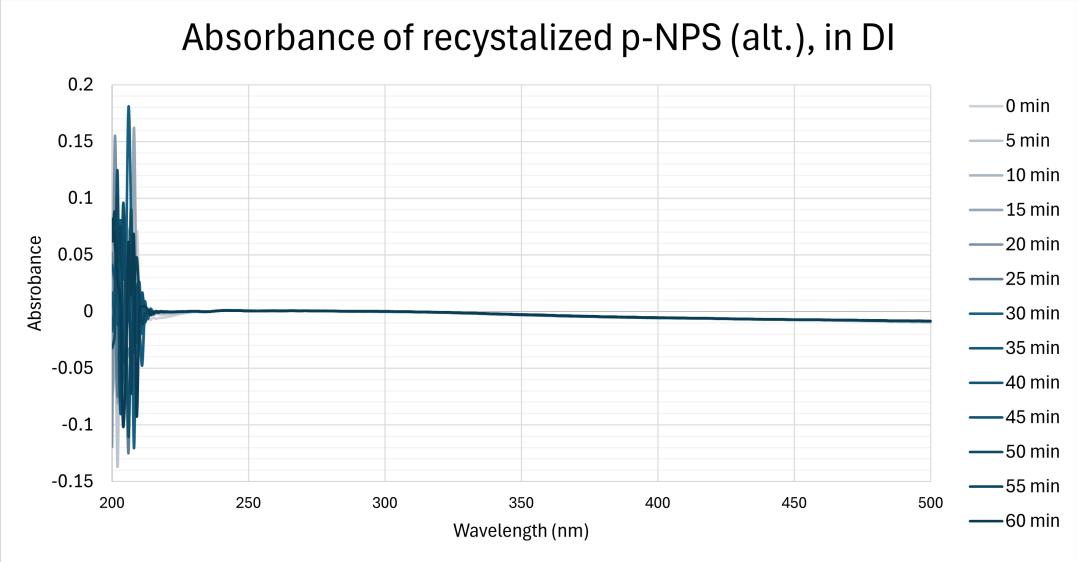

Figure 4.25: Absorbance at 37 °C of filtered and recrystalized pNPS, synthesized by the alternate method, solved in DI. Scans were taken at an interval of 5 min for a total duration of 60 min, in the 200-500 nm range. The experiment was performed on October 30th 2025.

Figure 4.26 shows the absorbance of recrystalized p-NPS, synthesized by the alternative method, solved in DI water at 37 °C. Scans were done in the UV-Vis range between 200 and 500 nm. The experiment was performed on November 4th.

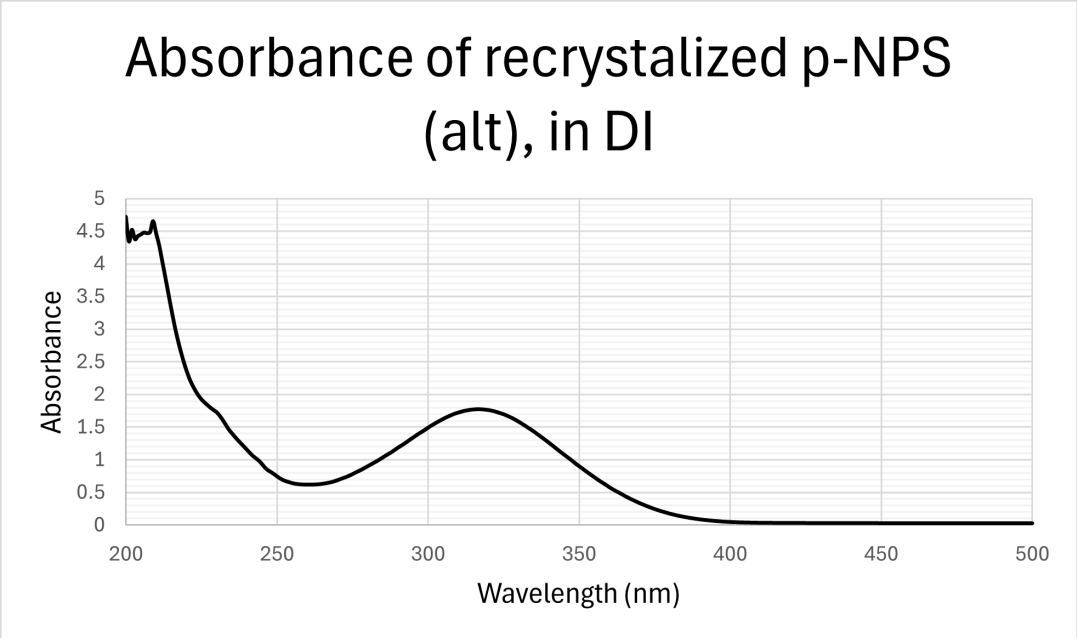

Figure 4.26: Absorbance in the 200-500 nm range at 37 °C of filtered and recrystalized pNPS, synthesized by the alternate method, solved in DI. The experiment was performed on November 4th 2025.

Figure 4.27 shows the absorbance of p-NPS, synthesized by the alternative method,

solved in 0.2 M Tris buffer at 37 °C. The scan was done in the UV-Vis range between 200 and 500 nm on October 15th.

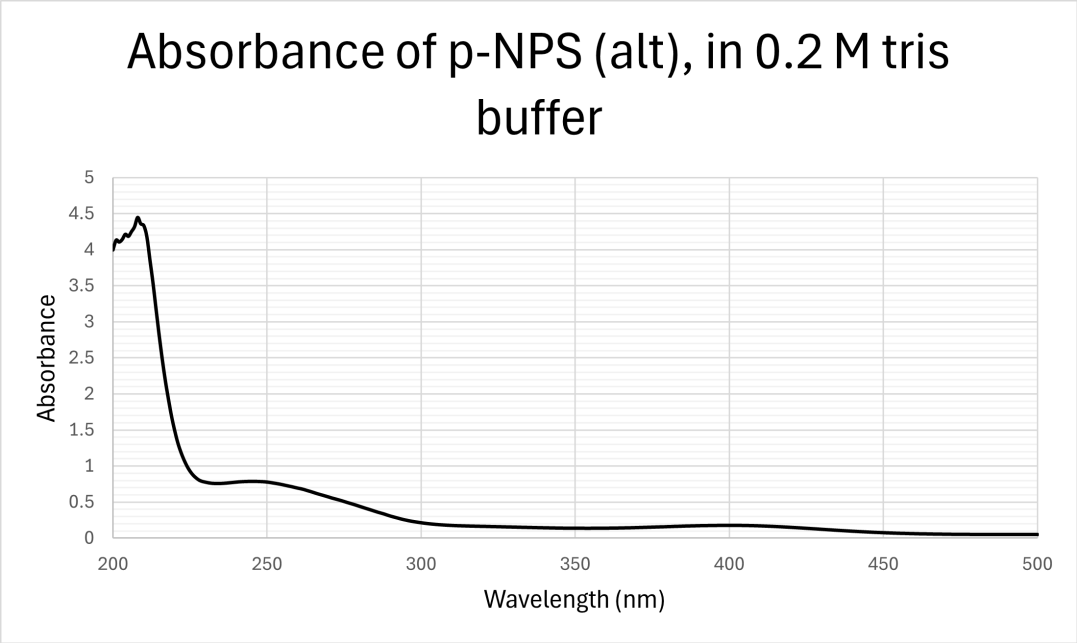

Figure 4.27: Absorbance of p-NPS synthesized by the alternative method, solved in 0.2 M Tris buffer at 37 °C, in the 200-500 nm range. The experiment was performed on October 15th 2025.

Figure 4.28 shows the absorbance of recrystalized p-NPS, synthesized by the alternative method, solved in 0.05 M Tris buffer at 37 °C. The scans were done every 5 minutes for 35 minutes, in the UV-Vis range between 200 and 500 nm on October 27th.

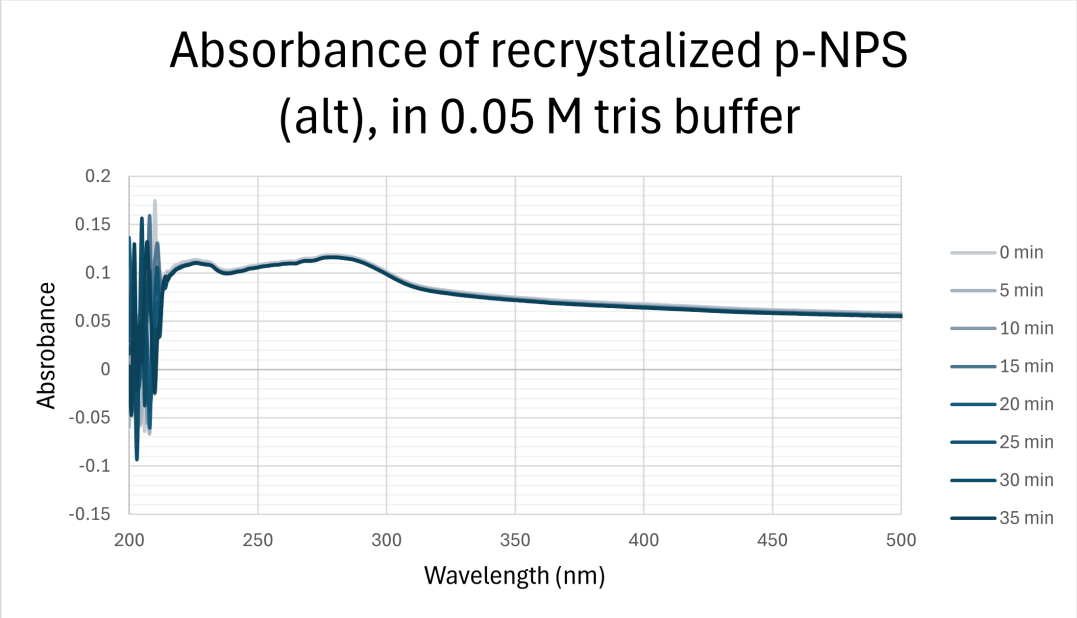

Figure 4.28: Absorbance at 37 °C of filtered and recrystalized p-NPS, synthesized by the alternate method, solved in 50 mM Tris buffer. Scans were taken at an interval of 5 min for a total duration of 35 min, in the 200-500 nm range. The experiment was performed on October 27th 2025.

4.11 Absorbance spectra of sulfatases

To verify stability of the enzymes under experimental conditions, the kinetics program on the UV-Vis Spectrophotometer was used on isolated reference samples of sulfatases, simultaneously to corresponding enzymatic assays.

Figure 4.29 shows the absorbance of the sulfatase from *Helix pomatia* in 0.015 M Tris buffer at 37 °C. Scans were done every 5 minutes for 120 minutes, in the 200-500 nm range. Two sources of *Helix pomatia sulfatase* was used, this being the one arbitrarily denoted "1". This experiment was performed on October 9th, in conjunction with the assays displayed in *Figures* 4.32 and 4.33.

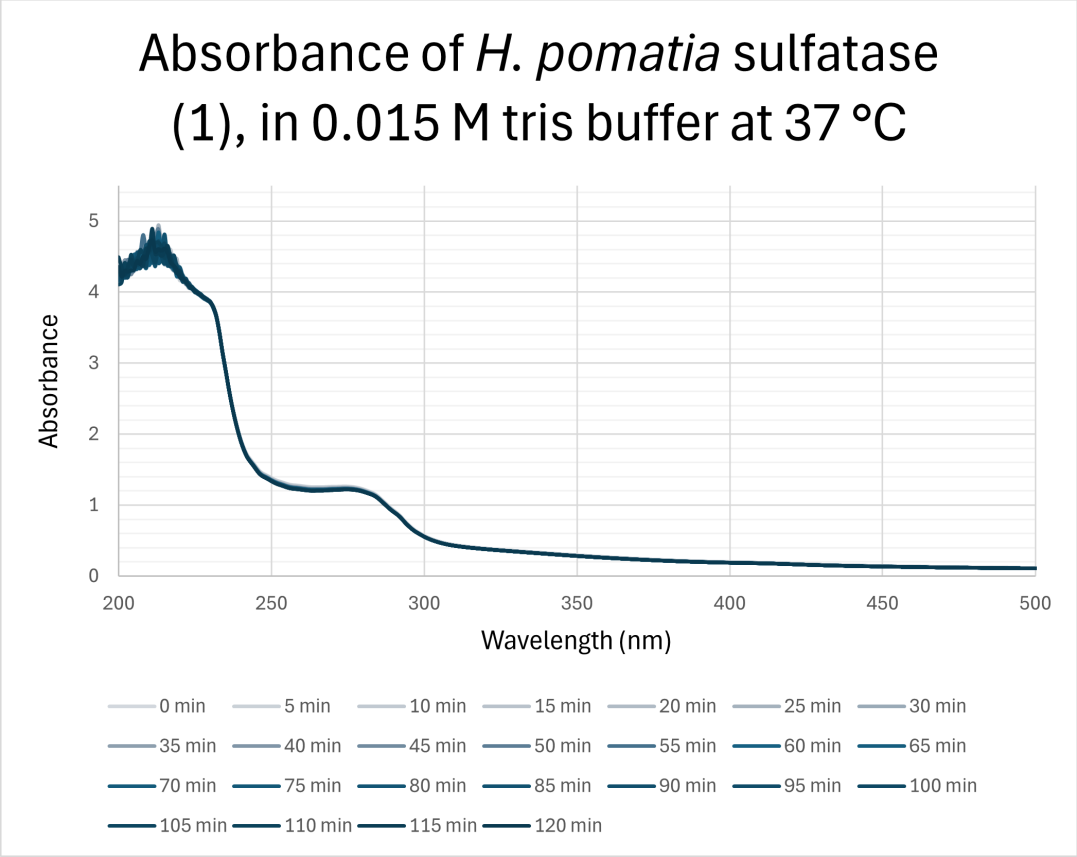

Figure 4.29: Absorbance of *Helix pomatia* sulfatase (source 1), in 15 mM Tris buffer at 37 °C. Scans were taken every 5 minutes for 120 minutes, between 200-500 nm. The experiment was performed on October 9th.

Figure 4.30 shows the absorbance of sulfatase from *Helix pomatia*, solved in 0.5 M Tris buffer at 37 °C. The source was the one arbitrarily denoted "2". The scan was done in the UV-Vis range between 200 and 500 nm on November 6th.

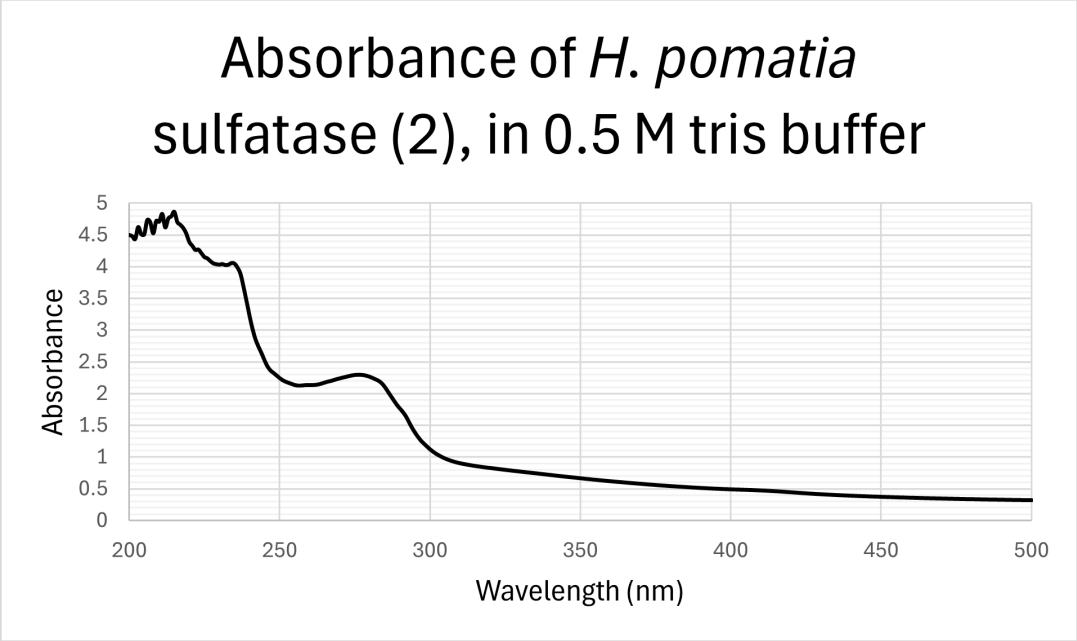

Figure 4.30: Absorbance of *Helix pomatia* sulfatase (source 2), in 0.5 M Tris buffer at 37 °C, in the 200-500 nm range. The experiment was performed on November 6th.

Figure 4.31 shows the absorbance of sulfatase from *Helix pomatia*, solved in 0.5 M NaOAc buffer at 37 °C. The source was the one arbitrarily denoted "2". The scan was done in the UV-Vis range between 200 and 500 nm on November 6th.

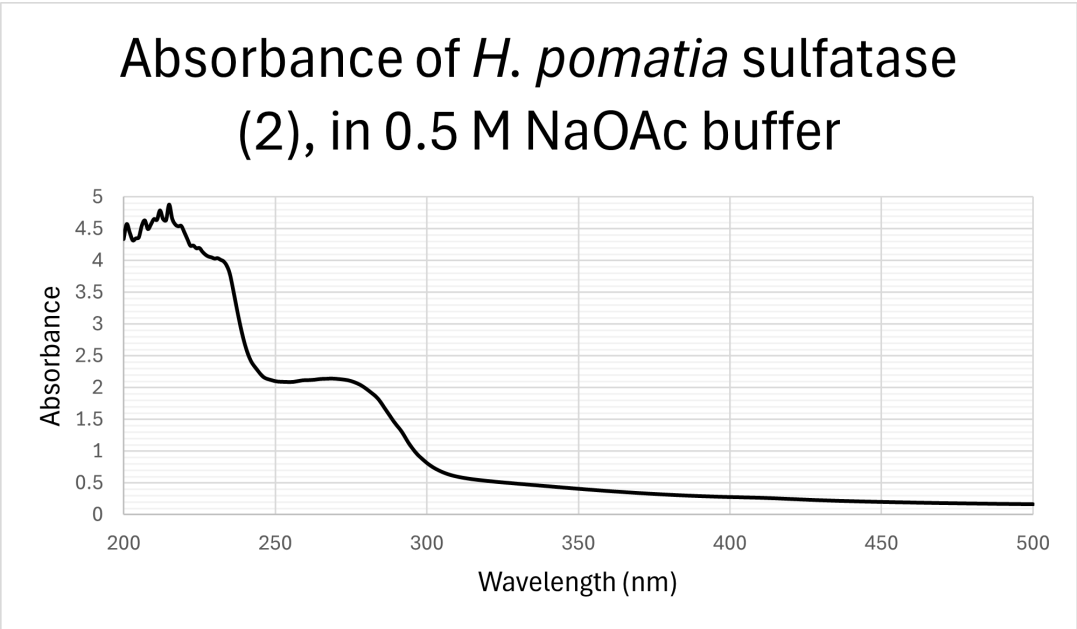

Figure 4.31: Absorbance of *Helix pomatia* sulfatase (source 2), in 0.5 M NaOAc buffer at 37 °C, in the 200-500 nm range. The experiment was performed on November 6th.

4.12 Enzymatic assays via absorbance spectroscopy

4.12.1 Helix pomatia 1 and pNPS (std) in 0.015 M Tris

Figure 4.32 shows the enzymatic assay of *Helix pomatia* sulfatase (source 1) on p-NPS synthesized by the standard method, in 0.015 M Tris buffer at 37 °C. Scans where made every 5 minutes for 120 minutes, in the 200-500 nm range, on October 9th. Corresponding reference measurements of p-NPS and enzyme are available in *Figures* 4.22 and 4.29, respectively.

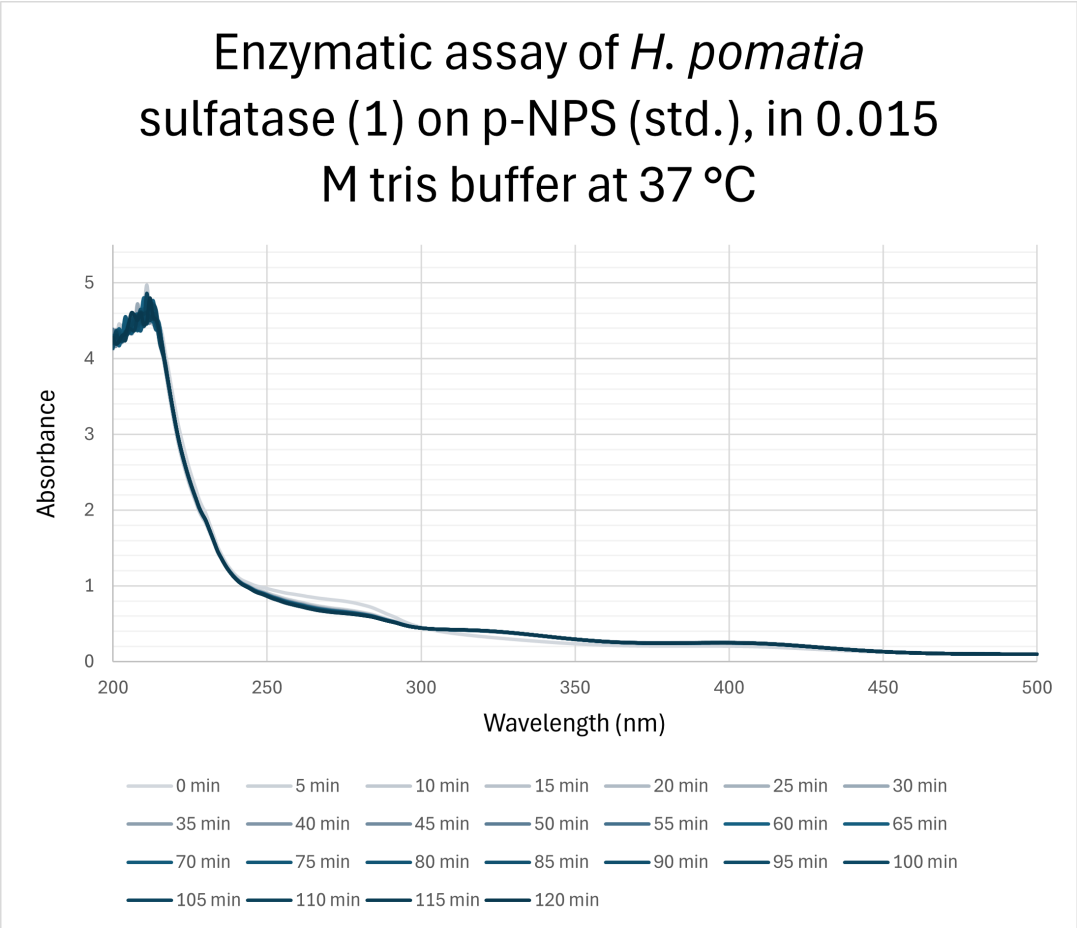

Figure 4.32: Enzymatic assay of *Helix pomatia* sulfatase (source 1) on p-NPS synthesized by the standard method, in 0.015 M Tris buffer at 37 °C. Scans where made every 5 minutes for 120 minutes, in the 200-500 nm range, on October 9th 2025.

Figure 4.33 shows the enzymatic assay of *Helix pomatia* sulfatase (source 1) on p-NPS synthesized by the standard method, in 0.015 M Tris buffer at RT. Scans where made every 5 minutes for 120 minutes, in the 200-500 nm range, on October 9th. Corresponding reference measurements of p-NPS and enzyme are available in *Figures* 4.22 and 4.29, respectively.

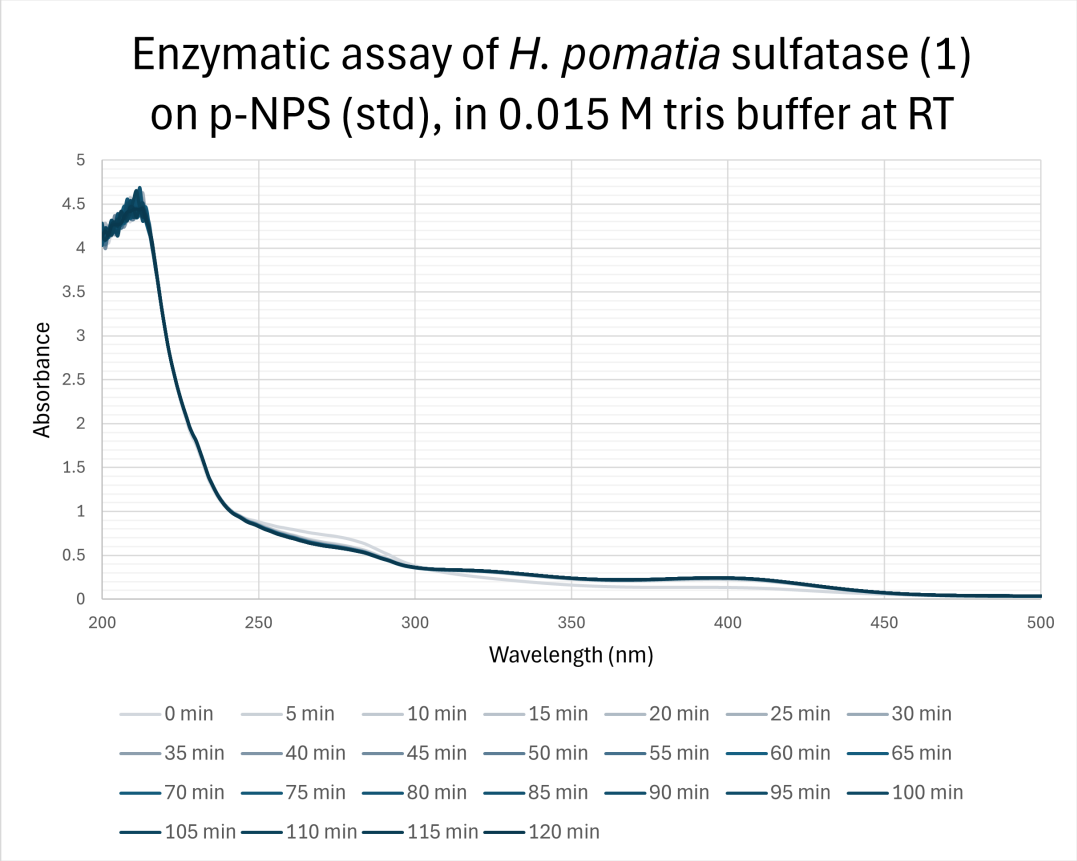

Figure 4.33: Enzymatic assay of *Helix pomatia* sulfatase (source 1) on p-NPS synthesized by the standard method, in 0.015 M Tris buffer at RT. Scans where made every 5 minutes for 120 minutes, in the 200-500 nm range, on October 9th 2025.

4.12.2 Helix pomatia 1 and pNPS (std) in 0.5 M Tris

Figure 4.34 shows the enzymatic assay of *Helix pomatia* sulfatase (source 1) on p-NPS synthesized by the standard method, in 0.5 M Tris buffer at 37 °C. Scans where made every 5 minutes for 120 minutes, in the 200-500 nm range, on October 8th.

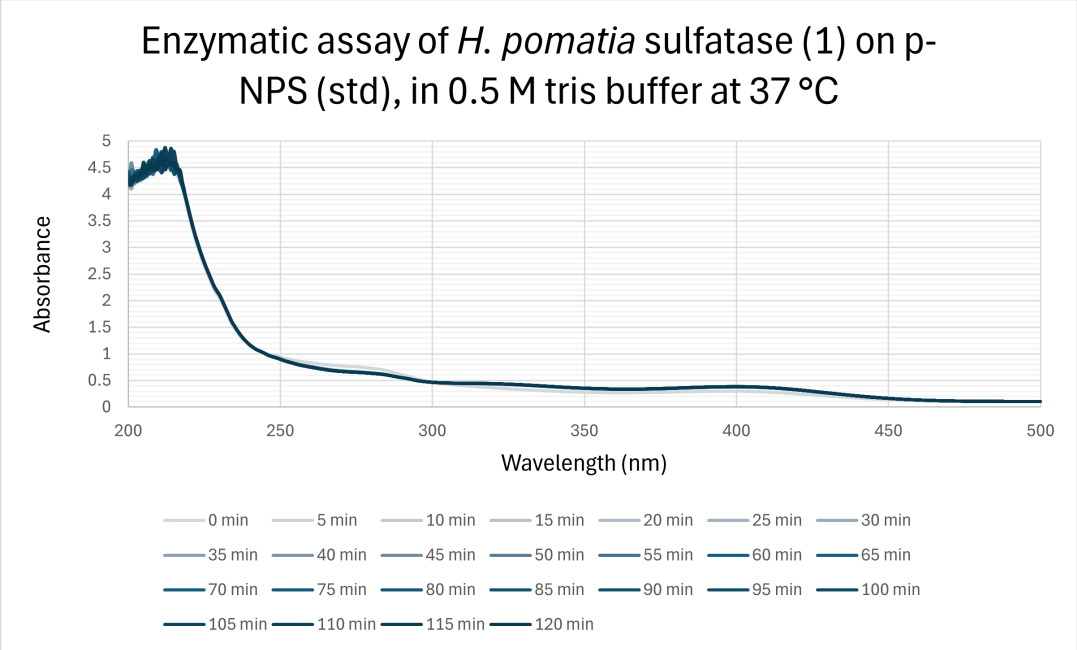

Figure 4.34: Enzymatic assay of *Helix pomatia* sulfatase (source 1) on p-NPS synthesized by the standard method, in 0.5 M Tris buffer at 37 °C. Scans where made every 5 minutes for 120 minutes, in the 200-500 nm range, on October 8th 2025.

Figure 4.35 shows the enzymatic assay of *Helix pomatia* sulfatase (source 1) on p-NPS synthesized by the standard method, in 0.5 M Tris buffer at RT. Scans where made every 5 minutes for 120 minutes, in the 200-500 nm range, on October 8th.

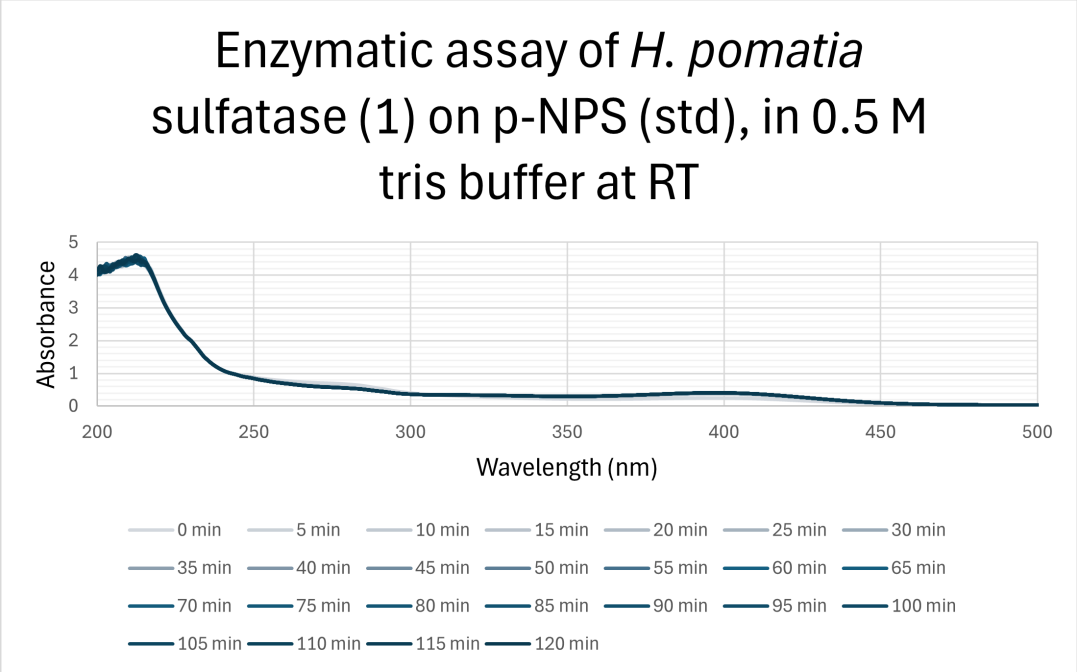

Figure 4.35: Enzymatic assay of *Helix pomatia* sulfatase (source 1) on p-NPS synthesized by the standard method, in 0.5 M Tris buffer at RT. Scans where made every 5 minutes for 120 minutes, in the 200-500 nm range, on October 8th 2025.

4.12.3 Helix pomatia 2 and (recrystalized) pNPS (std) in 0.5 M Tris

Figure 4.36 shows the enzymatic assay of *Helix pomatia* sulfatase (source 2) on recrystallized p-NPS, synthesized by the standard method, in 0.5 M Tris buffer at 37 °C. Scans where made every 2.5 minutes for 15 minutes, in the 200-500 nm range, on November 6th.

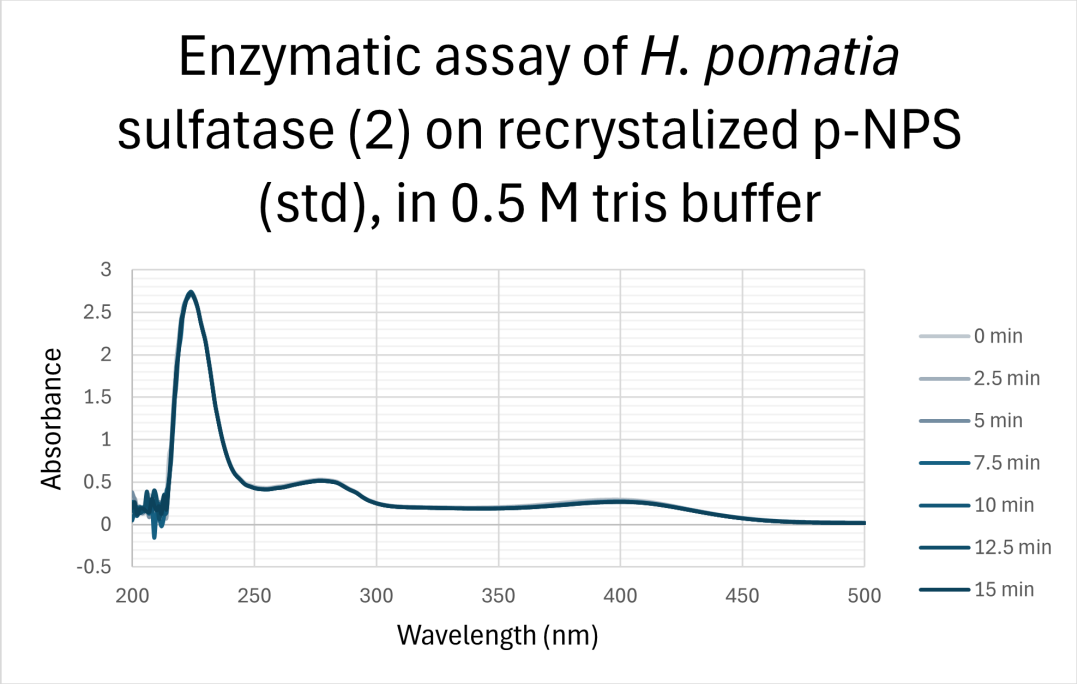

Figure 4.36: Enzymatic assay of *Helix pomatia* sulfatase (source 2) on recrystallized p-NPS, synthesized by the standard method, in 0.5 M Tris buffer at 37 °C. Scans where made every 2.5 minutes for 15 minutes, in the 200-500 nm range, on November 6th 2025.

4.12.4 Helix pomatia 1 and (recrystalized) p-NPS (std) in 0.5 M NaOAc

Figure 4.37 shows the enzymatic assay of *Helix pomatia* sulfatase (source 1) sulfatase on recrystallized p-NPS, synthesized by the standard method, in 0.5 M NaOAc buffer at 37 °C. Scans where made every 2.5 minutes for 60 minutes, in the 200-500 nm range, on November 4th.

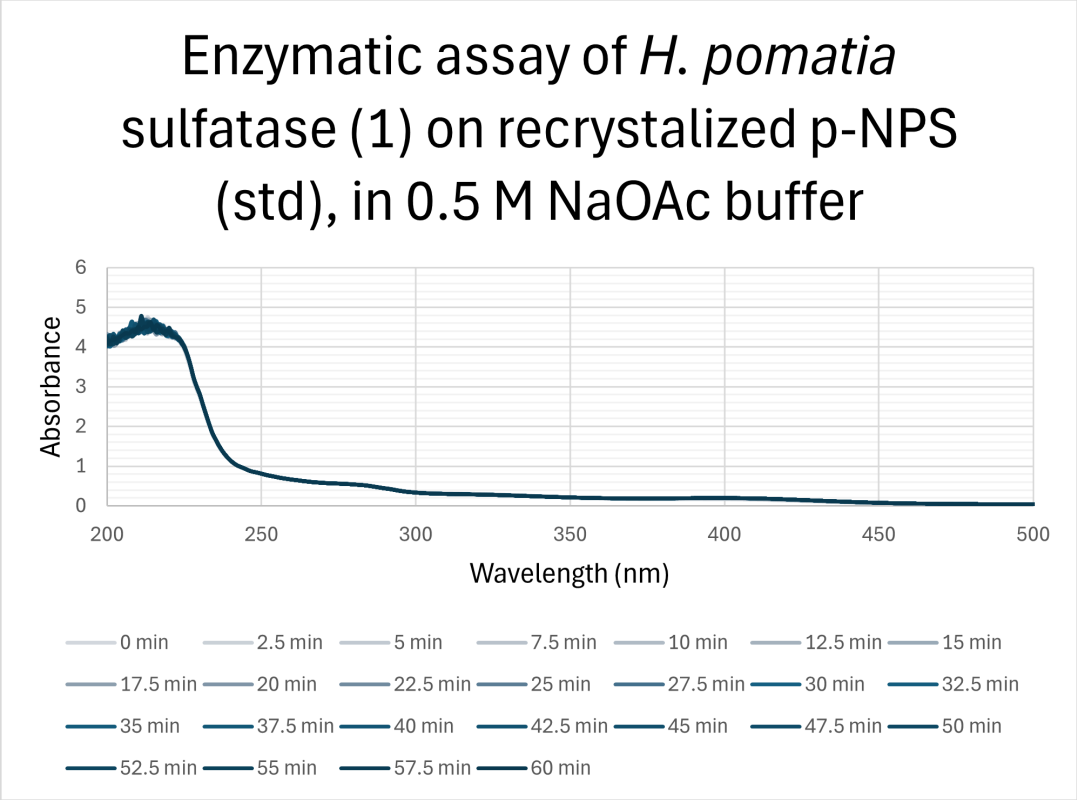

Figure 4.37: enzymatic assay of *Helix pomatia* sulfatase (source 1) sulfatase on recrystallized p-NPS, synthesized by the standard method, in 0.5 M NaOAc buffer at 37 °C. Scans where made every 2.5 minutes for 60 minutes, in the 200-500 nm range, on November 4th 2025.

4.12.5 Helix pomatia 2 and recrystallized p-NPS (std) in 0.5 M NaOAc

Figure 4.38 shows the enzymatic assay of *Helix pomatia* sulfatase (source 2) sulfatase on recrystallized p-NPS, synthesized by the standard method, in 0.5 M NaOAc buffer at 37 °C. Scans where made every 2.5 minutes for 30 minutes, in the 200-500 nm range, on November 6th.

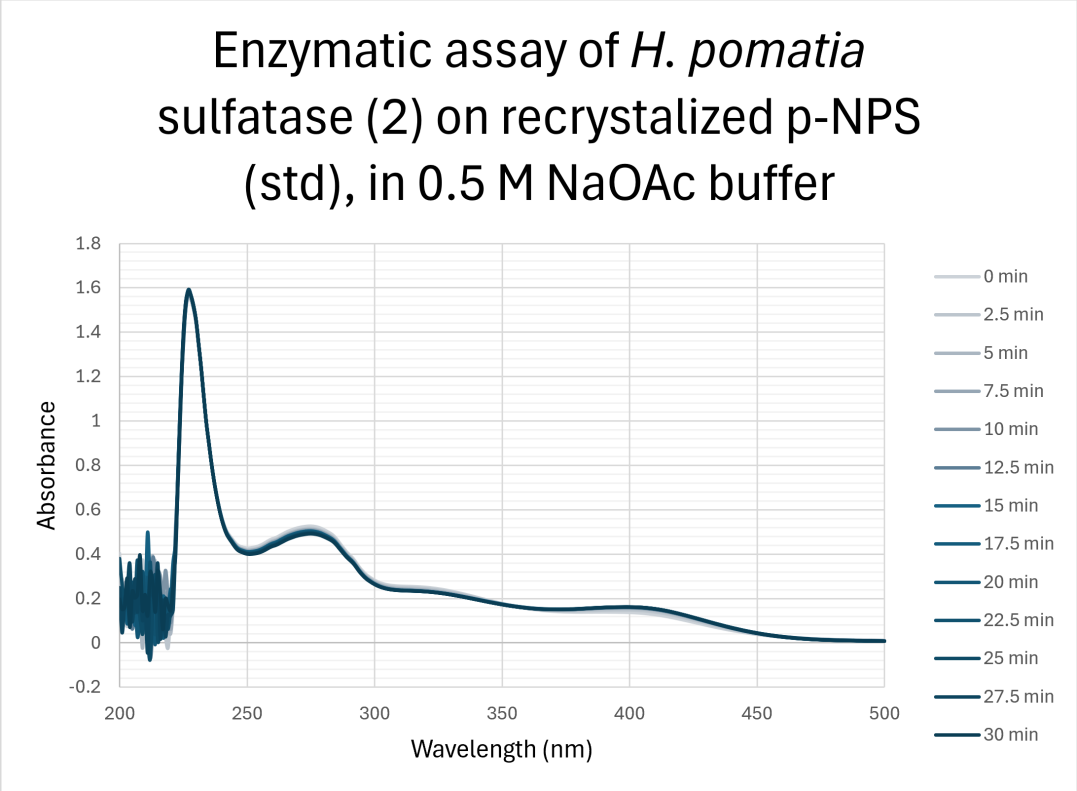

Figure 4.38: Enzymatic assay of *Helix pomatia* sulfatase (source 2) sulfatase on recrystallized p-NPS, synthesized by the standard method, in 0.5 M NaOAc buffer at 37 °C. Scans where made every 2.5 minutes for 30 minutes, in the 200-500 nm range, on November 6th 2025.

4.12.6 Pseudomonas aeruginosa sulfatase and recrsytallized p-NPS (alt) in 0.05 M Tris

Figure 4.39 shows the enzymatic assay of PAS on recrystallized p-NPS, synthesized by the alternative method, in 50 mM Tris buffer at 37 °C. Scans where made every 5 minutes for 35 minutes, in the 200-500 nm range, on October 27th.

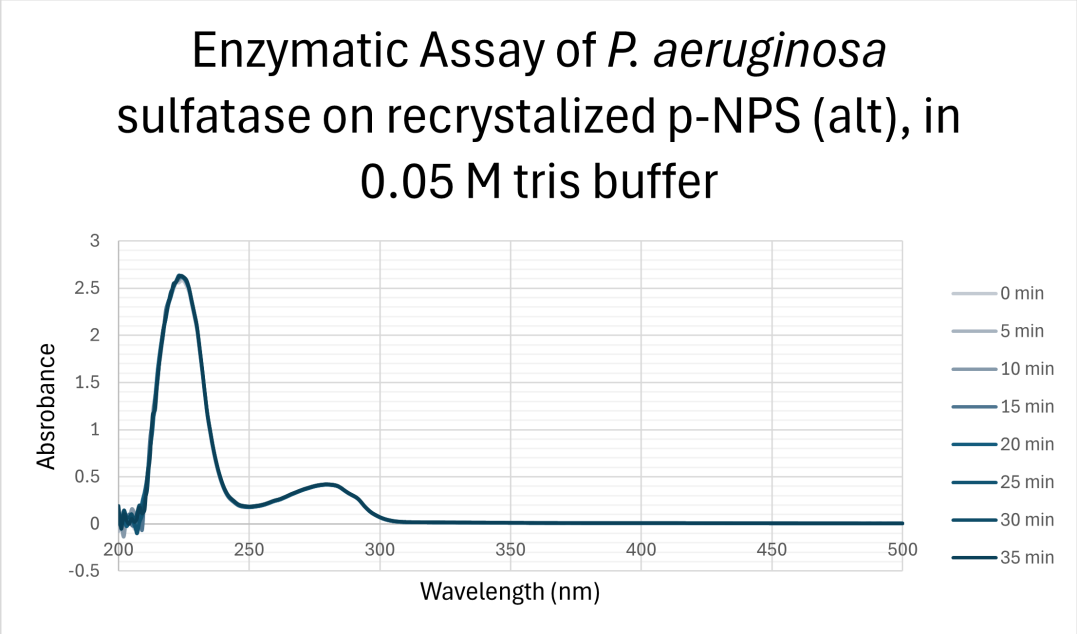

Figure 4.39: Enzymatic assay of PAS on recrystallized p-NPS, synthesized by the alternative method, in 50 mM Tris buffer at 37 °C. Scans where made every 5 minutes for 35 minutes, in the 200-500 nm range, on October 27th 2025.

4.12.7 Pseudomonas aeruginosa sulfatase and recrystallized p-NPS (alt) in DI

Figure 4.40 shows the enzymatic assay of PAS on recrystallized p-NPS, synthesized by the alternative method, in DI water at 37 °C. Scans where made every 5 minutes for 60 minutes, in the 200-500 nm range, on October 30th.

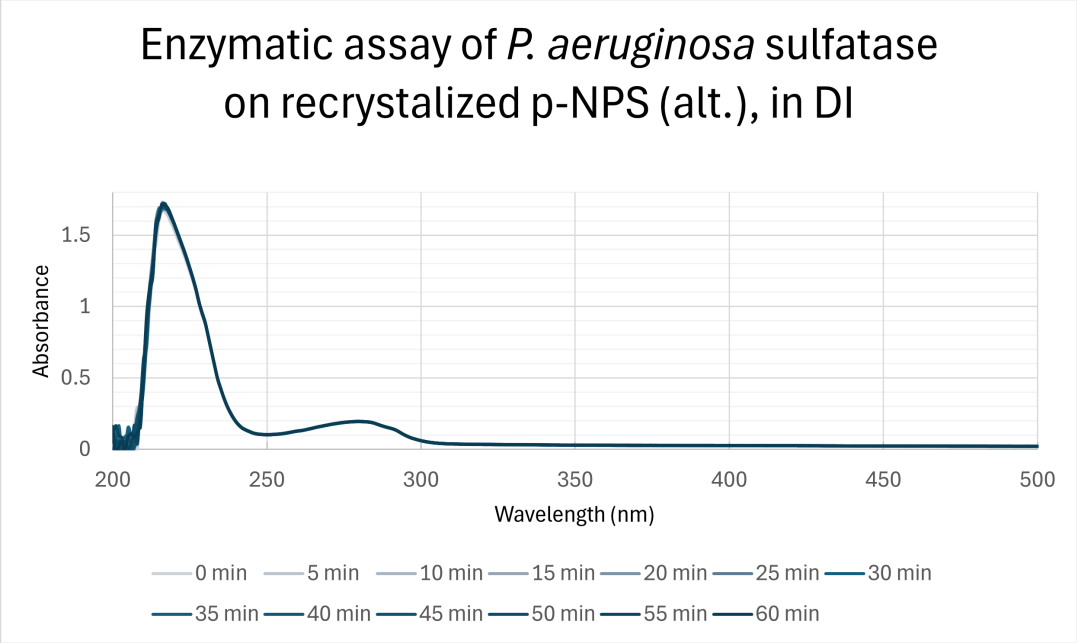

Figure 4.40: Enzymatic assay of PAS on recrystallized p-NPS, synthesized by the alternative method, in DI water at 37 °C. Scans where made every 5 minutes for 60 minutes, in the 200-500 nm range, on October 30th

5
Discussion

The absorbance peak below 230 nm in each buffer solution could either be a $\sigma \rightarrow \sigma^*$ and weak $n \rightarrow \sigma^*$ transitions for amines, or protonated amines, depending on pH. For reference, see figures in section 4.3.

As seen in *Figure* 4.10, in section 4.5, absorbance is highest for each sample at the low end of the evaluated range, at 300 nm. The nominal difference in absorbance between sulfated and "non-sulfated" (in actuality sulfated but blocked by AZ-salt) CNC, henceforth designated $\Delta_{Abs}(CNC, sulfate)$, increases with the dry weight. One explanation for this apparent increase in $\Delta_{Abs}(CNC, sulfate)$ could be the different production dates, people involved in said production, different source material, as well as the resulting non-equal sulfate content (before addition of AZ, in the case of the "non-sulfated batch). This behavior is nonetheless interesting, and could warrant future studies, since it could be indicative of different aggregation behavior. In order to isolate and draw conclusions on the potential impact on absorbance of the sulfate groups being freely accessible on the surface versus them being blocked by AZ salts, the blocking agent would have preferably been added to the same batch used as the sulfated reference, rather then synthesizing two separate batches.

The absorbance spectra of TO and CNC in section 4.6 notably show three peaks in the 400-550 nm range. The peaks at 440 nm corresponds to H-aggregate complexes of TO, aided by the CNC in suspension [7]. Those at 470 nm correspond to TO dimers, and those at 500 nm to TO monomers [7]. See *Figure* 1.4 for reference. For 0.05 WT% CNC and a 1:1 mole ratio of TO to surface sulfate on the CNC (sulfated batch, 265 µmol sulfate/g CNC), shown in *Figure* 4.11, all three forms are roughly equal in proportion at 17.5 µM TO, and at 35 µM TO, but H.aggregates are more prevalent compared to dimers and monomers at 70 µM TO. Doubling the molar ratio to 2:1 TO:sulfate on CNC, as seen in *Figure* 4.12 yields spectra that show higher prevalence of monomers and dimers than H-aggregates for all concentrations of TO, with a stronger trend at 35 µM TO. Interestingly, when the WT% too is doubled, as seen in *Figure* 4.13 the relative occurrence of H-aggregates is highest for 70 mM TO, like in *Figure* 4.11, but for 17.5 and 35 µM TO, dimers and monomers have the highest occurence, like in *Figure* 4.12. As for the absorbance of TO alone (in DSP buffer), *Figure* 4.8 shows how, as the concentration of TO increases, the ratio of dimer to monomer increases, but no peak at 440 nm corresponding to H-aggregates is observed. Taking these observations into account, the H-aggregate response of TO-CNC complexes observed by Jademyr is seemingly corroborated [7].

Comparing the fluorescence spectra of TO in 5 mM DSP, seen in *Figure* 4.14, to the repeat of the experiment performed on the same samples approximately two weeks thereafter, seen in *Figure* 4.15, there is notably a significant decrease in fluorescence in the latter. While the lack of signal for 70 mM TO in *Figure* 4.14 might be explained of as an equipment or handling error, the complete lack of signal for all three concentrations in *Fiure* 4.15 is unlikely to be explained by the same. Also of note is the weak fluorescent signal in the 370-470 nm range of *Figure* 4.15, that was not present in the fresh solutions of TO on December 15th. Possible explanations are degradation of the dye during storage, or - since absorbance shifts are observed due to dimerization and other aggregation patterns of TO, as seen in figures in sections 4.4 and 4.6 - unpredicted aggregation changing the absorbance and thus emission intensity at the chosen excitation wavelength.

The non-linearity of fluorescence intensity (in relation to concentration) that was observed in *Figure* 4.19 and 4.20 - i.e. that doubling of concentration did not double the intensity, assuming real fluorescence occurs - could be explained by the inner filter effect. It arises when the fluorophore concentration is high enough for emitted light to be reabsorbed by the solution itself and thus the measured emission to under-represent the real amount of fluorophore [42], as described further in section 2.6. Since the effect is more prominent for the higher the concentration is, it would also explain why going from 17.5 to 35 µM TO is closer to doubling the intensity than when going from 35 to 70 µM. See

Figures 4.17 and 4.18 belong to the only experiment where two excitation wavelengths were used on the same sample on the same day, which should exclude variation in equipment setting and sample preparation, as well as sample degradation between experiments, as factors. Note that the peaks (within the detected range of wavelengths) are either the same as or double the excitation wavelength of 380 nm.

The apparent emission peaks (of TO, CNC, and mixtures of both) in the fluorescence spectra in sections 4.7, 4.8, and 4.9, are likely to partly or mainly be scattering artifact. This is because they consistently and for all samples (with a wide enough detection range of wavelengths) only occur exactly at or double the excitation wavelength itself, which would be expected for first and second order diffraction, respectively [41], as further described in section 2.6. A complicating factor is the fact that 2nd order diffraction artifacts tend to overlap somewhat with real emission peaks, making definitive conclusions either way harder [41]. It is possible the corresponding emission spectrum in Jademyr's study, see *Figure* 1.5, also was the product of such scattering effects, rather then true emission, since it is also double the excitation wavelength used [7]. An interesting observation is that intensity of emission of combined CNC and TO, as shown in *Figure* 1.5 (Fig. 18 in the report by Jademyr), decreases with increased concentration of TO [7]. But, as illustrated in *Figure* 4.19 and 4.20 in this study, the opposite is seemingly true. A direct comparison of emission spectra of just TO in DSP is not possible, however, as the study by Jademyr did not include such a reference sample [7]. The lack of such a reference makes any comment on possible 2nd order artifacts also in Jademyr's study difficult, since

fluorescence of TO in complex with CNC is expected to be higher due to rotational constriction (as discussed in section 2.2) due to aggregation.

The TO likely degraded or aggregated due to unexpected instability when stored in RT on the lab bench. Of note is the non-uniformity with which the changes in absorbance occur, visible in comparison of *Figures* 4.8 and 4.9: When fresh on December 1st, peaks corresponding to dimers (at 470 nm) and monomers (at 500 nm) are clear, and absorbance increases with concentration of TO; but two weeks later, on December 15th, samples with 17.5 and 70 µM TO are almost completely absent, while some absorbance and distinct peaks remain for the 35 µM TO sample. aggregation or interaction effects, rather than purely degradation. Nonetheless, changes make inter-day comparisons less reliable due to the unknown scale and character of changes. If experiments are repeated, storage in fridge would be preferable.

NMR spectra of TO in *Figure* 4.1 in section 4.1 is consistent with expected theoretical values, indicating correct synthesis and no impurities present. Similarly, NMR spectra of p-NPS in section 4.2, in *Figure* 4.2 synthesized by the standard method and in *Figure* 4.3 by the alternative method, too are consistent with correct synthesis and no impurities. Recrystallization of p-NPS was done to minimize risk of contaminants being the cause of observed errors in the first assays, but comparison of absorbance spectra, e.g. between *Figures* **??** and **??** show no noticeable improvement, supporting the evidence of correct and uncontaminated initial synthesis seen in the NMR spectra in section 4.2. Unfortunately, data storage error resulted in the loss of absorbance data for p-NPS (alt) in NaOAc.

In order to rule out contamination of the source material for the buffer, the three different sources of Tris base available in the lab were tested by UV-Vis spectroscopy. The resulting data, shown in *Figure* 4.5, indicates no contamination in any source.

As seen in the assays in section 4.12, there is little to no enzymatic activity. Since there is seemingly no contamination of buffer solutions, and NMR spectra affirm correct synthesis of the substrate, an obvious aspect to examine is the sulfatase functionality itself. The assays were prepared at room temperature, and performed in the same or at 37 °C, well within the recommended range as discussed in subsections 2.4.1 and 2.4.2. Similarly, the pH of buffer solutions, too, were in acceptable ranges, thus indicating these two parameters likely are not the main contributors to the absent activity. Instead, the preparation and storage are more likely causes, seeing as the enzymes underwent multiple freeze-thaw cycles already before the project, though this is hard to determine after the fact. A more likely explanation is in the enzyme itself being degraded or otherwise low-functioning, or that potential miscalculations caused the concentration of buffer solutions to end up outside the functional range, i.e. being too strong or weak. The case of too strong buffer solutions would, however, not explain the lack of activity in DI water, as seen in *Figure* 4.40, but if some component of the buffers are strictly necessary for measurable activity,the latter case of too weak buffers could partly be to blame. Unfortunately, data storage error resulted in the loss of absorbance data for the assay of PAS on

p-NPS in NaOAc.

Since there is likely more than one sulfatase in the product from *Helix pomatia*, as mentioned in subsection 2.4.1 in section 2.4, it could explain why it is hard to figure out the unexpected lack of activity. One of the enzymes might degrade faster than the others, they might interact or aggregate over time, e.g. when thawing and refreezing in ways that didn't come into effect until after the previous experiments by Horn. However, accounting for factors such as recommended storage temperatures and retest period, as described in section 2.4, neither enzyme is likely to have been significantly degraded in storage, since storage temperature and duration since purchase was within recommendations.

One source of error in the comparison of effects between sulfated and non-sulfated CNC is due to the batches being synthesized independently, i.e. at different times and by different technicians, which introduces variability not accounted for. Another is the assumption that all, or the vast majority of, surface sulfate groups in the latter batch are functionally blocked by the azitidinium salt(s) present in it. If not, an unknown and potentially non-constant apparent sulfate content is used in the experiments to compare to the so called *sulfated CNC batch*. A third source of potential error is introduced if the salt(s) have notable interactions with solvents and substrates, or otherwise affect the absorption and fluorescence spectra during experiments, thus skewing the data in unpredictable ways.

Had the expected signal shifts indicative of successful desulfation of p-NPS in the enzymatic assays been observed, one promising choice of inhibition to evaluate is the addition of a chelator, since it targets the crucial metal-ion present in the active site of the relevant class of enzyme. A chelator such as EDTA, when added to the mixture of enzyme and substrate, will preferentially bind to e.g. the Ca2+ ions in the solution and in the active sites of the enzymes, rendering them permanently inert, with no expected interaction with the substrate (and later on CNC).

Recommendations for further and future study on the topic include ANOVA and multiple testing for scientific rigor, controlled rescue tests of chelator-based inhibition, e.g. using EDTA to target Ca2+ ions in the sulfatases, fluorescence microscopy to study film formation, along with polarized microscopy. For structural analysis atomic force microscopy, scanning or transmission electron microscopy may be utilized, as well as to verify sulfate group removal after successful enzymatic assays.

6
Conclusion

The final outcomes of this project can be directly measured against its seven establishing objectives. The first objective was fully realized, with results aligning with the response observed by Jademyr and corroborating his H-aggregation hypothesis. The second objective was partly realized, in that only reference cases of CNC, TO, and CNC and TO, were examined due to time constraints and unexpected results in references. Results indicate no emission was observed, with peaks instead corresponding to scattering of excitation light. Similarly, the third objective was also only partly realized due to fluorescence spectrometry likely yielding scattering artifacts instead of true emission. Absorbance measurements showed increased nominal difference between sulfated and functionally non-sulfated CNC batches as (i) wt% increases, and as (ii) wavelength increases. This pattern could indicate differential aggregation behavior, but no conclusive statements can be made on current data. Additionally, they showed that absorbance increases with decreased wavelength (in the tested range). The fourth objective was not realized due to time constraints after unforeseen problems with fluorescence and enzymatic assays. The fifth objective was realized, but enzymatic activity could not be validated for any of the experimental conditions. The likeliest (though not necessarily likely) causes are degradation of enzymes due to suboptimal storage and handling, and miscalculations causing buffer concentrations to be too high or low for proper function of said enzymes. The sixth objective was realized, but enzymatic activity was not observed for any of the experimental conditions. The seventh objective was not realized, because enzymatic activity was not successfully reproduced.

One main conclusion is that one or more chemicals had become degraded before or during the study, the reasons behind which could not be unequivocally determined. To address this and ensure a more successful future study, the obvious course of action is to order fresh enzyme, and to thoroughly validate the purity of both buffers. Another is to establish new storage and handling protocols to minimize the risk of degradation. Suggestions include the use of aliquots of standardized concentrations to minimize avoid freeze-thaw cycles, proper labeling of dates on similar containers to ensure batches are used fully and in order of age, and the implementation of a physical log of when each batch was received, first opened and aliquoted, and when and by whom these in turn were used. Yet another main conclusion, based on the interpretation that all observed "fluorescent emission" peaks are likely to be mere artifacts of Rayleigh scattering, is that either i) the theoretical excitation wavelength of TO and CNC was incorrect, ii) the fluorimeter was incorrectly calibrated, set-up, or used, or iii) TO and CNC was incorrectly synthesized, degraded, or contaminated,

or iv) sampled in too low or high concentrations. Since the NMR spectra of TO in A.1.3 is consistent with theoretical expectations of the pure substance, and the pattern of peaks being whole number multiples of excitation wavelength (that is typical of Rayleigh scattering) is seemingly the same for TO as for CNC and mixtures of the two, (iii) can be more or less ruled out.

Bibliography

[1] I. Boltes et al., "1.3 Å Structure of Arylsulfatase from Pseudomonas aeruginosa Establishes the Catalytic Mechanism of Sulfate Ester Cleavage in the Sulfatase Family," *Structure*, vol. 9, no. 6, pp. 483–491, Jun. 2001, ISSN: 09692126. DOI: 10.1016/S0969-2126(01)00609-8.

[2] K. Malekpour, A. Hazrati, A. Khosrojerdi, L. Roshangar, and M. Ahmadi, "An overview to nanocellulose clinical application: Biocompatibility and opportunities in disease treatment," *Regenerative Therapy*, vol. 24, pp. 630–641, Dec. 2023, ISSN: 23523204. DOI: 10.1016/j.reth.2023.10.006.

[3] Y. Xu, Z. Wu, A. Li, N. Chen, J. Rao, and Q. Zeng, "Nanocellulose Composite Films in Food Packaging Materials: A Review," *Polymers*, vol. 16, no. 3, p. 423, Feb. 2024, ISSN: 2073-4360. DOI: 10.3390/polym16030423.

[4] P. Bose, *The Applications of Crystalline Nanocellulose (CNC)*, Nov. 2019. [Online]. Available: https://www.azonano.com/article.aspx?ArticleID=5328.

[5] Y. Lee, H. Zhang, H.-Y. Yu, and K. C. Tam, "Electroconductive cellulose nanocrystals — Synthesis, properties and applications: A review," *Carbohydrate Polymers*, vol. 289, p. 119 419, Aug. 2022, ISSN: 01448617. DOI: 10.1016/j.carbpol.2022.119419.

[6] E. Marino, R. A. LaCour, and T. E. Kodger, "Emergent Properties from Three-Dimensional Assemblies of (Nano)particles in Confined Spaces," *Crystal Growth & Design*, vol. 24, no. 14, pp. 6060–6080, Jul. 2024, ISSN: 1528-7483. DOI: 10.1021/acs.cgd.4c00260.

[7] S. Jademyr, *Nanocrystalline Cellulose as a Drug Carrier of Cyanine Dyes to DNA*, Gothenburg, 2016. [Online]. Available: https://hdl.handle.net/20.500.12380/240591.

[8] E. Horn, *The Enzymatic Desulfation of Cellulose Nanocrystals using Sulfatase*, Gothenburg, 2024. [Online]. Available: https://hdl.handle.net/20.500.12380/308484.

[9] S. R. Hanson, M. D. Best, and C.-H. Wong, "Sulfatases: Structure, Mechanism, Biological Activity, Inhibition, and Synthetic Utility," *Angewandte Chemie International Edition*, vol. 43, no. 43, pp. 5736–5763, Nov. 2004, ISSN: 1433-7851. DOI: 10.1002/anie.200300632.

[10] H. J. Karlsson, M. Eriksson, E. Perzon, B. Åkerman, P. Lincoln, and G. Westman, "Groove-binding unsymmetrical cyanine dyes for staining of DNA: syntheses and characterization of the DNA-binding," *Nucleic Acids Research*,

vol. 31, no. 21, pp. 6227–6234, Nov. 2003, ISSN: 1362-4962. DOI: 10.1093/nar/gkg821.

[11] United Nations Department of Economic and Social Affairs, *THE 17 GOALS*. [Online]. Available: https://sdgs.un.org/goals.

[12] C. Liu, Y. Lu, S. He, Q. Wang, L. Zhao, and X. Zeng, "The nature of the styrylindolium dye: transformations among its monomer, aggregates and water adducts," *Journal of Materials Chemistry C*, vol. 1, no. 31, p. 4770, 2013, ISSN: 2050-7526. DOI: 10.1039/c3tc30768a.

[13] S. Beck and J. Bouchard, "Auto-catalyzed acidic desulfation of cellulose nanocrystals," *Nordic Pulp & Paper Research Journal*, vol. 29, no. 1, pp. 6–14, Jan. 2014, ISSN: 2000-0669. DOI: 10.3183/npprj-2014-29-01-p006-014.

[14] S. Elazzouzi-Hafraoui, Y. Nishiyama, J.-L. Putaux, L. Heux, F. Dubreuil, and C. Rochas, "The Shape and Size Distribution of Crystalline Nanoparticles Prepared by Acid Hydrolysis of Native Cellulose," *Biomacromolecules*, vol. 9, no. 1, pp. 57–65, Jan. 2008, ISSN: 1525-7797. DOI: 10.1021/bm700769p.

[15] National Nanotechnology Initiative, *Applications of Nanotechnology*. [Online]. Available: https://www.nano.gov/about-nanotechnology/applications-nanotechnology/.

[16] A. Yurtsever et al., "Molecular insights on the crystalline cellulose-water interfaces via three-dimensional atomic force microscopy," *Science Advances*, vol. 8, no. 41, Oct. 2022, ISSN: 2375-2548. DOI: 10.1126/sciadv.abq0160.

[17] K. Heise et al., "Spatioselective surface chemistry for the production of functional and chemically anisotropic nanocellulose colloids," *Journal of Materials Chemistry A*, vol. 10, no. 44, pp. 23 413–23 432, 2022, ISSN: 2050-7488. DOI: 10.1039/D2TA05277F.

[18] S. Llàcer Navarro, "Role of Sulfate Half-Ester Groups on Oxidative Modifications and Network Formation of Cellulose Nanocrystals," Ph.D. dissertation, Chalmers University of Technology, Gothenburg, 2023, ISBN: 978-91-7905-856-2. [Online]. Available: https://research.chalmers.se/en/publication/536143.

[19] R. Kádár, S. Spirk, and T. Nypelö, "Cellulose Nanocrystal Liquid Crystal Phases: Progress and Challenges in Characterization Using Rheology Coupled to Optics, Scattering, and Spectroscopy," *ACS Nano*, vol. 15, no. 5, pp. 7931–7945, May 2021, ISSN: 1936-0851. DOI: 10.1021/acsnano.0c09829.

[20] S. Saffarionpour, "Nanocellulose for Stabilization of Pickering Emulsions and Delivery of Nutraceuticals and Its Interfacial Adsorption Mechanism," *Food and Bioprocess Technology*, vol. 13, no. 8, pp. 1292–1328, Aug. 2020, ISSN: 1935-5130. DOI: 10.1007/s11947-020-02481-2.

[21] Smart Glass World, *What is a Liquid Crystal?* [Online]. Available: https://www.smartglassworld.net/what-is-a-liquid-crystal.

[22] J. Majoinen et al., "Controlling the Nematic Liquid Crystallinity of Cellulose Nanocrystals with an Alcohol Ethoxy Sulfonate Surfactant," *Biomacromolecules*, vol. 25, no. 7, pp. 3909–3919, Jul. 2024, ISSN: 1525-7797. DOI: 10.1021/acs.biomac.3c01375.

[23] I. Dierking and S. Al-Zangana, "Lyotropic Liquid Crystal Phases from Anisotropic Nanomaterials," *Nanomaterials*, vol. 7, no. 10, p. 305, Oct. 2017, ISSN: 2079-4991. DOI: 10.3390/nano7100305.

[24] A. Fox, "A study of optical propagation in polymer liquid crystal nanocomposites for photolithography applications," Ph.D. dissertation, Drexel University, 2009. DOI: https://doi.org/10.17918/ETD-3106.

[25] G. M. Ziarani, H. Kruger, R. Moradi, and N. Lashgari, *Metal-Free Synthetic Organic Dyes*. Elsevier, 2018, pp. 127–152, ISBN: 9780128156476. DOI: 10.1016/C2017-0-03672-8.

[26] K. Ilina and M. Henary, "Cyanine Dyes Containing Quinoline Moieties: History, Synthesis, Optical Properties, and Applications," *Chemistry – A European Journal*, vol. 27, no. 13, pp. 4230–4248, Mar. 2021, ISSN: 0947-6539. DOI: 10.1002/chem.202003697.

[27] N. Svanvik, G. Westman, D. Wang, and M. Kubista, "Light-Up Probes: Thiazole Orange-Conjugated Peptide Nucleic Acid for Detection of Target Nucleic Acid in Homogeneous Solution," *Analytical Biochemistry*, vol. 281, no. 1, pp. 26–35, May 2000, ISSN: 00032697. DOI: 10.1006/abio.2000.4534.

[28] M. Liang et al., "A Convenient Thiazole Orange Fluorescence Assay for the Evaluation of DNA Duplex Hybridization Stability," *Molecular Imaging and Biology*, vol. 11, no. 6, pp. 439–445, Nov. 2009, ISSN: 1536-1632. DOI: 10.1007/s11307-009-0221-4.

[29] MedChemExpress, *Thiazole Orange*. [Online]. Available: https://www.medchemexpress.com/Thiazole-Orange.html.

[30] T. G. Gardner and Z. N. Senwo, "Enzymatic Hydrolysis of an Organic Sulfur Compound," *Advances in Enzyme Research*, vol. 07, no. 01, pp. 1–13, 2019, ISSN: 2328-4846. DOI: 10.4236/aer.2019.71001.

[31] Thermo Scientific Chemicals, *4-Nitrophenyl sulfate, potassium salt, 99+%*. [Online]. Available: https://www.thermofisher.com/order/catalog/product/227490010.

[32] Nomenclature Committee of the International Union of Biochemistry and Molecular Biology, "The Enzyme List Class 3 — Hydrolases," in *The Enzyme List*, International Union of Biochemistry and Molecular Biology (IUBMB), 2023, ch. 3. [Online]. Available: https://www.enzyme-database.org/downloads.php.

[33] E. C. Webb, *Enzyme nomenclature 1992 : recommendations of the Nomenclature Committee of the International Union of Biochemistry and Molecular Biology on the nomenclature and classification of enzymes*. Published for the International Union of Biochemistry and Molecular Biology by Academic Press, 1992, p. 862, ISBN: 9780122271649.

[34] M. Stam, P. Lelièvre, M. Hoebeke, E. Corre, T. Barbeyron, and G. Michel, "SulfAtlas, the sulfatase database: state of the art and new developments," *Nucleic Acids Research*, vol. 51, no. D1, pp. D647–D653, Jan. 2023, ISSN: 0305-1048. DOI: 10.1093/nar/gkac977.

[35] T. A. Brandao and A. C. Hengge, "Phosphoryl and Sulfuryl Transfer," in *Comprehensive Natural Products II*, Elsevier, 2010, pp. 315–348. DOI: 10.1016/B978-008045382-8.00684-5.

[36] Merck, *Sulfatase from Helix pomatia*, 2026. [Online]. Available: https://www.sigmaaldrich.com/FR/en/product/sigma/s9626?srsltid=AfmBOopw102_sjhFMLRaIg-wLopt_O1eDQbqcf45qeZx-w7MXzN7ovaI.

[37] U. Wittstock, M. Fischer, I. Svendsen, and B. A. Halkier, "Cloning and Characterization of Two cDNAs Encoding Sulfatases in the Roman Snail, Helix pomatia," *IUBMB Life*, vol. 49, no. 1, pp. 71–76, Jan. 2000, ISSN: 1521-6543. DOI: 10.1080/713803591.

[38] S. P. Diggle and M. Whiteley, "Microbe Profile: Pseudomonas aeruginosa: opportunistic pathogen and lab rat," *Microbiology*, vol. 166, no. 1, pp. 30–33, Jan. 2020, ISSN: 1350-0872. DOI: 10.1099/mic.0.000860.

[39] Merck, *Arylsulfatase, Enhanced, Recombinant*. [Online]. Available: https://www.sigmaaldrich.com/FR/en/product/sigma/sae0213?srsltid=AfmBOorH838DLKZZY3Gli.

[40] LibreTexts, *2.1.5: Spectrophotometry*. [Online]. Available: https://chem.libretexts.org/Bookshelves/Physical_and_Theoretical_Chemistry_Textbook_Maps/Supplemental_Modules_(Physical_and_Theoretical_Chemistry)/Kinetics/02%3A_Reaction_Rates/2.01%3A_Experimental_Determination_of_Kinetics/2.1.05%3A_Spectrophotometry.

[41] Edinburgh Instruments, *Second Order Diffraction through a Monochromator – Common Errors in Fluorescence Spectroscopy*, Jul. 2021. [Online]. Available: https://www.edinst.com/resource/second-order-diffraction-through-a-monochromator-common-errors-in-fluorescence-spectroscopy/.

[42] J. Lakowicz, *Principles of Fluorescence Spectroscopy*, J. R. Lakowicz, Ed. Boston, MA: Springer US, 2006, ISBN: 978-0-387-31278-1. DOI: 10.1007/978-0-387-46312-4.

[43] G. Barnå, J. Benjaminsson, M. Clark, W. Lundström, V. Preinitz Gärdinge, and A. Young, *Mekaniska och aktiva egenskaper hos strukturer av nanokristallin cellulosa*, Gothenburg, 2023. [Online]. Available: https://hdl.handle.net/20.500.12380/306441.

[44] K. Mori, *Method for producing p-nitrophenyl sulfate*, Jul. 2017.

[45] Agilent Technologies, "Cary 3500 Multicell UV-Vis Spectrophotometer," [Online]. Available: https://www.agilent.com/en/product/molecular-spectroscopy/uv-vis-uv-vis-nir-spectroscopy/uv-vis-uv-vis-nir-systems/cary-3500-multicell-uv-vis-spectrophotometer.

A

Supporting figures

A.1 NMR spectra

A.1.1 NMR spectra of p-NPS by standard method

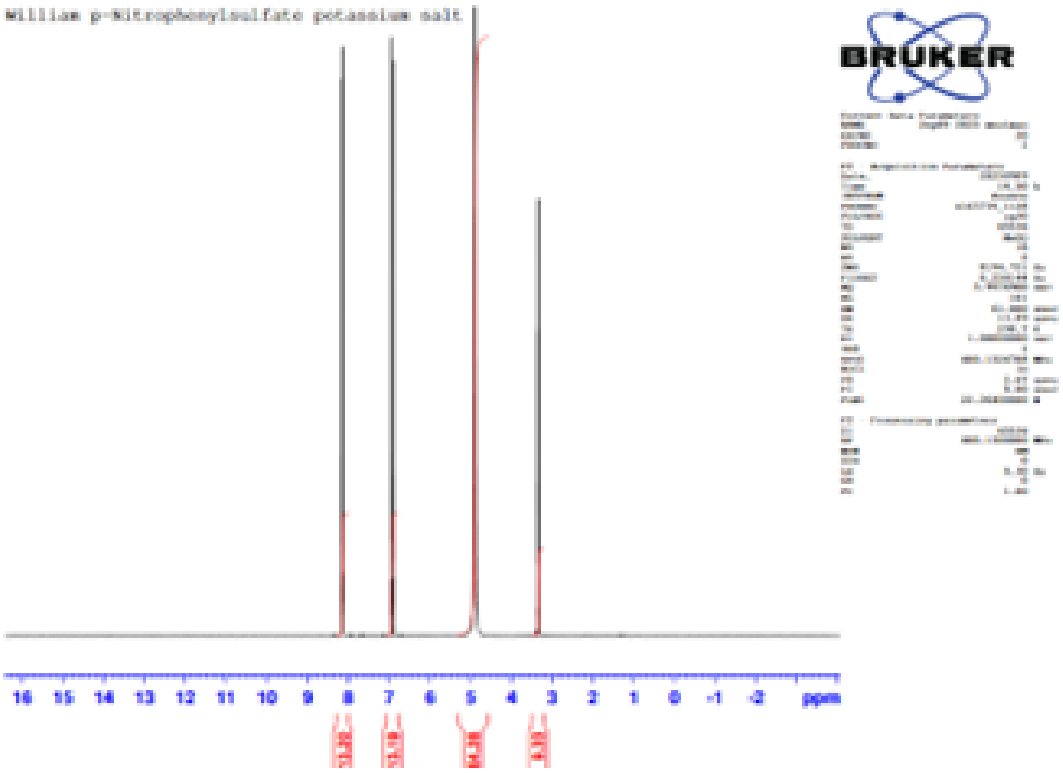

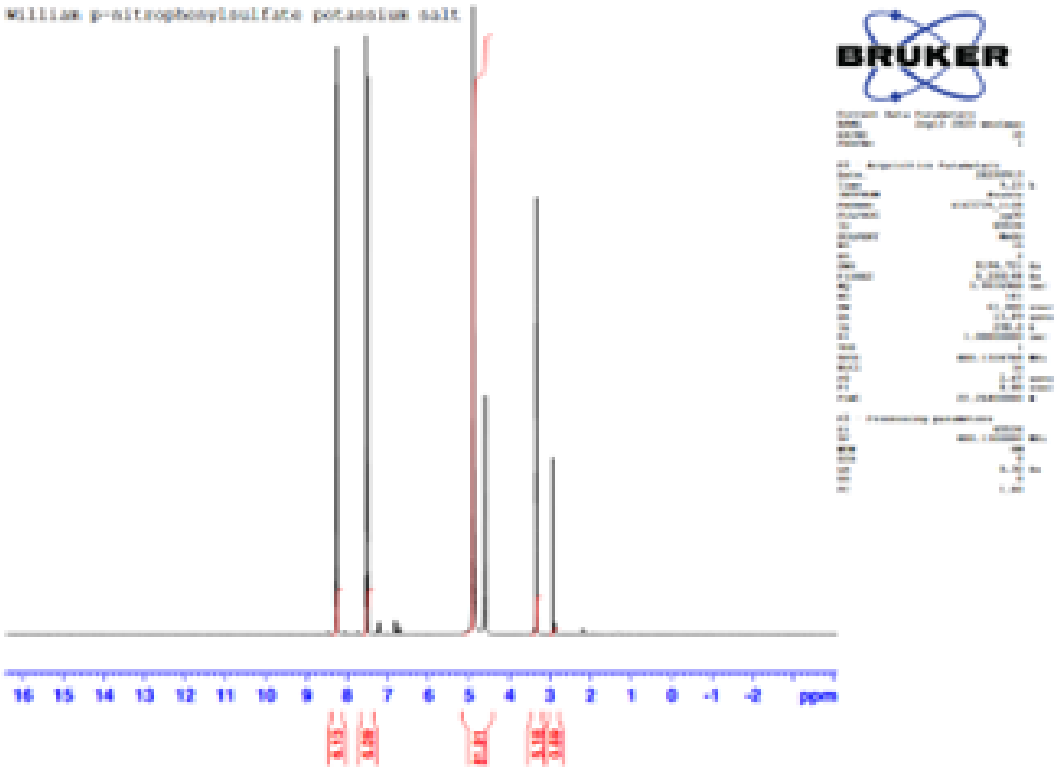
William p-nitrophenylsulfate potassium salt
BRUKER
16 15 14 13 12 11 10 9 8 7 6 5 4 3 2 1 0 -1 -2 ppm

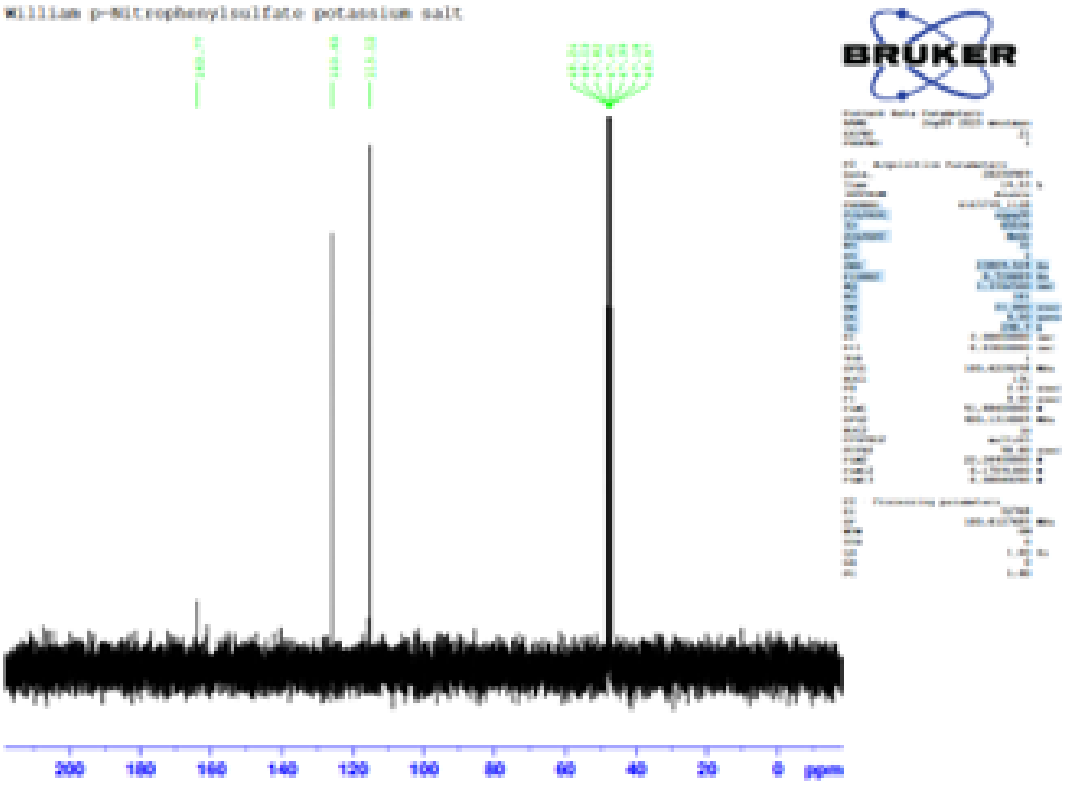
William p-Nitrophenylsulfate potassium salt
BRUKER
200 180 160 140 120 100 80 60 40 20 0 ppm

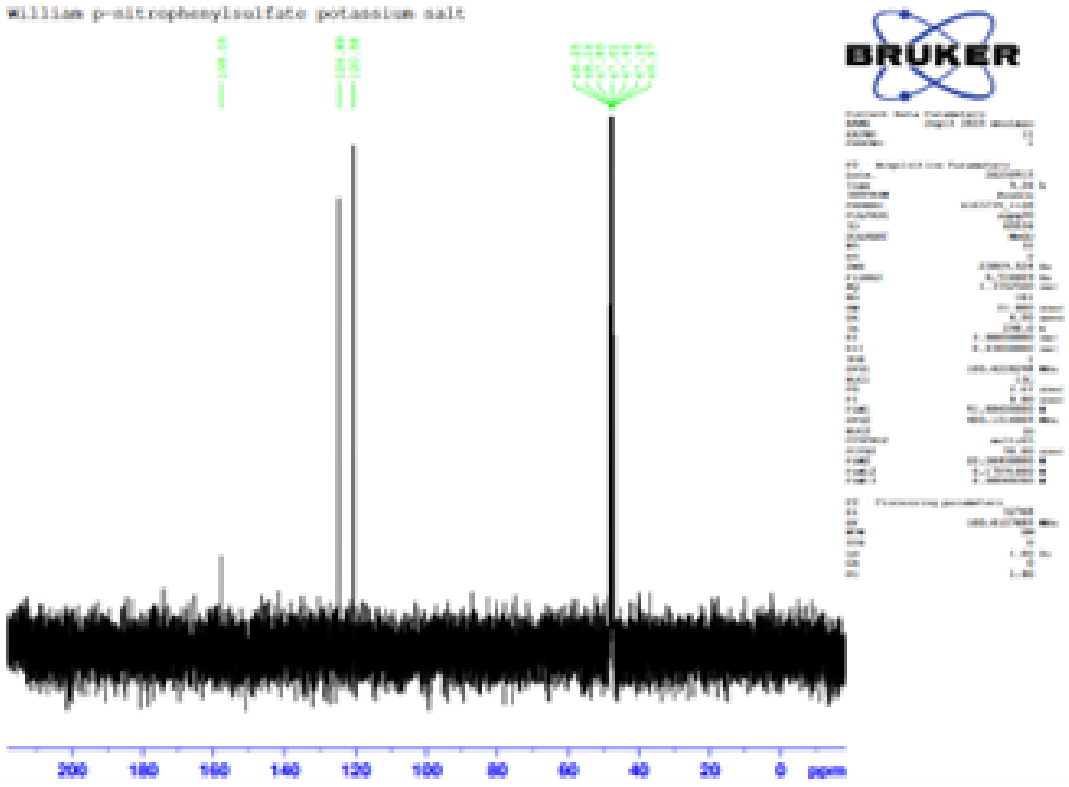

A.1.2 NMR spectra of p-NPS by alternate method

IV

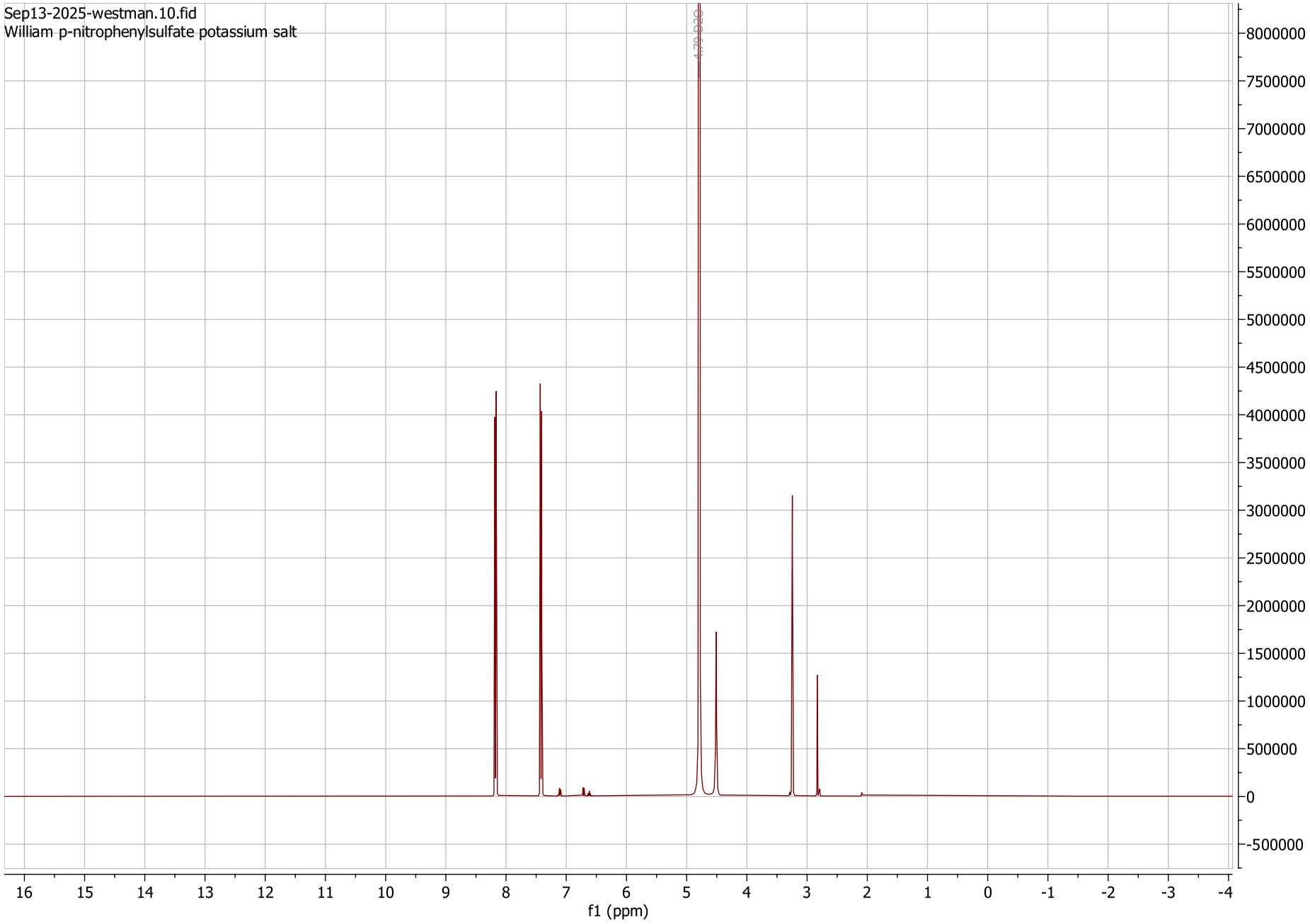
Sep13-2025-westman.10.fid
William p-nitrophenylsulfate potassium salt
4.936
8000000
7500000
7000000
6500000
6000000
5500000
5000000
4500000
4000000
3500000
3000000
2500000
2000000
1500000
1000000
500000
0
-500000
16
15
14
13
12
11
10
9
8
7
6
5
4
3
2
1
0
-1
-2
-3
-4
f1 (ppm)

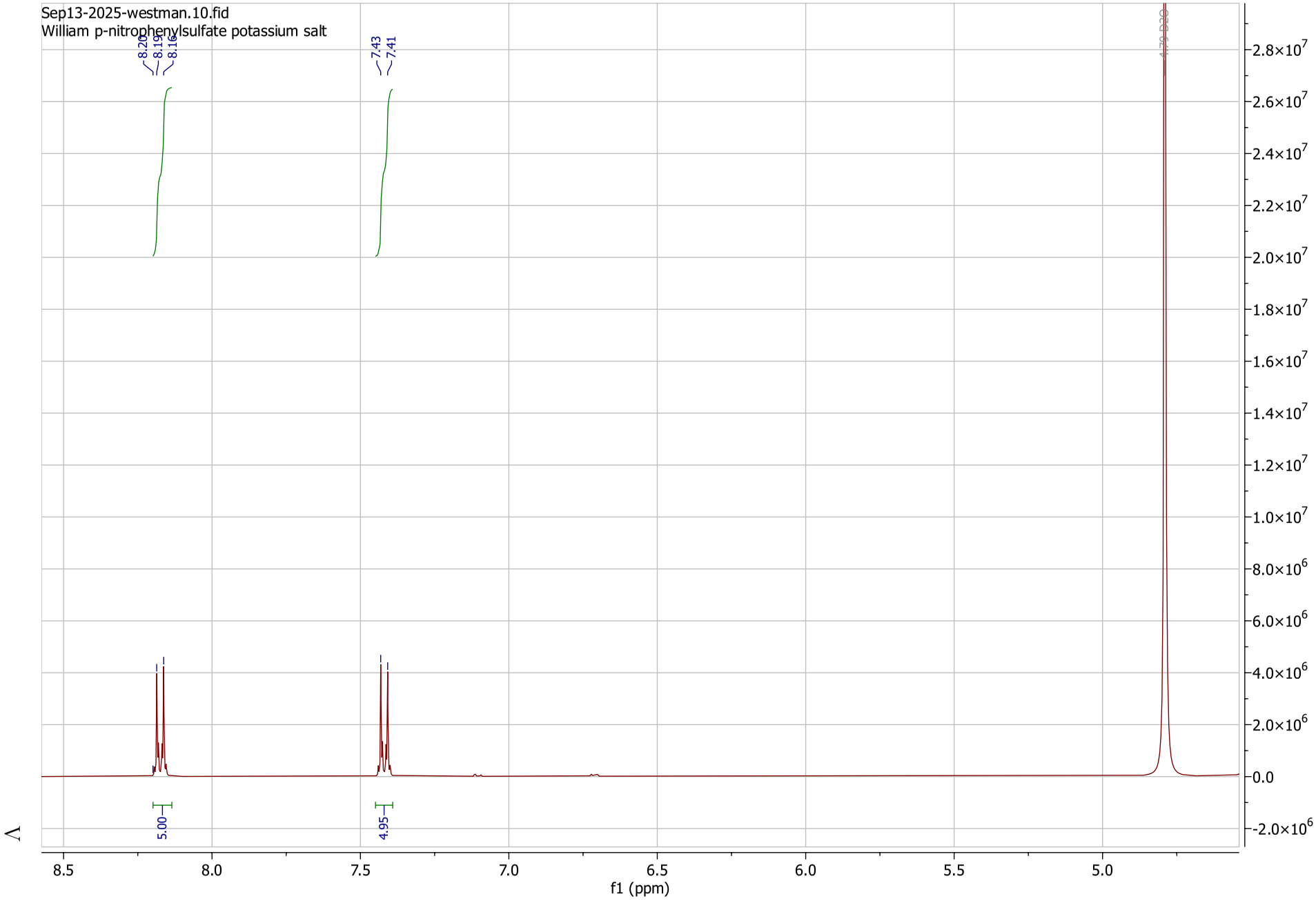
Sep13-2025-westman.10.fid
William p-nitrophenylsulfate potassium salt
8.20
8.19
8.16
7.43
7.41
4.70
5.00
4.95
2.8×10^7
2.6×10^7
2.4×10^7
2.2×10^7
2.0×10^7
1.8×10^7
1.6×10^7
1.4×10^7
1.2×10^7
1.0×10^7
8.0×10^6
6.0×10^6
4.0×10^6
2.0×10^6
0.0
-2.0×10^6
8.5
8.0
7.5
7.0
6.5
6.0
5.5
5.0
f1 (ppm)

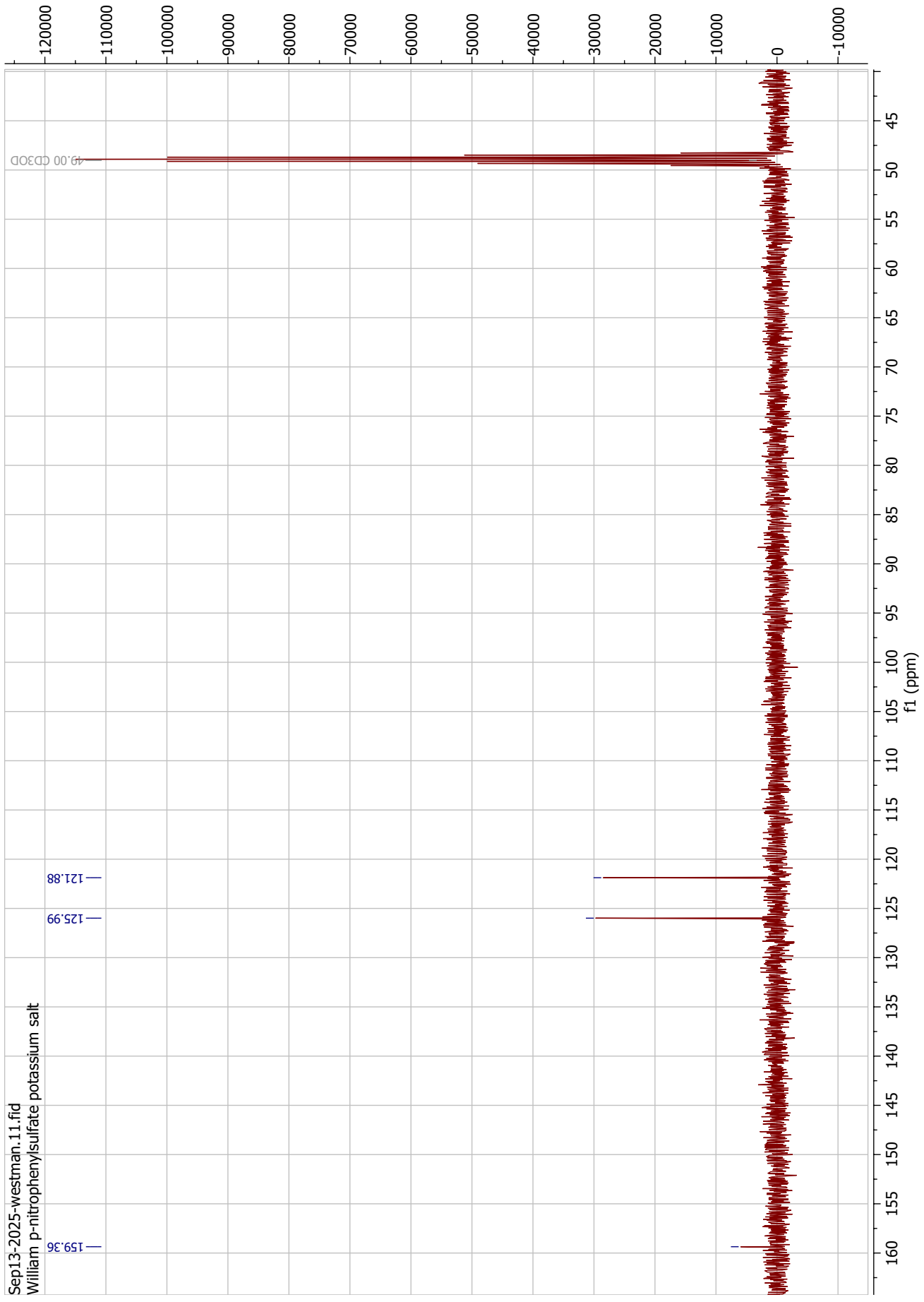
Sep13-2025-westman.11.fid
William p-nitrophenylsulfate potassium salt
49.00 CD3OD
121.88
125.99
159.36
f1 (ppm)

A.1.3 NMR spectra of TO

VIII

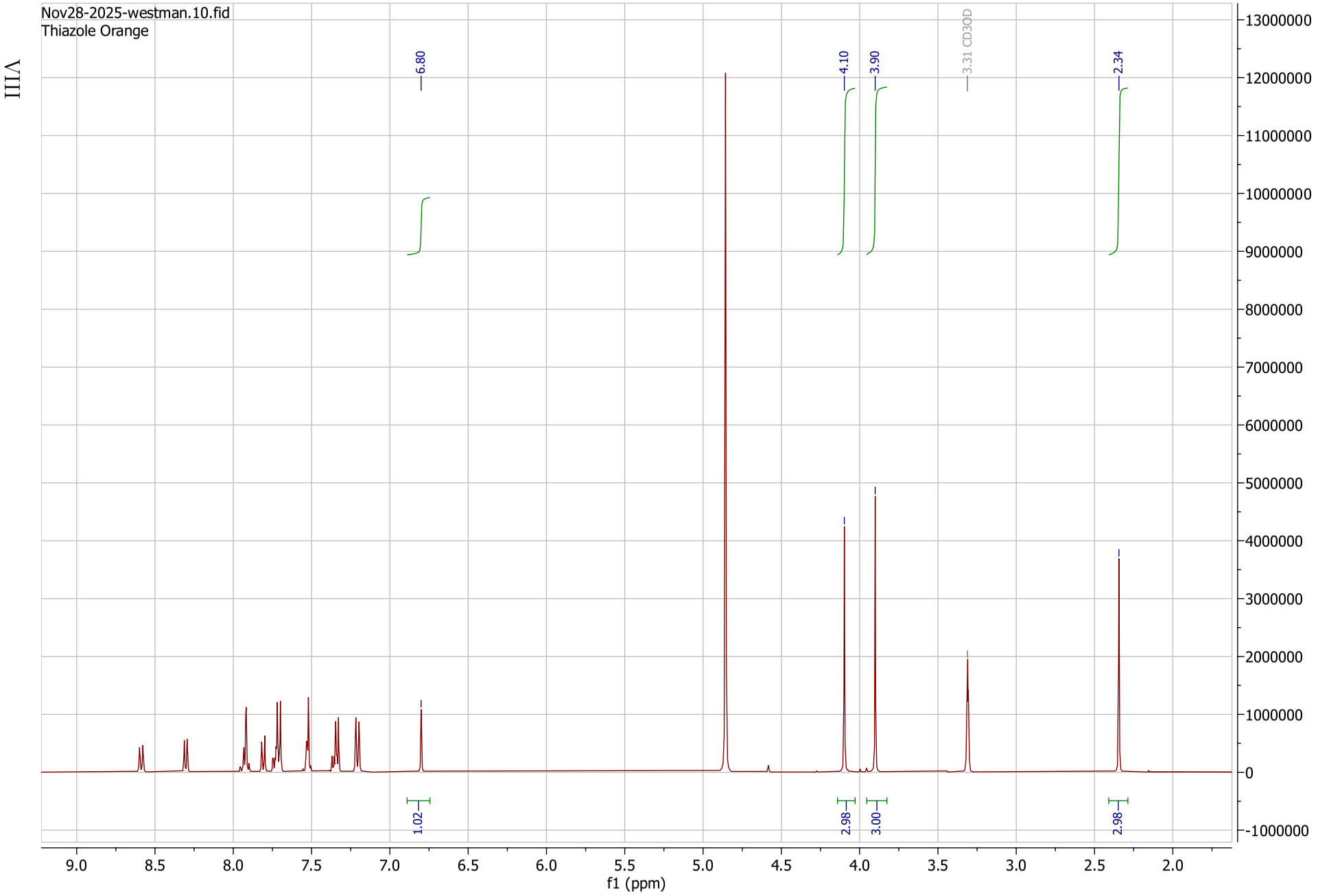
Nov28-2025-westman.10.fid
Thiazole Orange
6.80
4.10
3.90
3.31 CD3OD
2.34
1.02
2.98
3.00
2.98
f1 (ppm)

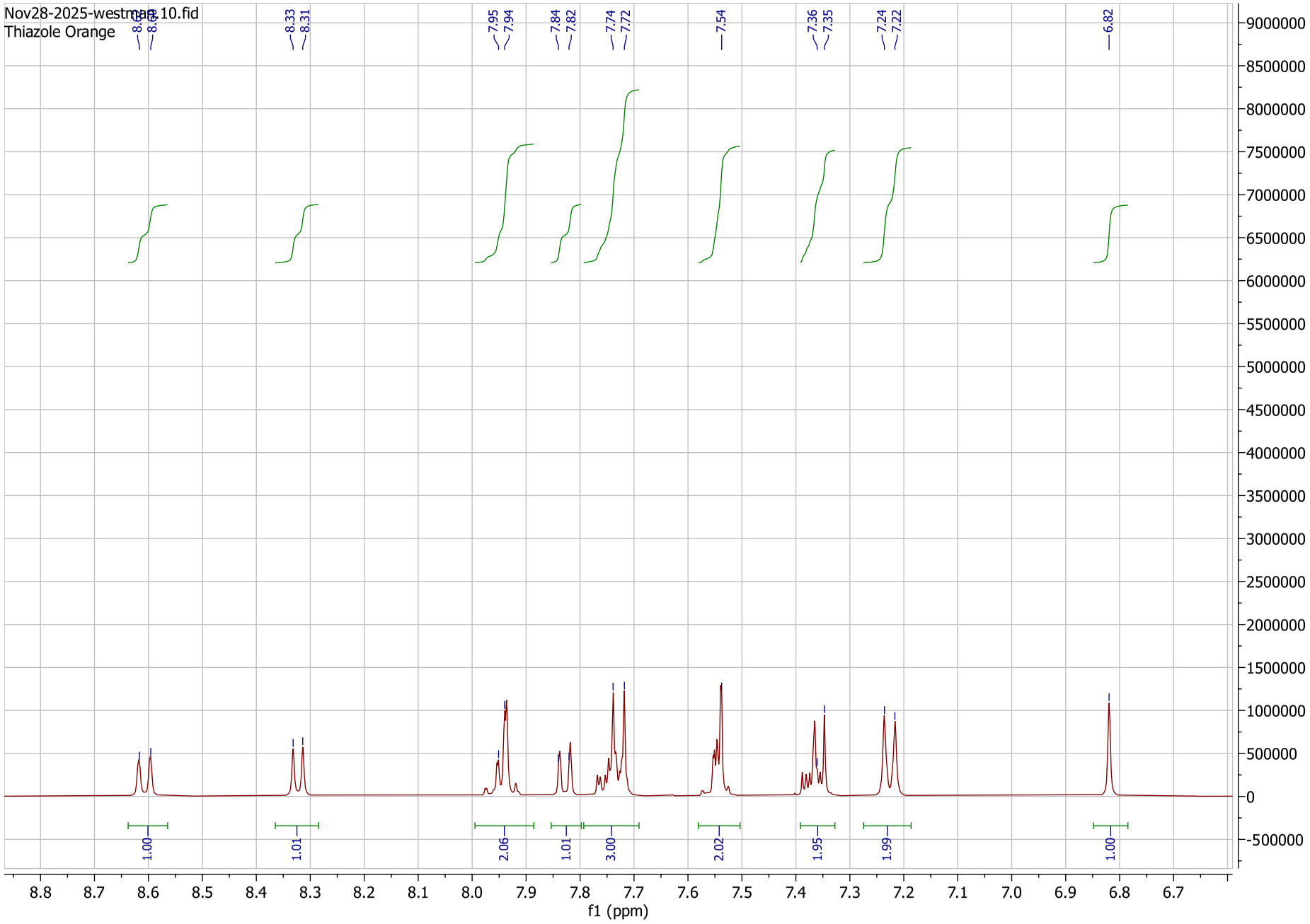
Nov28-2025-westman 10.fid
Thiazole Orange
8.33
8.31
7.95
7.94
7.84
7.82
7.74
7.72
7.54
7.36
7.35
7.24
7.22
6.82
1.00
1.01
2.06
1.01
3.00
2.02
1.95
1.99
1.00
f1 (ppm)

XI

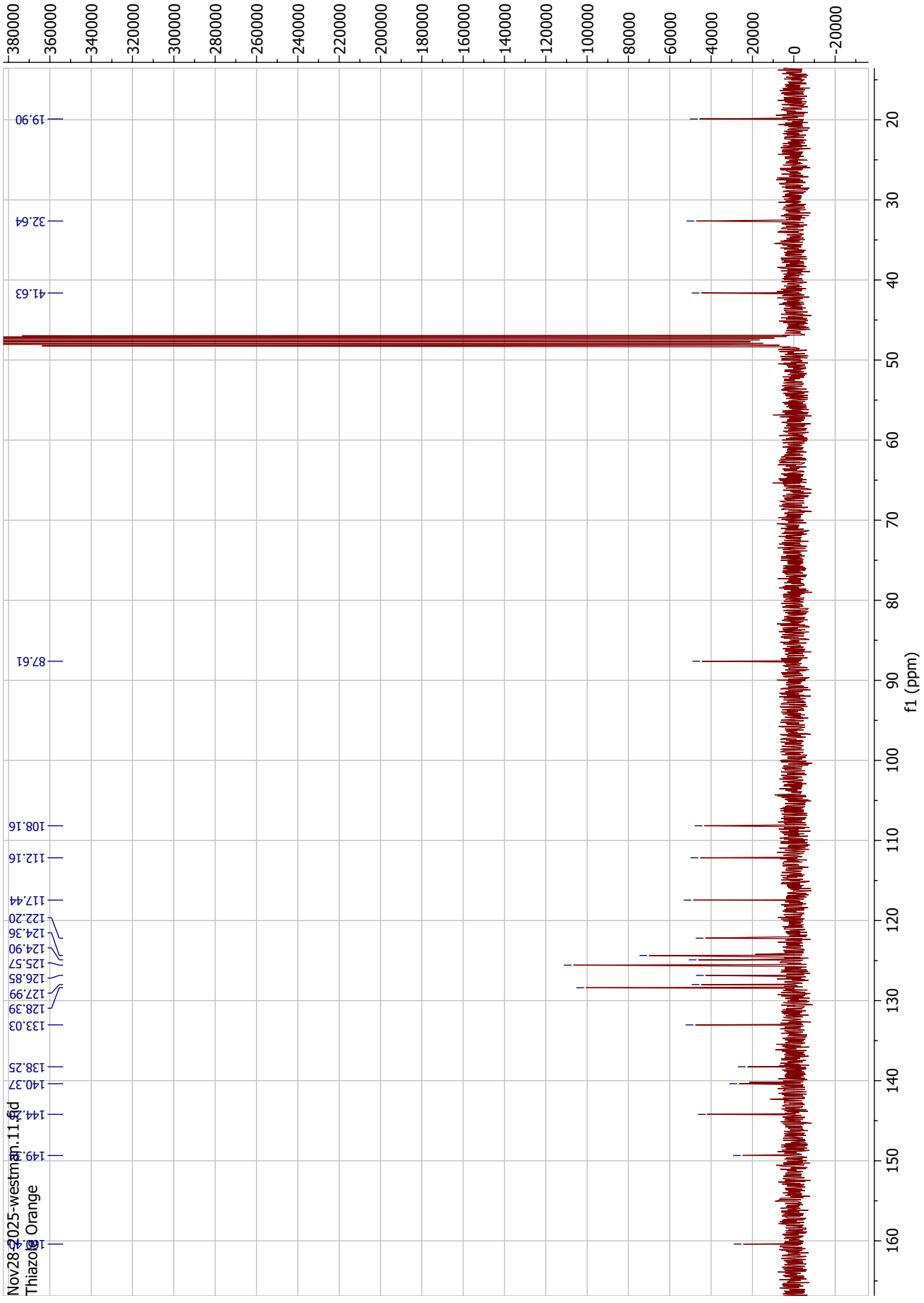

Nov28-2025-westman.11.fid
Thiazole Orange
f1 (ppm)
19.90
32.64
41.63
87.61
108.16
112.16
117.44
122.20
124.36
124.90
125.57
126.85
127.99
128.39
133.03
138.25
140.37
144.26
149.31
160.42

X

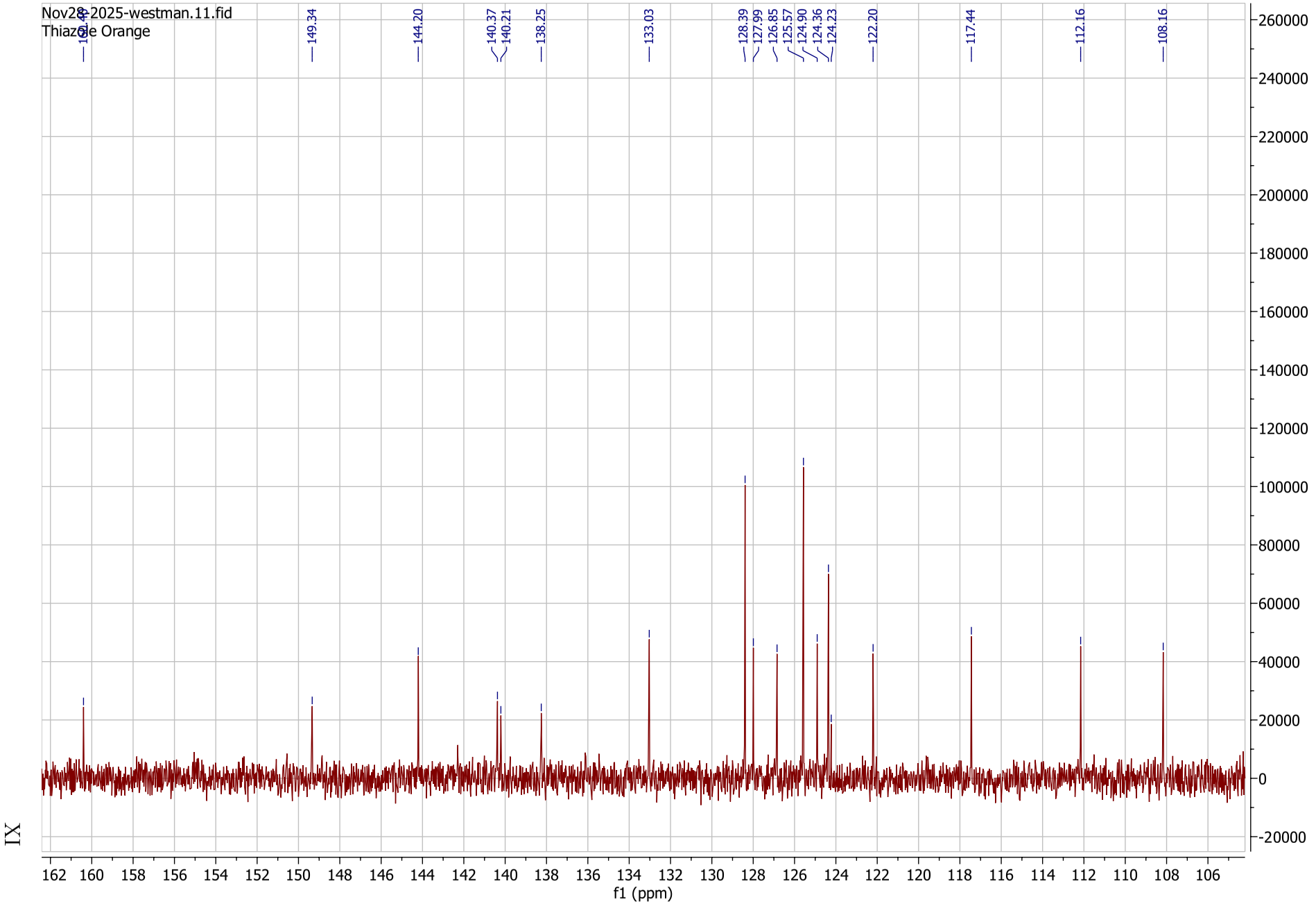
Nov28-2025-westman.11.fid
Thiazole Orange
159.44
149.34
144.20
140.37
140.21
138.25
133.03
128.39
127.99
126.85
125.57
124.90
124.36
124.23
122.20
117.44
112.16
108.16
260000
240000
220000
200000
180000
160000
140000
120000
100000
80000
60000
40000
20000
0
-20000
162 160 158 156 154 152 150 148 146 144 142 140 138 136 134 132 130 128 126 124 122 120 118 116 114 112 110 108 106
f1 (ppm)

IX

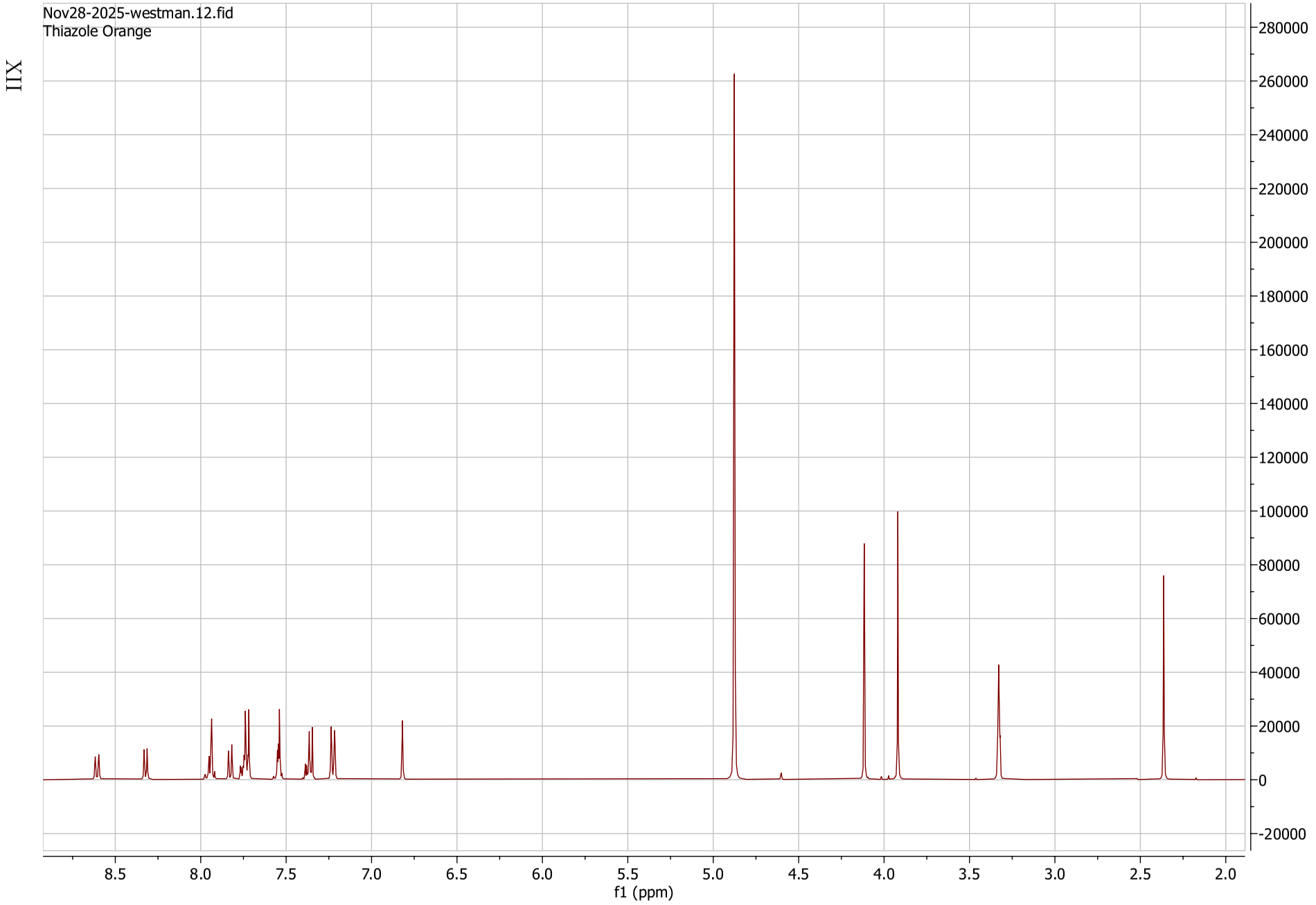
Nov28-2025-westman.12.fid
Thiazole Orange
XII
280000
260000
240000
220000
200000
180000
160000
140000
120000
100000
80000
60000
40000
20000
0
-20000
8.5
8.0
7.5
7.0
6.5
6.0
5.5
5.0
4.5
4.0
3.5
3.0
2.5
2.0
f1 (ppm)

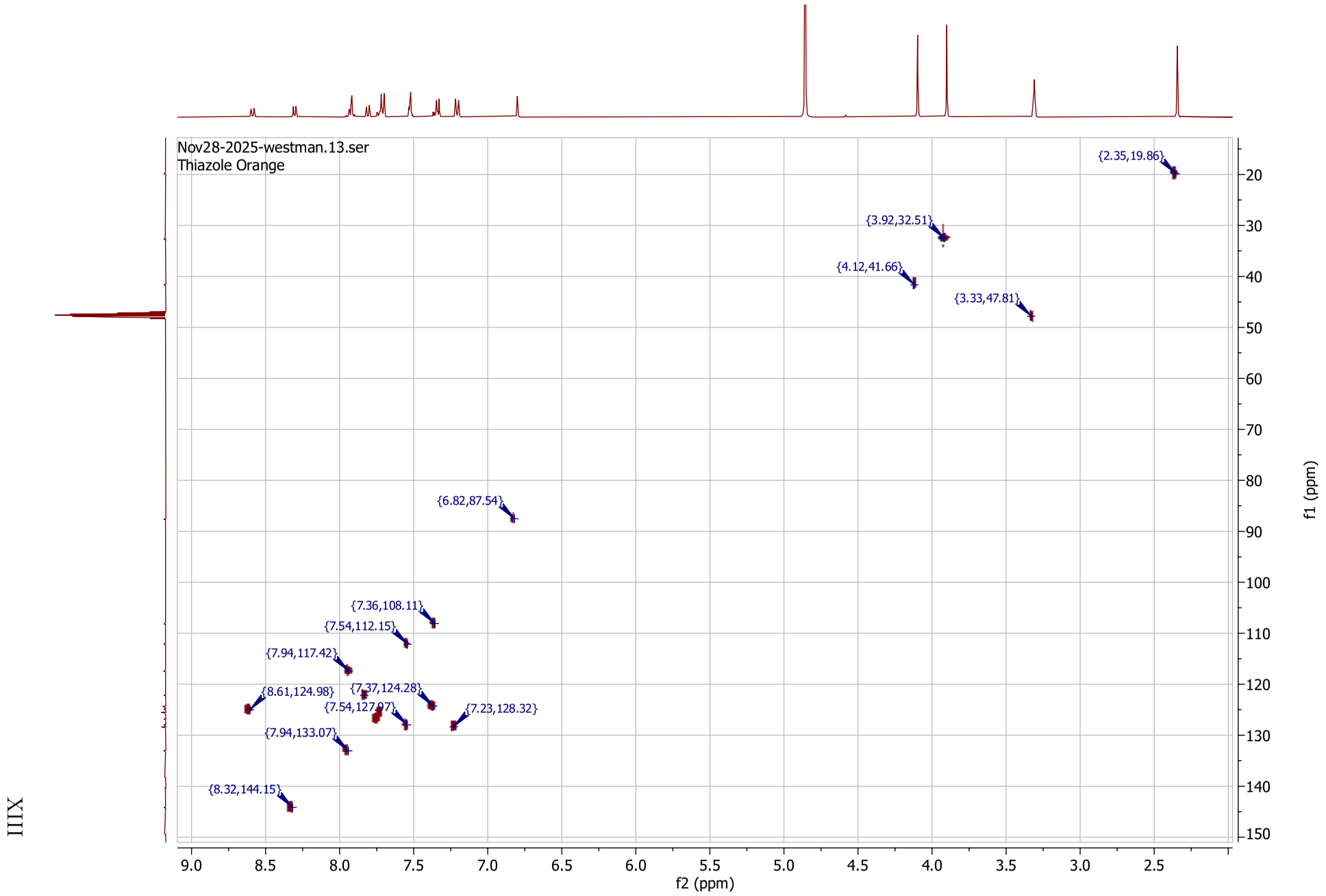
Nov28-2025-westman.13.ser
Thiazole Orange
{2.35,19.86}
{3.92,32.51}
{4.12,41.66}
{3.33,47.81}
{6.82,87.54}
{7.36,108.11}
{7.54,112.15}
{7.94,117.42}
{8.61,124.98}
{7.37,124.28}
{7.54,127.97}
{7.23,128.32}
{7.94,133.07}
{8.32,144.15}
f2 (ppm)
f1 (ppm)

XIII

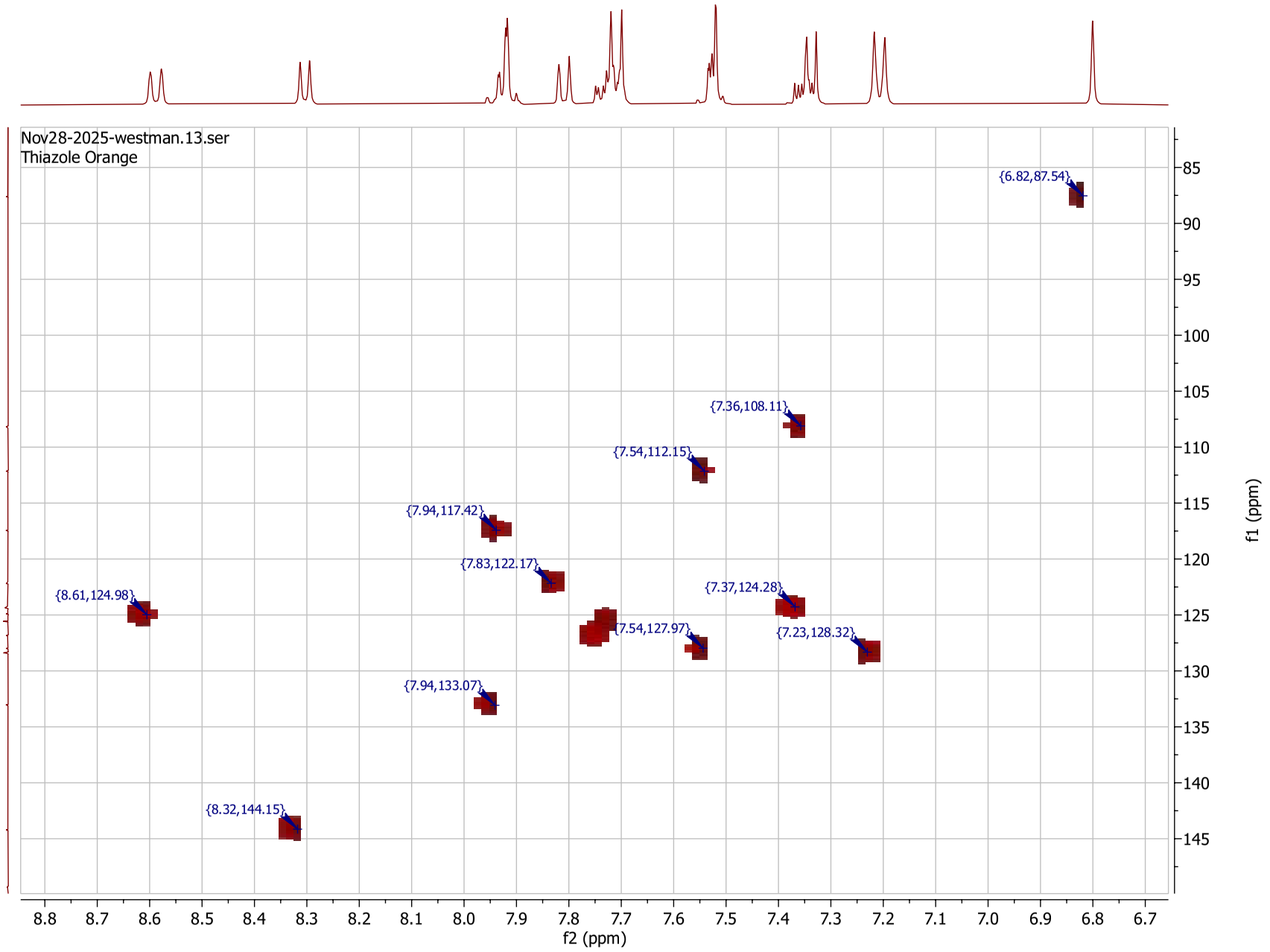
Nov28-2025-westman.13.ser
Thiazole Orange
{6.82,87.54}
{7.36,108.11}
{7.54,112.15}
{7.94,117.42}
{7.83,122.17}
{8.61,124.98}
{7.37,124.28}
{7.54,127.97}
{7.23,128.32}
{7.94,133.07}
{8.32,144.15}
f1 (ppm)
f2 (ppm)

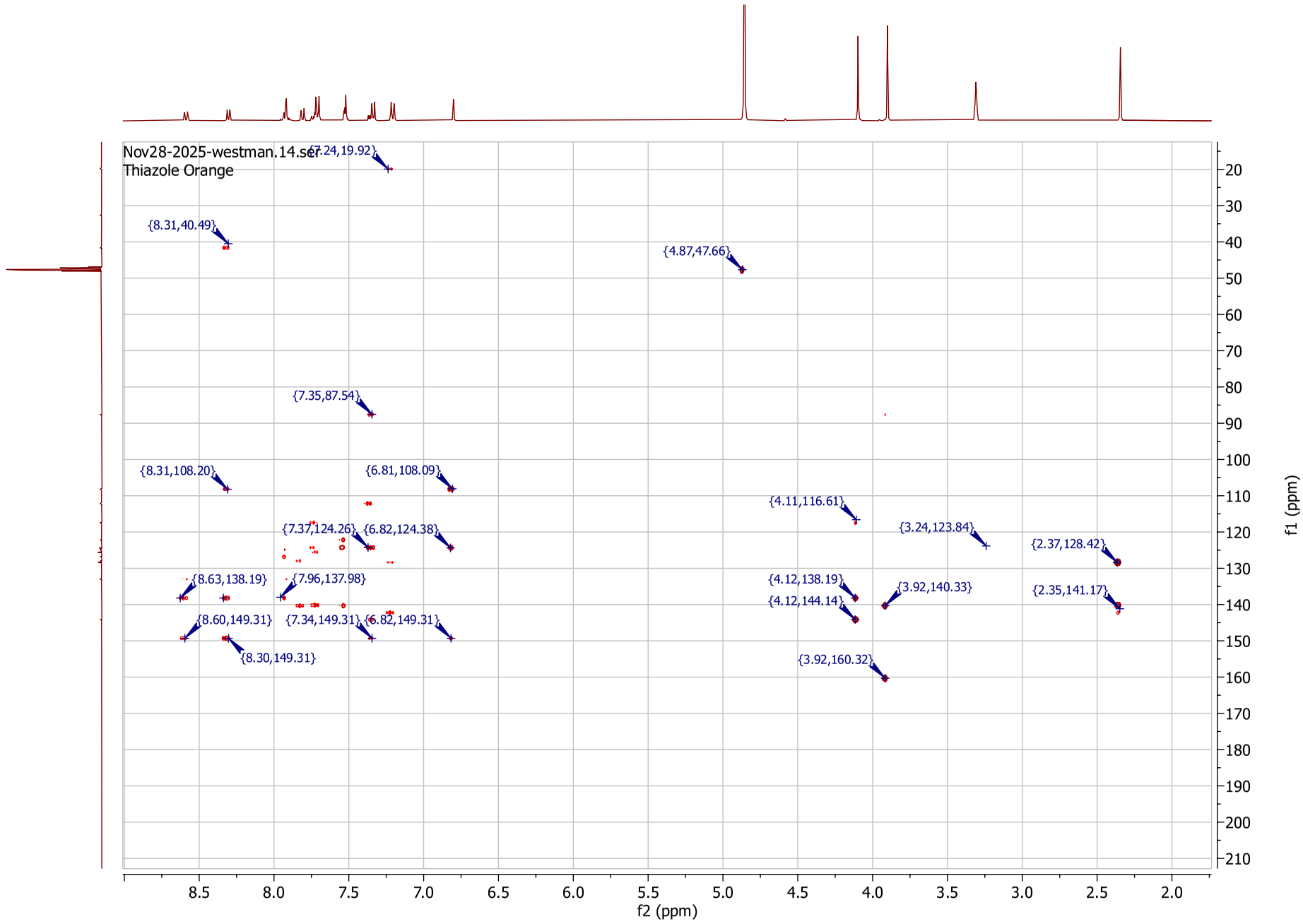
Nov28-2025-westman.14.ser
Thiazole Orange
{7.24,19.92}
{8.31,40.49}
{4.87,47.66}
{7.35,87.54}
{8.31,108.20}
{6.81,108.09}
{4.11,116.61}
{7.37,124.26}
{6.82,124.38}
{3.24,123.84}
{2.37,128.42}
{8.63,138.19}
{7.96,137.98}
{4.12,138.19}
{3.92,140.33}
{2.35,141.17}
{4.12,144.14}
{8.60,149.31}
{7.34,149.31}
{6.82,149.31}
{8.30,149.31}
{3.92,160.32}
f2 (ppm)
f1 (ppm)
XY

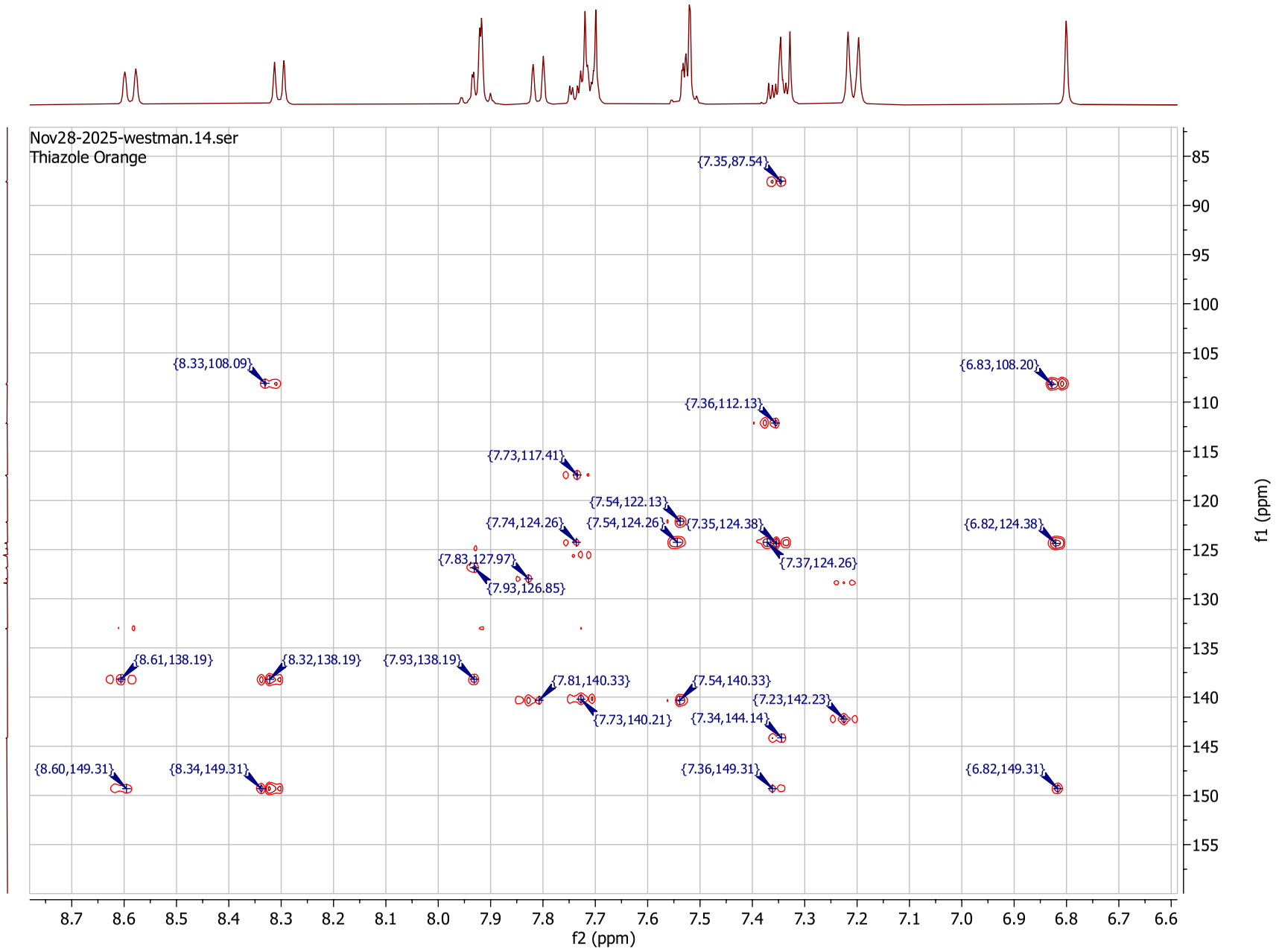
Nov28-2025-westman.14.ser
Thiazole Orange
{7.35,87.54}
{8.33,108.09}
{6.83,108.20}
{7.36,112.13}
{7.73,117.41}
{7.54,122.13}
{7.74,124.26}
{7.54,124.26}
{7.35,124.38}
{6.82,124.38}
{7.83,127.97}
{7.37,124.26}
{7.93,126.85}
{8.61,138.19}
{8.32,138.19}
{7.93,138.19}
{7.81,140.33}
{7.54,140.33}
{7.23,142.23}
{7.73,140.21}
{7.34,144.14}
{8.60,149.31}
{8.34,149.31}
{7.36,149.31}
{6.82,149.31}
f2 (ppm)
f1 (ppm)

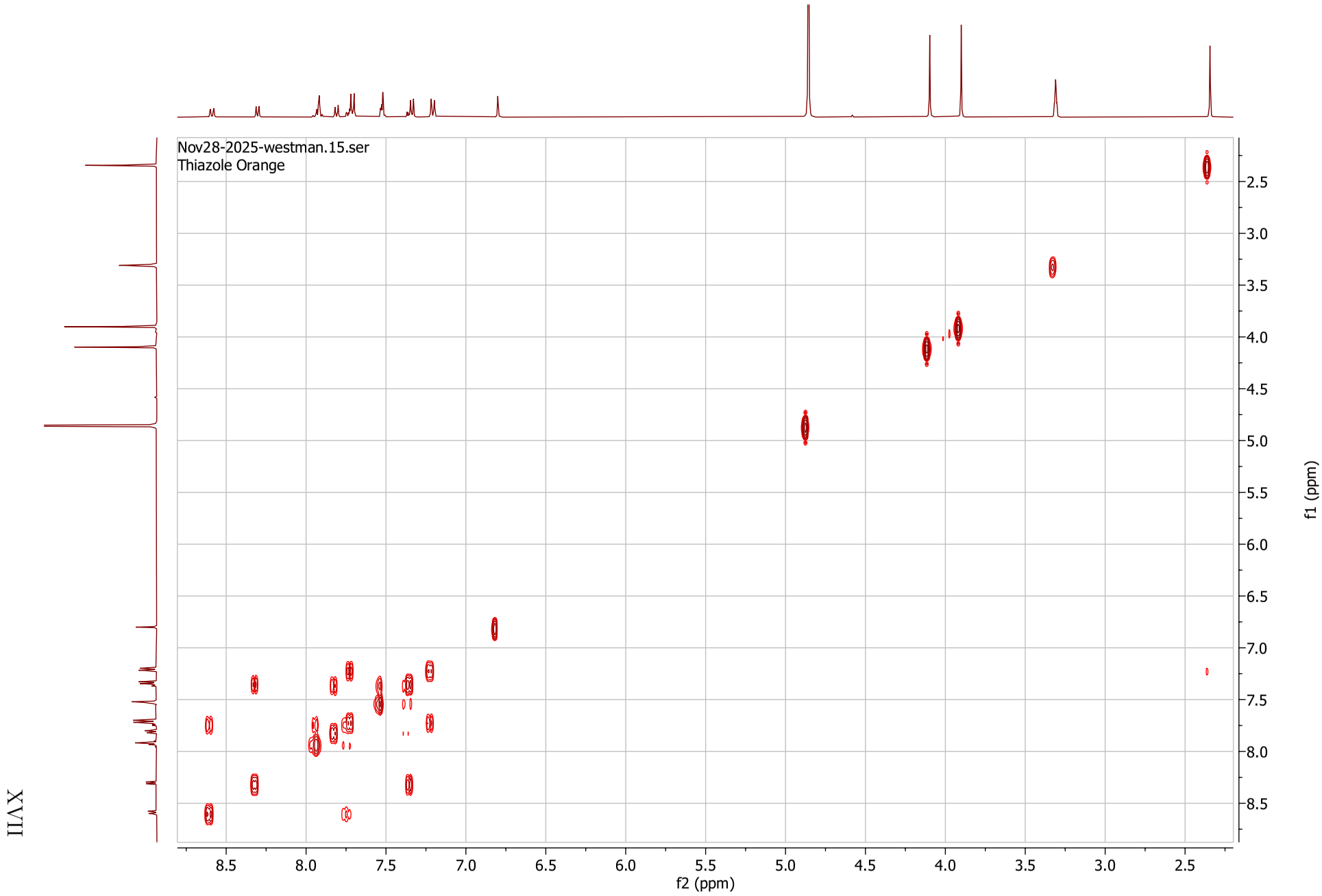
Nov28-2025-westman.15.ser
Thiazole Orange
f2 (ppm)
f1 (ppm)
XVII

XVIII

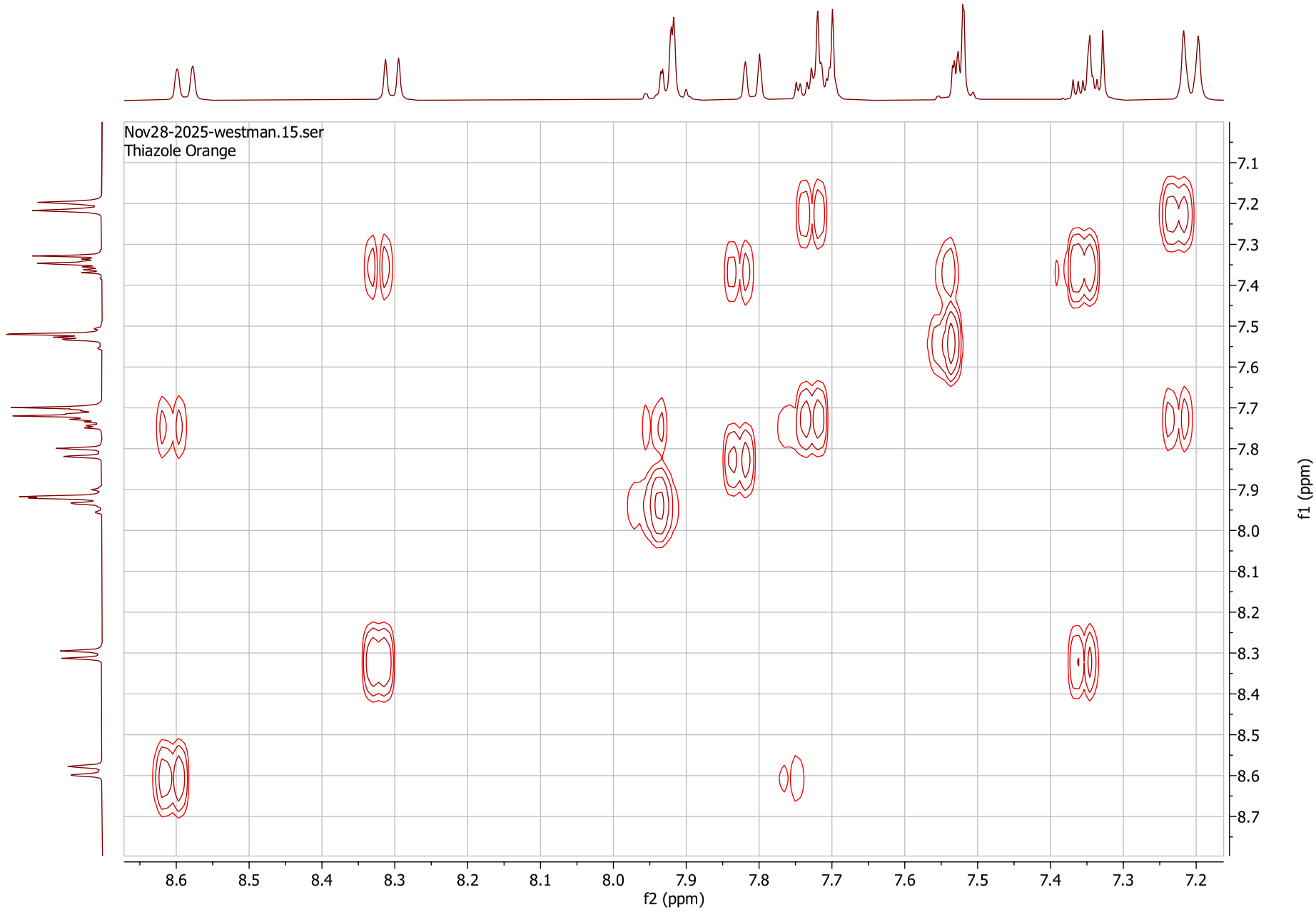
Nov28-2025-westman.15.ser
Thiazole Orange
8.6
8.5
8.4
8.3
8.2
8.1
8.0
7.9
7.8
7.7
7.6
7.5
7.4
7.3
7.2
f2 (ppm)
7.1
7.2
7.3
7.4
7.5
7.6
7.7
7.8
7.9
8.0
8.1
8.2
8.3
8.4
8.5
8.6
8.7
f1 (ppm)

B

Standard Operating Procedures

B.1 Synthesis of CNC

B.1.1 Measurement of dry weight and sulfate content

B.2 Potentiometric and Conductometric Titration

Good to know

- Titrations are performed in triplicate, preferably all three on the same day.
- They are sensitive—check calculations carefully and weigh precisely. Treat all samples the same.
- Use Milli-Q (MQ) water for everything. Rinse containers once with MQ water before use to remove excess ions.

Generally, for CNC

- Prepare a total suspension volume of 20 mL (total mass $\approx$ 20 g).
- Choose concentration as needed; 0.5 wt% is generally suitable. Avoid too high concentrations to prevent coagulation.

Procedure—sample preparation

1. Prepare three samples, all containing the same amount of CNC and NaCl. Samples should be prepared from one stock solution:
   1.1. Make a 60 mL stock solution of CNC at the desired wt%.
   1.2. Use the wide plastic flask with red lid if collected at room temperature.
2. Final volume per sample: 20 mL, composed of:
   - 19.6 mL CNC suspension at the desired wt%.
   - 40 µL of 0.5 M NaCl (to ensure conductivity, especially if running a conductometric titration simultaneously).

Collecting data using the Titrando machine

1. Ensure you have a booked slot (calendar in the room).
2. Verify that calibration was performed within the last 7 days (see log-book in the drawer). If not, contact Jelka.
3. Start the Titrando software; it should indicate that at least one device is connected.
4. Add a flea stir bar to the vessel.
5. Select the method of choice (mostly *SCZ pH 3 to 10*) and name the experiment.
6. Rinse the pH electrode and place it in the suspension—the bulb must be covered but not at risk of being struck by the stir bar.
7. If running a conductometric titration, rinse the conductivity electrode with MQ water and place it in the suspension—ensure it will not foul the stir bar.
8. Rinse the automatic filling tube.
9. Place the filling tube in the suspension—ensure it is immersed but not interfering with the stir bar.
10. Run the method. With *SCZ pH 3 to 10*, the software first measures pH; it should be around 3 to capture the equivalence point.
11. Continuously monitor to ensure proper stirring and that no components are colliding.

After the titration

1. Remove electrodes, rinse, and place them back in the appropriate storage solutions.
2. Clean the workspace.
3. Save and transfer data:
   3.1. Right-click on the graph measuring points.
   3.2. Copy the data and paste into a plain-text editor (e.g., Notepad).
   3.3. Email the file to yourself.

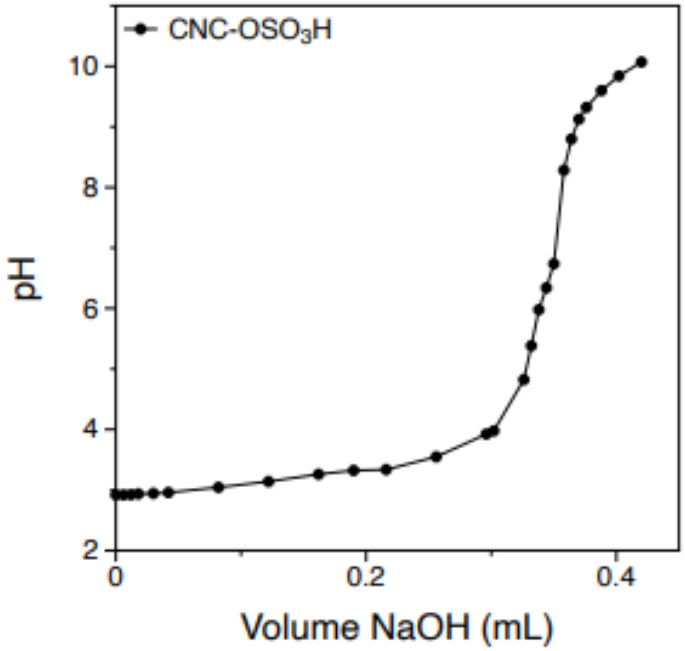

Figure B.1: Typical potentiometric titration curve for sulfated CNC against NaOH.

Calculations

Using the values in the plain-text file, sulfate content (in $mmol \cdot g^{-1}$)is calculated according to equation B.1: where C and V_e is the concentration and volume, respectively, of NaOH at the point of equivalence, M_s M_s is the total weight of the suspension, and D_s its concentration. Keep in mind to:

- Use the volume corresponding to each of the two local maximum ERC values for the calculation.
- Perform the calculation for all three samples, for a total of six.
- Carry out statistical analysis on the results to ensure accuracy.

$$\text{Sulfate content}\,(mmol \cdot g^{-1}) = \frac{C \cdot V_\mathrm{e}}{M_\mathrm{s} \cdot D_\mathrm{s}} \cdot 100 \tag{B.1}$$

DEPARTMENT OF SOME SUBJECT OR TECHNOLOGY
CHALMERS UNIVERSITY OF TECHNOLOGY
Gothenburg, Sweden
www.chalmers.se



CHALMERS
UNIVERSITY OF TECHNOLOGY